Existence, Stability and Slow Dynamics of Spikes in a 1D Minimal Keller–Segel Model with Logistic Growth

Fanze Kong[*], Michael J. Ward[†], and Juncheng Wei[‡]

Dept. of Mathematics, University of British Columbia, Vancouver, Canada, V6T 1Z2

We analyze the existence, linear stability, and slow dynamics of localized 1D spike patterns for a Keller–Segel model of chemotaxis that includes the effect of logistic growth of the cellular population. Our analysis of localized patterns for this two-component reaction-diffusion (RD) model is based, not on the usual limit of a large chemotactic drift coefficient, but instead on the singular limit of an asymptotically small diffusivity $d_2 = \epsilon^2 \ll 1$ of the chemoattractant concentration field. In the limit $d_2 \ll 1$, steady-state and quasi-equilibrium 1D multi-spike patterns are constructed asymptotically. To determine the linear stability of steady-state N-spike patterns we analyze the spectral properties associated with both the "large" $O(1)$ and the "small" $o(1)$ eigenvalues associated with the linearization of the Keller-Segel model. By analyzing a nonlocal eigenvalue problem characterizing the large eigenvalues, it is shown that N-spike equilibria can be destabilized by a zero-eigenvalue crossing leading to a competition instability if the cellular diffusion rate d_1 exceeds a threshold, or from a Hopf bifurcation if a relaxation time constant τ is too large. In addition, a matrix eigenvalue problem that governs the stability properties of an N-spike steady-state with respect to the small eigenvalues is derived. From an analysis of this matrix problem, an explicit range of d_1 where the N-spike steady-state is stable to the small eigenvalues is identified. Finally, for quasi-equilibrium spike patterns that are stable on an $O(1)$ time-scale, we derive a differential algebraic system (DAE) governing the slow dynamics of a collection of localized spikes. Unexpectedly, our analysis of the KS model with logistic growth in the singular limit $d_2 \ll 1$ is rather closely related to the analysis of spike patterns for the Gierer-Meinhardt RD system.

KEYWORDS: Chemotaxis, logistic growth, spikes, matched asymptotic expansions, nonlocal eigenvalue problem.

1 Introduction

The study of pattern formation phenomena for RD systems originates from the pioneering work of Alan M. Turing [49]. In an attempt to understand the mechanism underlying biological morphogenesis, he discovered that spatially homogeneous steady-states of reaction kinetics for multi-component systems that are linearly stable can be destabilized in the presence of diffusion. This diffusion-induced instability, now commonly referred to as a Turing instability, typically leads to the formation of stable spatial patterns that break the symmetry of the spatially uniform state. Based on this insight, modern bifurcation-theoretic tools such as weakly nonlinear multi-scale analysis and Lyapunov-Schmidt reductions have been used ubiquitously to characterize pattern formation near onset for RD systems. However, to analyze localized patterns for RD systems away from the onset of where a Turing instability occurs, new theoretical approaches are needed. Over the past two decades, there has been a focus on developing such novel analytical tools to study the existence, stability, and dynamical behavior of

---

[*]Fanze Kong: fzkong@math.ubc.ca

[†]Michael Ward: ward@math.ubc.ca

[‡]Juncheng Wei: jcwei@math.ubc.ca

"far-from-equilibrium" spatially localized patterns, such as stripes and spots, for two-component RD systems that combine only diffusion and nonlinear reactions (see [59], [12], [8], [53] and references therein).

In contrast, the analytical study of localized pattern formation for RD systems that combine diffusion, non-linear reactions, and *advection* poses many new theoretical challenges (cf. [2, 9, 48, 52]. The most common such RD models are chemotaxis-type systems, such as the prototypical Keller–Segel (KS) system [27, 28], that are widely used to model how cells or bacteria direct their movements in response to an environmental chemical stimulus, such as observed in some foundational experiments (cf. [13], [1], [5]). Chemotactic effects have been shown to play a key role in a wide variety of other biological processes such as, cell-cell interactions in the immune system, the organization of tissues during embryogenesis, and the growth of tumor cells [4, 41, 45].

In 1971, Keller and Segel [27, 28] proposed the following coupled RD system to model chemotaxis:

$$
\begin{cases}
\tau u_t = \overbrace{d_1 \Delta u}^{\text{cellular diffusion}} - \overbrace{\chi \nabla \cdot (S(u,v)\nabla v)}^{\text{advection}} + \overbrace{f(u)}^{\text{source}}, & x \in \Omega, \, t > 0, \\
 \underbrace{}_{\text{chemical signal diffusion}} \underbrace{}_{\text{chemical production/consumption}} \\
v_t = \overbrace{d_2 \Delta v}^{} + \overbrace{g(u,v)}^{}, & x \in \Omega, \, t > 0.
\end{cases}
\tag{K-S}
$$

Here Ω is either a bounded domain with smooth boundary $\partial\Omega$ or the whole space $\mathbb{R}^N$ with $N \geq 1$. In (K-S), u is the cellular density, v is the chemotactic concentration, τ is the reaction time constant, d_1 and d_2 are diffusivities of u and v, respectively, while $S(u,v)$ models the chemotactic or directed movement. The chemotactic drift coefficient χ measures the relative strength of this directed motion. In a bounded domain, no-flux boundary conditions are usually imposed on (K-S) to ensure that the cellular aggregation is spontaneous.

One main research focus on the chemotaxis PDE system (K-S) is the study of self-aggregating pattern-formation phenomena and the determination of whether finite-time singularities can occur. There are two well-known approaches to study the possibility of such blow-up behavior. The first approach is to analyze the well-posedness and global existence of solutions, which can rule out the trivial dynamics. The other approach is to construct spatially inhomogeneous patterns and to study their local and long time behaviors. For a survey of diverse applications and some mathematical results for (K-S) and its variants see [3, 17, 20–22, 43].

Our goal is to analyze certain pattern-formation properties for a KS model with logistic growth, given by

$$
\begin{cases}
\tau u_t = d_1 \Delta u - \chi \nabla \cdot (u\nabla v) + \mu u(\bar{u} - u), & x \in \Omega, \, t > 0, \\
v_t = d_2 \Delta v - v + u, & x \in \Omega, \, t > 0, \\
\frac{\partial u}{\partial \mathbf{n}}(x,t) = \frac{\partial v}{\partial \mathbf{n}}(x,t) = 0, & x \in \partial\Omega, \, t > 0,
\end{cases}
\tag{1.1}
$$

where $u(x,0) = u^0(x)$ and $v(x,0) = v^0(x)$ are non-negative initial data. Here S and g in (K-S) are taken to be linear, i. e. $S(u,v) = u$ and $g(u,v) = u - v$. In (1.1), $f(u) = \mu u(\bar{u} - u)$ describes the cellular population growth dynamics, where $\mu > 0$ denotes the logistic growth rate and $\bar{u} > 0$ represents the carrying capacity of the habitat for cells. Before discussing some previous results for (1.1), we will highlight some results for the case $f(u) \equiv 0$.

Without logistic growth, (1.1) in 2D admits blow-up phenomenon, which depends on the cellular mass $M := \int_\Omega u(x,0)\,dx$. In particular, if $M < M_0 := 4\pi/\chi$ for the bounded domain or $M < M_0 := 8\pi/\chi$ for the whole space $\mathbb{R}^2$, the solution to (1.1) will globally exist [38]; otherwise (1.1) admits finite time blow-up solutions [10, 16, 39, 46, 50]. For the steady-state problem of (1.1) in 2D, the pioneering study of Lin, Ni and Takagi [35, 40] constructed large amplitude stationary solutions analytically. Motivated by this seminal work, it has been subsequently revealed that non-constant steady states with $f(u) \equiv 0$ can exhibit a wide range of solution behaviors [7, 11, 15]. In particular, Wei and Del Pino [11] constructed a multi-spike equilibrium to (1.1) in 2D via the "localized energy method". In contrast to the 2D case, the solution to (1.1) in 1D with $f \equiv 0$ is uniformly bounded in time [37, 42]. For the stationary counterpart, spatially non-uniform steady states were constructed in [9, 18, 26, 52]. In particular, Wang and Xu [52] adopted an innovative bifurcation-theoretic approach to directly treat the steady-state problem for (1.1) in 1D without relying significantly on the special structure of (1.1).

With the logistic source term, i.e. when $f(u) = \mu u(\bar{u} - u)$, Winkler et al. [36, 60–64] showed that the solution of (1.1) globally exists in any dimension when the effect of the logistic growth is strong enough. Some results regarding the construction of spatially inhomogeneous equilibria for (1.1) are given in [25, 31, 33, 34, 51]. However, the dynamics of (1.1) can be highly intricate and are not nearly as well understood as for the case where $f(u) \equiv 0$. Hillen and Painter et al. [19, 44] studied (1.1) numerically and revealed the possibility of periodic and chaotic dynamics consisting of repeated spike nucleation and amalgamation events.

From a formal asymptotic analysis together with numerical simulations, Kolokolnikov et al. [31] showed that there exists three types of spiky steady states to (1.1) in 1D. In particular, they constructed a locally stable single interior spike solution, which does not occur in the minimal KS model without the logistic source term. To more fully understand how a logistic source term allows for spiky patterns, the focus in this paper is to study the existence, stability, and dynamics of spiky solutions to the 1D version of (1.1), which is formulated as

$$\tau u_t = d_1 u_{xx} - \chi (u v_x)_x + \mu u(\bar{u} - u), \quad |x| < 1, \; t > 0; \qquad u_x(\pm 1, t) = 0, \tag{1.2a}$$

$$v_t = d_2 v_{xx} - v + u, \quad |x| < 1, \; t > 0; \qquad v_x(\pm 1, t) = 0, \tag{1.2b}$$

with $u(x, 0) = u^0(x)$ and $v(x, 0) = v^0(x)$. Our main goal is to construct N-spike equilibria for (1.2) with equal heights in the limit where the diffusivity d_2 is small, and to analyze the linear stability properties of these localized steady-state patterns. Labeling $d_2 = \epsilon^2 \ll 1$, the steady-state problem for (1.2) on $|x| < 1$ is

$$d_1 u_{xx} - \chi (u v_x)_x + \mu u(\bar{u} - u) = 0, \qquad \epsilon^2 v_{xx} - v + u = 0; \qquad u_x(\pm 1) = v_x(\pm 1) = 0. \tag{1.3}$$

We will also explicitly construct quasi-equilibrium patterns for (1.2) where the spike locations evolve dynamically on some asymptotically long time scale as $\epsilon \to 0$ towards their steady-state locations.

We emphasize that our analysis of localized pattern formation for (1.2) in the singular limit $d_2 \to 0$ is in distinct contrast to the previous analytical and numerical studies of pattern formation properties for (1.2) that were undertaken in the more traditional large chemotactic drift limit $\chi \gg 1$ (cf. [34], [33], [25], and [51]). In the singular limit $d_2 \ll 1$, our analysis and results for the existence, linear stability, and slow dynamics of 1D spike patterns for (1.2) will be shown to be rather closely related to corresponding studies of 1D spike patterns for the Gierer-Meinhardt (GM) RD model (cf. [24], [23], [55], [58]).

The outline of this paper is as follows. In §2, we construct N-spike quasi-equilibrium spike patterns for (1.2) using the method of matched asymptotic expansions in the limit $\epsilon \ll 1$. Our analysis reveals a novel, analytically tractable, sub-inner asymptotic structure that characterizes the spatial profile of a localized spike. With regards to the linear stability analysis, in §3 and §4 we analyze the large and small eigenvalues in the discrete spectrum of the linearization of (1.2) around an N-spike steady-state, respectively. The spectral properties for the large eigenvalues are shown to be governed by a nonlocal eigenvalue problem (NLEP), which has a somewhat similar form to the NLEP that arises in the study of spike stability in the GM model. For $\tau = 0$, our NLEP linear stability analysis will provide a range of d_1 values for which the N-spike equilibrium is linearly stable. Moreover, for $\tau > 0$, we show that spike amplitude oscillations can occur via a Hopf bifurcation associated with the NLEP. Hypergeometric functions are shown to be key for accurately calculating the stability thresholds from the NLEP. For the small eigenvalues, in §4.2 we will determine analytically an explicit range of d_1 for which the steady-state solution is linearly stable to translation instabilities.

A differential-algebraic (DAE) system characterizing slow spike dynamics for quasi-equilibrium patterns is derived in §5. The slow dynamics obtained from this DAE system are favorably compared with corresponding results computed from full PDE numerical simulations of (1.2). Moreover, in §5.1 we show that the explicit expressions for the small eigenvalues that are obtained in §4 can also be derived from a linearization of the DAE dynamics around the steady-state spike locations. In §6, we suggest a few open problems, and we compare and contrast the analytical approach used and results previously obtained for spike patterns in the 1D GM model with that obtained herein for the KS model (1.2).

2 Asymptotic Analysis of the N-Spike Quasi-equilibrium

In this section, we construct N-spike quasi-steady state solutions to (1.3) in the limit $\epsilon \ll 1$ by using the method of matched asymptotic expansions. We define the centers of the spikes as x_j, for $j = 1, \ldots, N$, and assume that they are well-separated in the sense that $|x_j - 1| = O(1)$, $|x_j + 1| = O(1)$, and $|x_i - x_j| = O(1)$ for $i \neq j$.

2.1 Inner Solution

In the inner region near each x_j where the cellular density u and the chemical concentration v are localized, we introduce new local variables $y = \epsilon^{-1}(x - x_j)$, $U_j(y) = u(x_j + \epsilon y)$, and $V_j(y) = v(x_j + \epsilon y)$, and we expand

$$U_j(y) = U_{0j}(y) + \epsilon^2 U_{1j}(y) + \ldots, \quad V_j(y) = V_{0j}(y) + \epsilon^2 V_{1j}(y) + \ldots, \quad y = \epsilon^{-1}(x - x_j). \tag{2.1}$$

Here the subscripts 0 and 1 in (U_{0j}, V_{0j}) and (U_{1j}, V_{1j}) are the orders of the expansion, while j refers to the jth inner region. The leading order terms, found by substituting (2.1) into (1.3), yield on $-\infty < y < \infty$ that

$$(U'_{0j} - \bar{\chi} U_{0j} V'_{0j})' = 0, \quad U'_{0j}(0) = 0; \quad V''_{0j} - V_{0j} + U_{0j} = 0, \quad V'_{0j}(0) = 0. \tag{2.2}$$

In this so-called *core problem*, we define $\bar{\chi} := \chi/d_1$. Below, for simplicity, we omit the subscript j for U_{0j} and V_{0j}. Moreover, in the analysis below, terms such as h_x and H' denote differentiation in x and y, respectively.

Upon imposing $U_0 \to 0$ as $|y| \to \infty$, (2.2) yields $U_0 = C_j e^{\bar{\chi} V_0}$, where the constant $C_j > 0$ will be determined below. Then, from (2.2), we conclude that the spike profile is characterized by a homoclinic solution V_0 to

$$V''_0 + Q(V_0) = 0, \quad -\infty < y < +\infty; \quad V'_0(0) = 0; \quad V_0 \to s_j, \quad V'_0, V''_0 \to 0, \quad \text{as } |y| \to \infty, \tag{2.3}$$

where $Q(V_0) := -V_0 + C_j e^{\bar{\chi} V_0}$ and s_j satisfies $Q(s_j) = 0$, so that $C_j e^{\bar{\chi} s_j} = s_j$. The first integral of (2.3) is

$$\frac{1}{2}(V'_0)^2 + K(V_0; C_j) = 0, \quad K(V_0; C_j) := \int_{s_j}^{V_0} Q(\xi) \, d\xi = \frac{1}{2}\left(s_j^2 - V_0^2\right) + \frac{C_j}{\bar{\chi}}\left(e^{\bar{\chi} V_0} - e^{\bar{\chi} s_j}\right). \tag{2.4}$$

Imposing that V_0 is even and monotone decreasing in $y > 0$, we obtain from (2.4) that

$$V'_0 = -\sqrt{-2K(V_0; C_j)} \quad \text{for} \quad 0 \leq y < \infty. \tag{2.5}$$

By separating variables in (2.5), we obtain an implicit equation for V_0, defined on $y \geq 0$, given by

$$y = \int_{V_0}^{v_{\max j}} \frac{d\xi}{\sqrt{-2K(\xi; C_j)}}, \tag{2.6}$$

where $v_{\max j} := V_0(0)$ is the amplitude of V_0. By setting $V'_0(0) = 0$ in (2.5) and using $s_j = C_j e^{\bar{\chi} s_j}$, it follows that $v_{\max j}$ satisfies the nonlinear algebraic equation

$$-\frac{1}{2}v_{\max j}^2 + \frac{1}{2}s_j^2 + \frac{C_j}{\bar{\chi}}e^{\bar{\chi} v_{\max j}} - \frac{s_j}{\bar{\chi}} = 0. \tag{2.7}$$

In the outer region, defined at $O(1)$ distances from the centers of the spikes, we will construct a solution where u and v are $o(1)$ as $\epsilon \to 0$. As a result, we anticipate from the matching condition that $s_j = o(1)$ as $\epsilon \to 0$, which allows us to approximate our implicit form of V_0 given by (2.6). To this end, we suppose that $s_j = o(1)$ and $v_{\max j}^{-1} = o(1)$ when $\epsilon \ll 1$, so that (2.7) reduces to

$$\frac{C_j}{\bar{\chi}}e^{\bar{\chi} v_{\max j}} \sim \frac{1}{2}v_{\max j}^2. \tag{2.8}$$

4

Next, we introduce new variables z and $\tilde{V}_0$, which constitute a sub-layer within the inner region, defined by

$$z = y\, v_{\max j}, \qquad V_0(y) = v_{\max j} + \tilde{V}_0(z).$$

By using (2.8), and where primes now indicate derivatives in z, we can rewrite the V_0-equation in (2.3) as

$$v_{\max j}^2 \tilde{V}_0'' - (v_{\max j} + \tilde{V}_0) + \frac{\bar{\chi}}{2} v_{\max j}^2 e^{\bar{\chi}\tilde{V}_0} = 0, \qquad \infty < z < +\infty. \tag{2.9}$$

In this j^{th} sub-inner region, we expand $\tilde{V}_0(z)$ as $\tilde{V}_0 = \tilde{V}_{00}(z) + o(1)$. From (2.9), and assuming that $v_{\max j} \gg 1$, we obtain an explicitly solvable leading order sub-inner equation

$$\tilde{V}_{00}'' + \frac{1}{2}\bar{\chi} e^{\bar{\chi}\tilde{V}_{00}} = 0, \qquad \text{so that} \qquad \tilde{V}_{00} = \frac{1}{\bar{\chi}}\log\left[\text{sech}^2\left(\frac{\bar{\chi}}{2}z\right)\right], \qquad U_0 = C_j e^{\bar{\chi}V_0} \sim C_j e^{\bar{\chi}(v_{\max j} + \tilde{V}_{00})}. \tag{2.10}$$

We now summarize our results in the inner and sub-inner regions for the leading order profile of a quasi-equilibrium spike when $s_j \ll 1$ and $v_{\max j} \gg 1$. In the sub-inner region, where $|x - x_j| \le O\left(\frac{\epsilon}{v_{\max j}}\right)$, we have

$$u \sim U_0 \sim \frac{1}{2}\bar{\chi} v_{\max j}^2 e^{\bar{\chi}\tilde{V}_{00}(z)}, \qquad v \sim V_0 \sim v_{\max j} + \tilde{V}_{00}(z), \tag{2.11}$$

where $z = v_{\max j}\epsilon^{-1}(x - x_j)$ and $\tilde{V}_{00}$ is given by (2.10). In the inner region, where $|x - x_j| \le O(\epsilon)$, we have

$$u \sim C_j e^{\bar{\chi}V_0(y)}, \qquad v \sim V_0(y), \tag{2.12}$$

where $y = \epsilon^{-1}(x - x_j)$ and $V_0(y)$ is determined implicitly by (2.6). Here, the three constants C_j, s_j and $v_{\max j}$ satisfy the two nonlinear algebraic equations $C_j e^{\bar{\chi}s_j} = s_j$ and (2.7). The required additional equation arises below from matching the far-field of each inner solution to an outer solution. The far-field of the leading order inner solution (2.12) gives only that $u \sim v \to s_j$ as $|y| \to \infty$, but has no gradient information.

As such, we must refine our inner analysis to one higher order so as to match with any spatial gradients of the outer solution at the spike locations. To this end, we substitute (2.1) into (1.3) and obtain at next order that

$$\left[U_{1j}' - \bar{\chi}(U_0 V_{1j}') - \bar{\chi}(U_{1j} V_0')\right]' = \frac{\mu}{d_1}(U_0^2 - \bar{u}U_0), \quad -\infty < y < \infty; \qquad U_{1j}'(0) = 0, \tag{2.13a}$$

$$V_{1j}'' - V_{1j} + U_{1j} = 0, \quad -\infty < y < \infty; \qquad V_{1j}'(0) = 0. \tag{2.13b}$$

Upon integrating (2.13a) over $(0, y)$, we obtain the flux-balancing condition

$$U_{1j}' - \bar{\chi}U_{1j}V_0' - \bar{\chi}U_0 V_{1j}' = \frac{\mu}{d_1}\int_0^y \left[U_0^2(\xi) - \bar{u}U_0(\xi)\right] d\xi. \tag{2.14}$$

By letting $y \to \infty$, and assuming that $U_{1j}V_0'$ and U_0V_{1j}' are negligible in this limit, we obtain from (2.14) that

$$U_{1j}' \to \frac{\mu}{d_1}\int_0^\infty (U_0^2 - \bar{u}U_0)\, dy, \qquad \text{as} \quad y \to +\infty. \tag{2.15}$$

To explicitly determine U_{1j}' as $y \to +\infty$, we must estimate the two integrals in (2.15) involving U_0 and U_0^2. By using the sub-inner solution (2.11), we readily calculate that

$$\int_0^\infty U_0\, dy \sim v_{\max j}, \qquad \int_0^\infty U_0^2\, dy \sim \frac{1}{3}\bar{\chi} v_{\max j}^3. \tag{2.16}$$

5

In this way, by substituting (2.16) into (2.15), we obtain that $U'_{1j} \to \mu\bar{\chi}v^3_{\max j}/(3d_1)$ as $y \to +\infty$. In a similar way, we obtain from (2.13) that $U'_{1j} \to -\mu\bar{\chi}v^3_{\max j}/(3d_1)$ as $y \to -\infty$. Since the inner solution is expanded as $u \sim U_0 + \epsilon^2 U_{1j}$, and U_{0y} is exponentially small as $|y| \to \infty$, we obtain for the outer solution that $u_x \sim \epsilon U'_{ij}$ as $x \to x_j$ and $|y| \to \infty$. By using the expressions above for U'_{1j} as $y \to \pm\infty$, we conclude by matching the far-field behavaior of the inner solution to the outer solution that the outer solution must satisfy the limiting behavior

$$u_x \sim \pm\epsilon\frac{\mu\bar{\chi}}{3d_1}v^3_{\max j} \quad \text{as} \quad x \to x_j^{\pm}. \tag{2.17}$$

This matching condition shows that, in the outer region, u_x must have a jump discontinuity across each $x = x_j$.

Finally, we must confirm, through a self-consistency argument, that $U_{1j}V'_0$ and $U_0V'_{1j}$ for $y \to \infty$ can be neglected in (2.14). To do so, we observe that, although U_{1j} grows linearly for $|y|$ sufficiently large, the exponential decay of V'_0 ensures that $U_{1j}V'_0$ can be neglected as $y \to \infty$. Moreover, since $u \sim v$ in the outer region when $\epsilon \ll 1$, we obtain that $U_0 \sim V_0$ and $U_{1j} \sim V_{1j}$ as $y \to \pm\infty$. Combining these estimates with $U_0 \to s_j$ as $|y| \to +\infty$, we obtain $U_0V'_{1j} \approx s_jU'_{1j} \ll U'_{1j}$ in (2.14) since $s_j \ll 1$. As a result, our assumptions that $U_{1j}V'_0$ and $U_0V'_{1j}$ can be neglected in (2.14) as $|y| \to \infty$ are self-consistent.

2.2 Outer Solution and Matching

Next, we construct the solution in the outer region. When $\epsilon \ll 1$, we expand u and v as $u = u_o + o(1)$ and $v = v_o + o(1)$. From (1.3) for v we get $v_o = u_o$, so that (1.3) for u reduces to

$$u_{oxx} - \bar{\chi}(u_ou_{ox})_x + \frac{\mu}{d_1}u_o(\bar{u} - u_o) = 0, \quad x \in (-1,1)\backslash\bigcup_{j=1}^{N}x_j. \tag{2.18}$$

There are two ways to approximate the solution to (2.18). The first approach is to introduce the new variable

$$w := u_o - \frac{\bar{\chi}}{2}u_o^2. \tag{2.19}$$

In terms of w, we obtain from (2.18) that w satisfies

$$w_{xx} + \frac{\mu}{d_1}\left[\frac{\bar{u}}{\bar{\chi}} - \frac{2}{\bar{\chi}^2} + \left(\frac{2}{\bar{\chi}^2} - \frac{\bar{u}}{\bar{\chi}}\right)\sqrt{1 - 2w\bar{\chi}} + \frac{2w}{\bar{\chi}}\right] = 0, \qquad x \in (-1,1)\backslash\bigcup_{j=1}^{N}x_j. \tag{2.20}$$

We have $\sqrt{1 - 2\bar{\chi}w} \sim 1 - \bar{\chi}w$ since u_o is small in the outer region. With this approximation, and setting $w \sim w_o$, we obtain from (2.19) and (2.20) that $w_o \sim u_o$ in the outer region, where w_o solves the leading order problem

$$w_{oxx} + \frac{\bar{u}\mu}{d_1}w_o = 0, \qquad x \in (-1,1)\backslash\bigcup_{j=1}^{N}x_j. \tag{2.21}$$

Observe that (2.21) follows *exactly* from (2.20), with no approximation, for the special parameter set $\bar{u} = 2/\bar{\chi}$. The second way to approximate (2.18) is to collect the leading order terms in (2.18) directly. In fact, since u_o is small, $(u_ou_{ox})_x$ and u_o^2 are higher order terms in the outer region. By neglecting these terms in (2.18), we also obtain (2.21) since $u_o \sim w_o$. Finally, for (2.21), we require from (2.17) that w_o must satisfy the jump condition $w_{ox}(x_j^+) - w_{ox}(x_j^-) = \frac{2\bar{\chi}\mu}{3d_1}v^3_{\max j}\epsilon$ across each x_j. In this way, we obtain the leading order outer problem

$$\mathcal{L}_0w_o := \frac{d_1}{\mu}w_{oxx} + \bar{u}w_o = \frac{2\bar{\chi}}{3}\epsilon\sum_{k=1}^{N}v^3_{\max k}\delta(x - x_k), \quad -1 < x < 1; \qquad w_{ox}(\pm1) = 0. \tag{2.22}$$

6

To analyze the solvability of (2.22), we first observe that (2.22) admits the nontrivial homogeneous solution

$$w_{oh}(x) := \cos\left(\frac{m(x+1)\pi}{2}\right), \qquad \text{when} \quad d_1 = d_{1Tm} := \frac{4\mu\bar{u}}{m^2\pi^2}, \quad \text{for } m = 1, 2, \ldots. \tag{2.23}$$

As shown in Appendix A, the interpretation of these critical, or *resonant*, values of d_1 are that they correspond precisely to where there is a bifurcation from the spatially uniform solution $v = u = 0$ for (1.2) on $|x| < 1$. This trivial solution for (1.2) on $|x| < 1$ is linearly stable only when $d_1 > 4\mu\bar{u}/\pi^2$. When $d_1 = d_{1Tm}$, there is a solution (non-unique) to (2.22) only if a compatibility condition is satisfied. However, as shown in Appendix A this condition is automatically satisfied for an N-spike steady-state solution.

To solve (2.22) when $d_1 \neq d_{1Tm}$, we introduce the Helmholtz Green's function $G(x; x_k)$ satisfying

$$\frac{d_1}{\mu}G_{xx} + \bar{u}G = \delta(x - x_k), \quad -1 < x < 1; \qquad G_x(\pm 1; x_k) = 0. \tag{2.24}$$

For $d_1 \neq d_{1Tm}$, the explicit solution to (2.24) is

$$G(x; x_k) = \sqrt{\frac{\mu}{\bar{u}d_1}} \left[\tan(\theta(1 + x_k)) + \tan(\theta(1 - x_k))\right]^{-1} \begin{cases} \frac{\cos(\theta(1+x))}{\cos(\theta(1+x_k))}, & -1 < x < x_k, \\ \frac{\cos(\theta(1-x))}{\cos(\theta(1-x_k))}, & x_k < x < 1, \end{cases} \qquad \theta := \sqrt{\frac{\mu\bar{u}}{d_1}}. \tag{2.25}$$

In terms of (2.25), the solution to (2.22) when $d_1 \neq d_{1Tm}$ is

$$u_o \sim w_o = \frac{2\bar{\chi}}{3}\epsilon \sum_{k=1}^{N} v_{\max k}^3 G(x; x_k). \tag{2.26}$$

Our final step in the construction is to match the inner and outer solutions to obtain the third algebraic equation needed to determine s_j, C_j and $v_{\max j}$. Since $w_o \sim u_o$ in the outer region, we impose $w_o(x_j) = s_j$ to get

$$s_j = \frac{2\bar{\chi}}{3}\epsilon \sum_{k=1}^{N} v_{\max k}^3 G(x_j; x_k), \qquad j = 1, \ldots, N, \tag{2.27}$$

when $d_1 \neq d_{1Tm}$. Combining (2.27), (2.7), and $C_j e^{\bar{\chi}s_j} = s_j$, we obtain the following coupled algebraic system:

$$C_j e^{\bar{\chi}s_j} - s_j = 0, \qquad -\frac{1}{2}v_{\max j}^2 + \frac{1}{2}s_j^2 + \frac{C_j}{\bar{\chi}}e^{\bar{\chi}v_{\max j}} - \frac{s_j}{\bar{\chi}} = 0, \qquad s_j = \frac{2\bar{\chi}}{3}\epsilon \sum_{k=1}^{N} v_{\max k}^3 G(x_j; x_k). \tag{2.28}$$

Finally, we observe that the matching condition (2.17) between the inner and outer solutions holds only when the spike locations x_j are equally spaced, and are given by $x_j = x_j^0$ where

$$x_j^0 := -1 + \frac{2j-1}{N}, \qquad j = 1, \ldots, N. \tag{2.29}$$

Moreover, in (B.9) of Appendix B we calculate $\sum_{k=1}^{N} G(x_j; x_k)$ explicitly to show that it is independent of j when $x_j = x_j^0$, $x_k = x_k^0$, and $d_1 \neq d_{1Tm}$. As a result, for equally-spaced spikes we have $s_j = s_0$, where s_0 is given by

$$s_0 = \frac{2\bar{\chi}}{3}a_g v_{\max 0}^3 \epsilon \sim \epsilon a_g \int_{-\infty}^{\infty} U_0^2 \, dy, \qquad \text{with} \quad a_g := \sum_{k=1}^{N} G(x_j^0; x_k^0) = \frac{1}{2}\sqrt{\frac{\mu}{d_1\bar{\mu}}} \cot\left(\frac{\theta}{N}\right). \tag{2.30}$$

7

When $x_j = x_j^0$ and $d_1 \neq d_{1Tm}$, our N-spike quasi-equilibrium is the approximation to a true steady-state solution of (1.3). Setting $s_j = s_0$ for all j, we obtain from (2.28) that $C_j = C_0$ and $v_{\max j} = v_{\max 0}$ for all j, satisfy

$$C_0 = s_0 e^{-\bar{\chi} s_0}, \qquad -\frac{1}{2}v_{\max 0}^2 + \frac{1}{2}s_0^2 + \frac{C_0}{\bar{\chi}}e^{\bar{\chi} v_{\max 0}} - \frac{s_0}{\bar{\chi}} = 0, \quad \text{where} \quad s_0 = \frac{2\bar{\chi}}{3}\epsilon v_{\max 0}^3 a_g, \qquad (2.31)$$

with a_g as given in (2.30). By combining (2.31), we obtain a single nonlinear equation for $v_{\max 0}$ given by

$$-\frac{1}{2}v_{\max 0}^2 + \frac{2}{9}\bar{\chi}^2 v_{\max 0}^6 a_g^2 \epsilon^2 + \frac{2}{3}a_g v_{\max 0}^3 \epsilon e^{\bar{\chi} v_{\max 0} - \frac{2}{3}a_g \bar{\chi}^2 v_{\max 0}^3 \epsilon} - \frac{2}{3}a_g v_{\max 0}^3 \epsilon = 0. \qquad (2.32)$$

In terms of the solution $v_{\max 0}$ to (2.32), s_0 and C_0 are given by (2.31). Moreover, assuming $v_{\max 0} \gg 1$, $v_{\max 0}^3 \epsilon \ll 1$, and $a_g > 0$, a dominant balance argument on (2.32) for $\epsilon \ll 1$ yields that

$$\frac{1}{2}v_{\max 0}^2 \sim \frac{s_0}{\bar{\chi}}e^{\bar{\chi} v_{\max 0}} \sim \frac{2}{3}a_g v_{\max 0}^3 \epsilon e^{\bar{\chi} v_{\max 0}}. \qquad (2.33)$$

This shows that $v_{\max 0} = O(-\log \epsilon) \gg 1$, so that the consistency condition $v_{\max 0}^3 \epsilon \ll 1$ is satisfied. We summarize our results regarding the construction of the N-spike steady-state in the following formal proposition:

Proposition 2.1. *Let $\epsilon \ll 1$, assume that $d_1 \neq d_{1Tm}$, where d_{1Tm} is defined in (2.23). Label the set $\mathcal{I} := \{1, 2, \ldots, N\}$. Then, the N-spike quasi-equilibrium to (1.3), defined by (u_q, v_q), has the following asymptotic behavior in $-1 < x < 1$:*

$$
\begin{cases}
u_q(x) \sim \begin{cases}
\frac{1}{2}\bar{\chi}v_{\max k}^2 \text{sech}^2\left(\frac{\bar{\chi}}{2}\frac{v_{\max k}(x-x_k)}{\epsilon}\right), & x \in \left\{x \in \mathbb{R}\,\big|\,|x-x_k| \leq O\left(\frac{\epsilon}{|\log \epsilon|}\right), \exists k \in \mathcal{I}\right\}, \\
C_k e^{\bar{\chi} V_0\left(\frac{x-x_k}{\epsilon}\right)}, & x \in \left\{x \in \mathbb{R}\,\big|\,O\left(\frac{\epsilon}{|\log \epsilon|}\right) \ll |x-x_k| \leq O(\epsilon), \exists k \in \mathcal{I}\right\}, \\
\frac{2\bar{\chi}\epsilon}{3}\sum_{k=1}^{N} v_{\max k}^3 G(x; x_k), & x \in \left\{x \in \mathbb{R}\,\big|\,O(\epsilon) \ll |x-x_k|, \forall k \in \mathcal{I}\right\},
\end{cases} \\[2em]
v_q(x) \sim \begin{cases}
v_{\max k} + \frac{1}{\bar{\chi}}\log\left[\text{sech}^2\left(\frac{\bar{\chi}}{2}\frac{v_{\max k}(x-x_k)}{\epsilon}\right)\right], & x \in \left\{x \in \mathbb{R}\,\big|\,|x-x_k| \leq O\left(\frac{\epsilon}{|\log \epsilon|}\right), \exists k \in \mathcal{I}\right\}, \\
V_0\left(\frac{x-x_k}{\epsilon}\right), & x \in \left\{x \in \mathbb{R}\,\big|\,O\left(\frac{\epsilon}{\log \epsilon}\right) \ll |x-x_k| \leq O(\epsilon), \exists k \in \mathcal{I}\right\}, \\
\frac{2\bar{\chi}\epsilon}{3}\sum_{k=1}^{N} v_{\max k}^3 G(x; x_k), & x \in \left\{x \in \mathbb{R}\,\big|\,O(\epsilon) \ll |x-x_k|, \forall k \in \mathcal{I}\right\}.
\end{cases}
\end{cases}
\tag{2.34}
$$

Here $\bar{\chi} = \chi/d_1$, $G(x; x_k)$ is defined by (2.25) and V_0 is given implicitly by (2.6). Moreover, the constants $v_{\max j}$, s_j and C_j are determined by (2.28). When $x_j = x_j^0$, as given in (2.29), the spikes are equally spaced and (u_q, v_q) becomes an approximation to the true N-spike equilibrium solution (u_e, v_e) to (1.2), in which

$$v_{\max j} = v_{\max 0}, \quad s_j = s_0, \quad C_j = C_0, \quad \text{for} \quad j = 1, \ldots, N.$$

In terms of the solution $v_{\max 0}$ to (2.32), s_0 and C_0 are given by (2.31) where a_g is defined in (2.30).

When $d_1 = d_{1Tm}$, for $m = 1, \ldots, N-1$, we show in Appendix A that for a steady-state solution where the spike locations x_j satisfy (2.29), the outer problem (2.22) has a non-unique solution that can be found using a generalized Green's function. Finally, to establish the range of d_1 where our steady-state analysis is valid we must also ensure that the outer solution w_o is positive on $|x| < 1$. This constraint, discussed in Appendix A, motivates the following key remark that introduces the notion of an *admissible set* $\mathcal{T}_e$ for d_1.

Remark 2.1. *For an N-spike steady-state solution, where the spikes are centered at (2.29), the range of d_1 where (2.22) has a unique and positive solution w_o is characterized by an admissible set $\mathcal{T}_e$, which we define by*

$$\mathcal{T}_e := \{\, d_1 \mid d_1 > d_{1pN} := \frac{4\mu\bar{u}}{N^2\pi^2}, \quad d_1 \neq d_{1Tm} := \frac{4\mu\bar{u}}{m^2\pi^2}, \quad m = 1, \ldots, N-1\}. \qquad (2.35)$$

For $d_1 > d_{1pN}$, we have $a_g > 0$ in (2.30), so that $s_0 > 0$. As $d_1 \to d_{1pN}$ from above, $a_g \to 0^+$ and $v_{\max 0} \to +\infty$. Moreover, when $d_1 \in \mathcal{T}_e$, the outer solution w_o on the interval of width $2/N$ between two adjacent spikes, which is asymptotically close to the uniform state $u = 0$, is linearly stable. At the positivity threshold $d_1 = d_{1pN}$, the trivial solution $u = 0$ on a domain of length $2/N$ undergoes a Turing instability and this threshold appears to trigger a nonlinear spike nucleation event for (1.2) between adjacent spikes (see Figure 7 in §4.2 below). In contrast, for an N-spike quasi-equilibrium pattern, the outer solution w_o between spikes is positive when

$$d_1 > \frac{L_{max}^2 \mu \bar{u}}{\pi^2}, \qquad L_{max} := \max\{|x_1 + 1|\,;\, |x_N - 1|\,;\, |x_{j+1} - x_j|,\ j = 1, \ldots, N\}. \tag{2.36}$$

2.3 Global Balancing and Comparison with Numerics

As an analytical confirmation of our asymptotic results, we show that they are consistent with a global balancing condition. By integrating (1.3) for u over $|x| \le 1$, we obtain that the global balance condition

$$\int_{-1}^{1} u(\bar{u} - u)\, dx = 0, \tag{2.37}$$

must hold. Defining $f(u) := u(\bar{u} - u)$, we decompose the left-hand side of (2.37) into the two terms

$$\int_{-1}^{1} u(\bar{u} - u)\, dx = \overbrace{\int_{-1}^{1} [f(u) - f(s_0)]\, dx}^{I_1} + \overbrace{\int_{-1}^{1} f(s_0)\, dx}^{I_2}. \tag{2.38}$$

Since the inner and outer regions both contribute to I_1, we decompose I_1 as $I_{11} + I_{12}$, where I_{11} and I_{12} represent the N inner integrals and the outer integral, respectively. For I_{11}, since $u \to s_0$ as $y \to \pm\infty$, we have $f(u) - f(s_0) \to 0$ as $y \to \pm\infty$. Therefore, by using (2.5) and since there are N identical inner regions, we identify that

$$I_{11} \sim 2N\epsilon \int_0^\infty [f(U_0) - f(s_0)]\, dy = 2N\epsilon \int_{s_0}^{v_{\max 0}} \frac{f(C_0 e^{\bar{\chi}\xi}) - f(s_0)}{\sqrt{-2K(\xi; C_0)}}\, d\xi, \tag{2.39}$$

where K is given by (2.4). However, to estimate (2.39) we can more simply use the fact that $U_0 \gg 1$ in each sub-inner region. In this way, by using (2.16), we obtain that

$$I_{11} \sim 2N\epsilon \int_0^\infty (\bar{u}U_0 - U_0^2)\, dy \sim 2N\bar{u}v_{\max 0}\epsilon - \frac{2}{3}N\bar{\chi}v_{\max 0}^3\epsilon. \tag{2.40}$$

Next, by using the outer solution (2.26), together with $\int_{-1}^{1} G(x; x_k^0)\, dx = 1/\bar{u}$, we estimate the outer integral as

$$\begin{aligned}
I_{12} &\sim \int_{-1}^{1} f(w_o)\, dx - \int_{-1}^{1} f(s_0)\, dx, \\
&= \frac{2}{3}\bar{\chi}\bar{u}v_{\max 0}^3\epsilon \sum_{k=1}^{N} \int_{-1}^{1} G(x; x_k^0)\, dx - \left(\frac{2\bar{\chi}\bar{u}}{3}v_{\max 0}^3\epsilon\right)^2 \int_{-1}^{1} \left[\sum_{k=1}^{N} G(x; x_k^0)\right]^2 dx - \int_{-1}^{1} f(s_0)\, dx, \\
&= \frac{2}{3}N\bar{\chi}v_{\max 0}^3\epsilon - \int_{-1}^{1} f(s_0)\, dx + O(\epsilon^2 v_{\max 0}^6).
\end{aligned} \tag{2.41}$$

We substitute (2.40) and (2.41) into (2.38) to find $\int_{-1}^{1} u(\bar{u} - u)\, dx = O(\epsilon v_{\max 0}) \ll 1$, and so the global balancing condition is satisfied to this order as $\epsilon \to 0$.

9

| d_2	$d_1 = \chi$	$\bar{u}$	$u_{\max}$(num)	$u_{\max}$(asy)	$v_{\max}$(num)	$v_{\max}$(asy)
0.02	1	2	3.8935	3.4633	2.6937	2.6318
0.004	1	2	5.2575	5.0329	3.1702	3.1727
0.002	1	2	5.9773	5.8239	3.3955	3.4129
0.02	10	2	3.8599	3.1702	2.6623	2.5180
0.004	10	2	5.0958	4.6664	3.1099	3.0550
0.002	10	2	5.7514	5.4210	3.3218	3.2927
0.02	1	3	5.9159	4.4409	3.3970	2.9802
0.004	1	3	7.3629	6.2531	3.7971	3.5364
0.002	1	3	8.1535	7.1617	4.0023	3.7846

Table 1: The asymptotic results for $u_{\max}$ and $v_{\max}$, obtained from (2.34), for various d_2, d_1 and $\bar{u}$ are compared with FlexPDE7 numerical results.

d_2	$d_1 = \chi$	$\bar{u}$	u_{bdry}(num)	u_{bdry}(asy)	v_{bdry}(num)	v_{bdry}(asy)
0.02	1	2	0.4799	0.5195	0.5047	0.5195
0.004	1	2	0.3744	0.3923	0.3734	0.3923
0.002	1	2	0.3340	0.3412	0.3336	0.3412
0.02	10	2	0.4295	0.3824	0.4567	0.3824
0.004	10	2	0.3166	0.3047	0.3166	0.3047
0.002	10	2	0.2790	0.2695	0.2790	0.2695
0.02	1	3	0.3350	0.5538	0.3537	0.5538
0.004	1	3	0.2878	0.3883	0.2867	0.3883
0.002	1	3	0.2627	0.3305	0.2622	0.3305

Table 2: The asymptotic results for u_{bdry} and v_{bdry}, obtained from (2.34), for various d_2, d_1 and $\bar{u}$ are compared with FlexPDE7 [14] numerical results.
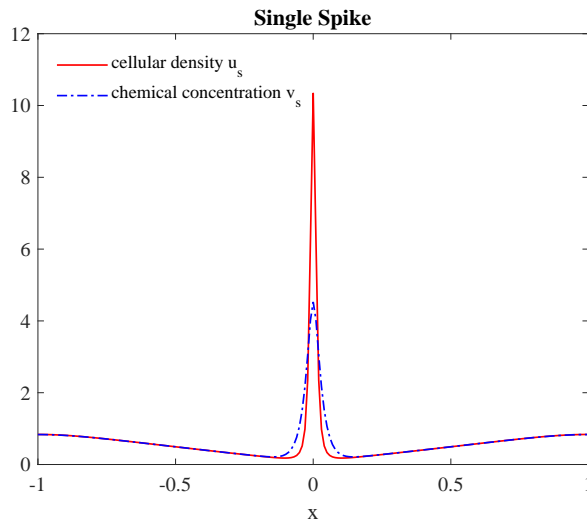
(a) a one-spike steady-state
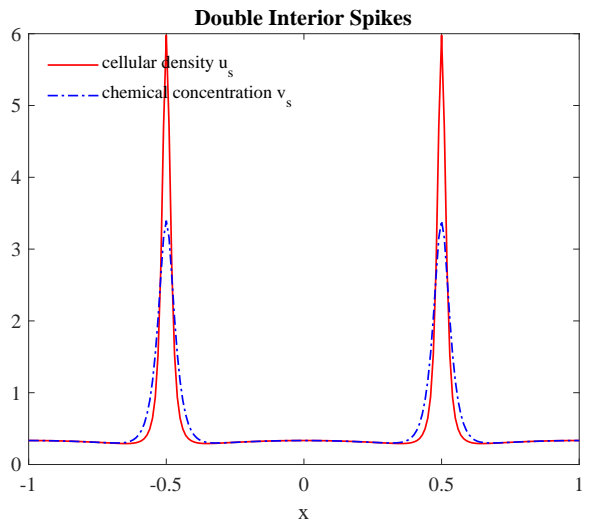
(b) a two-spike steady-state

Figure 1: *Numerically-computed one and two-spike steady-state solutions of (1.3) with $d_1 = \chi = 1$, $\bar{u} = 2$, $d_2 = 0.0005$ using FlexPDE7 [14].* The solid red curves are the cellular density u, while the dotted blue curves are the chemical concentration v. Observe that u and v increase in the outer region.

10

For a one-spike steady-state, we now compare our asymptotic results with corresponding full numerical results computed using FlexPDE7 [14]. For $\mu = 0.25$, in Table 1 we compare asymptotic and numerical results for the maximum values of u and v for both $\bar{u} = 2$ and for $\bar{u} = 3$. A similar comparison, but for the boundary values of u and v are shown in Table 2. We observe that the asymptotic results in (2.34) more closely approximate the numerical result when $\bar{u} = 2$ than when $\bar{u} = 3$. This improved agreement when $\bar{u} = 2$ is due to the fact that the $\sqrt{1 - 2w_o\bar{\chi}}$ term in (2.20) vanishes only when $\bar{u} = 2/\bar{\chi}$, and so the error does not include any $O(|\log \epsilon|^{-1})$ correction term as it does for the case when $\bar{u} = 3$. In Figure 1 we plot the numerically-computed one-spike and two-spike steady-state solutions computed using FlexPDE7 [14]. We observe that the half-profiles of u and v are not monotone decreasing and so their spatial behavior is rather different than for spike patterns of the classical KS model [52] without the logistic growth term.

2.4   Formulation of the Linear Stability Problem

To formulate the linear stability problem for the steady-state solution, denoted by (u_e, v_e), we introduce the following time-dependent perturbation (u, v) to (1.2):

$$u(x, t) = u_e(x) + e^{\lambda t}\phi(x), \qquad v(x, t) = v_e(x) + e^{\lambda t}\psi(x), \tag{2.42}$$

where $\phi \ll 1$ and $\psi \ll 1$. Upon substituting (2.42) into (1.2) and linearizing, we obtain the spectral problem

$$\frac{\tau\lambda}{d_1}\phi = \phi_{xx} - \bar{\chi}(u_e\psi_x)_x - \bar{\chi}(v_{ex}\phi)_x + \frac{\mu}{d_1}(\bar{u} - 2u_e)\phi, \quad -1 < x < 1; \quad \phi_x(\pm1) = 0, \tag{2.43a}$$

$$\lambda\psi = \epsilon^2\psi_{xx} - \psi + \phi, \quad -1 < x < 1; \quad \psi_x(\pm1) = 0. \tag{2.43b}$$

It is well known that linearized eigenvalue problems arising from the analysis of localized spike patterns of RD systems have two classes of eigenvalues (cf. [24]). The first type is referred to as the large eigenvalues since they are bounded away from zero as $\epsilon \to 0$. The second type are the small eigenvalues of order $o(1)$ as $\epsilon \to 0$.

In §3 and §4 we will analyze the large and small eigenvalues for (2.43), where the cellular diffusion rate d_1 is the main bifurcation parameter. Recall that $d_1 \in \mathcal{T}_e$ where the admissible set is defined in (2.35). Our main goal is to determine critical thresholds for $d_1 \in \mathcal{T}_e$, depending on N, that will provide the range of d_1 for which all large and small eigenvalues satisfy $\text{Re}(\lambda) < 0$. On this range, N-spike steady-states are linearly stable as $\epsilon \to 0$. Oscillatory instabilities in the amplitude of a one-spike steady-state are also shown to be possible as τ is increased from a Hopf bifurcation of the large eigenvalues.

3   Analysis of the Large Eigenvalues

This section is devoted to the study of large eigenvalues for an N-spike steady-state. These eigenvalues are bounded away from zero as $\epsilon \to 0$. To begin, we introduce local variables defined in the jth inner region by

$$y = \epsilon^{-1}(x - x_j), \qquad \Phi_j(y) := \phi(x_j + \epsilon y), \qquad \Psi_j(y) := \psi(x_j + \epsilon y), \tag{3.1}$$

and we expand

$$\Phi_j(y) = \Phi_{0j}(y) + \epsilon^2\Phi_{1j}(y) + \dots \quad \Psi_j(y) = \Psi_{0j}(y) + \epsilon^2\Psi_{1j}(y) + \dots, \quad \lambda \sim \lambda_0. \tag{3.2}$$

Since the spike profile (U_j, V_j) for the steady-state is the same for each j, as similar to (2.1) we expand

$$U_j(y) = U_0(y) + \epsilon^2U_1(y) + \dots \quad V_j(y) = V_0(y) + \epsilon^2V_1(y) + \dots. \tag{3.3}$$

11

Upon substituting (3.1)–(3.3) into (2.43), we obtain the following leading order problem on $-\infty < y < \infty$:

$$0 = \Phi_{0j}'' - \bar{\chi}(U_0\Psi_{0j}')' - \bar{\chi}(V_0'\Phi_{0j})' ; \qquad \Phi_{0j}'(0) = 0 , \tag{3.4a}$$

$$\lambda_0\Psi_{0j} = \Psi_{0j}'' - \Psi_{0j} + \Phi_{0j} ; \qquad \Psi_{0j}'(0) = 0 . \tag{3.4b}$$

Recalling that $U_0' = \bar{\chi}U_0V_0'$ from the core problem (2.2), it is convenient to define g_{0j} by

$$g_{0j} := \frac{\Phi_{0j}}{U_0} - \bar{\chi}\,\Psi_{0j} . \tag{3.5}$$

In terms of g_{0j}, the two problems in (3.4) are transformed on $-\infty < y < \infty$ to

$$\left(U_0 g_{0j}'\right)' = 0 , \quad g_{0j}'(0) = 0 ; \qquad \lambda_0\Psi_{0j} = \Psi_{0j}'' - \Psi_{0j} + \bar{\chi}U_0\Psi_{0j} + U_0 g_{0j} , \quad \Psi_{0j}'(0) = 0 . \tag{3.6}$$

Imposing that g_{0j} is bounded as $|y| \to \infty$, we obtain from the first equation of (3.6) that $g_{0j} = \tilde{C}_j$, where $\tilde{C}_j$ is to be determined. Then, the second equation in (3.6) becomes

$$\lambda_0\Psi_{0j} = \Psi_{0j}'' - \Psi_{0j} + \bar{\chi}U_0\Psi_{0j} + \tilde{C}_j U_0 , \quad -\infty < y < \infty ; \qquad \Psi_{0j}'(0) = 0 . \tag{3.7}$$

Before formulating the outer problem, we must determine the far-field behavior of the inner solution. In the outer region, we obtain from (2.43) that, for $\epsilon \ll 1$, $\phi \sim (\lambda_0 + 1)\psi$. As a result, we must have $\Phi_{0j} \sim (\lambda_0 + 1)\Psi_{0j}$ as $y \to \pm\infty$. By using this relation, together with $g_{0j} = \tilde{C}_j$ and $U_0 \sim s_0$ as $|y| \to \infty$, (3.5) yields that

$$\Phi_{0j} = \tilde{C}_j U_0 + \bar{\chi}U_0\Psi_{0j} \sim \tilde{C}_j s_0 + \bar{\chi}s_0\frac{\Phi_{0j}}{\lambda_0 + 1} ,$$

as $|y| \to \infty$. Since $s_0 \ll 1$, this expression provides the leading order far-field behavior

$$\Phi_{0j} \sim \tilde{C}_j s_j , \qquad \text{as} \quad |y| \to \infty . \tag{3.8}$$

Next, we construct the outer solution. Since $u_e = v_e = O(s_0) \ll 1$ in the outer region, (2.43a) yields that $\phi \sim \phi_o$, where

$$\frac{d_1}{\mu}\phi_{oxx} + \hat{u}\phi_o = 0 , \quad -1 < x < 1 , \quad x \neq x_j^0 , \qquad \text{where} \quad \hat{u} = \bar{u} - \frac{\tau\lambda_0}{\mu} . \tag{3.9}$$

From (3.8), one matching condition is $\phi_0(x_j^0) = \tilde{C}_j s_0$, while the other is obtained by deriving the appropriate jump condition for $[\phi_{ox}]_j := \phi_{ox}(x_j^{0+}) - \phi_{ox}(x_j^{0-})$. To derive this jump condition we write (2.43a) as

$$\frac{d_1}{\mu}\phi_{xx} + \hat{u}\phi = 2u_e\phi + \bar{\chi}(u_e\psi_x)_x + \bar{\chi}(v_{ex}\phi)_x . \tag{3.10}$$

We integrate (3.10) over an intermediate scale $x_j^0 - \sigma < x < x_j^0 + \sigma$ where $\epsilon \ll \sigma \ll 1$ and we pass to the limit $\sigma \to 0$, but with $\sigma/\epsilon \to \infty$. In terms of the inner coordinate y, where $u_e \sim U_0$ and $\phi \sim \Phi_{0j}$, and upon using the facts that $u_e = v_e = O(s_0) \ll 1$ at $x = x_j^0 \pm \sigma$, we obtain that the jump condition for the outer solution is

$$\frac{d_1}{\mu}[\phi_{ox}]_j \sim 2\epsilon \int_{-\infty}^{\infty} U_0\Phi_{0j}\,dy .$$

Then, by using $\Phi_{0j} \sim U_0\tilde{C}_j + \bar{\chi}U_0\Psi_{0j}$, as derived from (3.5) with $g_{0j} = \tilde{C}_j$, we conclude that

$$\frac{d_1}{\mu}[\phi_{ox}]_j \sim 2\epsilon \int_{-\infty}^{\infty} \left(U_0^2\tilde{C}_j + \bar{\chi}\Psi_{0j}U_0^2\right) dy . \tag{3.11}$$

In this way, we obtain the following multi-point boundary-value problem (BVP) for the outer solution ϕ_o:

$$\frac{d_1}{\mu}\phi_{oxx} + \hat{u}\phi_o = 0\,, \quad -1 < x < 1\,, \ x \neq x_j^0\,, \ j = 1,\ldots,N\,; \qquad \phi_{ox}(\pm 1) = 0\,, \tag{3.12a}$$

$$\frac{d_1}{\mu}[\phi_{ox}]_j = 2\epsilon \int_{-\infty}^{\infty} \left(U_0^2 \tilde{C}_j + \bar{\chi}\Psi_{0j}U_0^2 \right) dy\,, \quad \phi_0(x_j^0) = \tilde{C}_j s_0\,, \quad j = 1,\ldots,N\,. \tag{3.12b}$$

To solve (3.12), we introduce an eigenvalue-dependent Green's function $G_\lambda(x; x_k)$ defined by

$$\frac{d_1}{\mu}G_{\lambda xx} + \hat{u}G_\lambda = \delta(x - x_k)\,, \quad -1 < x < 1\,; \qquad G_{\lambda x}(\pm 1; x_k) = 0\,, \tag{3.13}$$

which exists provided that $d_1 \neq 4\mu\hat{u}/(m^2\pi^2)$ for $m = 1, 2, \ldots$. When these constraints are satisfied, the solution to (3.12) is represented as the superposition

$$\phi_o = 2\epsilon \sum_{k=1}^{N} \int_{-\infty}^{\infty} \left(\bar{\chi}U_0^2\Psi_{0k} + \tilde{C}_k U_0^2 \right) dy\, G_\lambda(x; x_k^0)\,. \tag{3.14}$$

By imposing $\phi_o(x_j^0) = s_0\tilde{C}_j$, and recalling from (2.30) that $s_0 = \epsilon a_g \int_{-\infty}^{\infty} U_0^2\, dy$, we obtain from (3.14) that

$$\tilde{C}_j = \frac{2}{a_g \int_{-\infty}^{\infty} U_0^2\, dy} \sum_{k=1}^{N} \left(\int_{-\infty}^{\infty} \bar{\chi}U_0^2\Psi_{0k}\, dy \right) G_\lambda\left(x_j^0; x_k^0\right) + \frac{2}{a_g} \sum_{k=1}^{N} \tilde{C}_k G_\lambda\left(x_j^0; x_k^0\right)\,, \tag{3.15}$$

where a_g was defined in (2.30). Then, by letting I be the $N \times N$ identity matrix, and introducing

$$\mathcal{G}_\lambda := \begin{pmatrix} G_\lambda(x_1^0; x_1^0) & \cdots & G_\lambda(x_1^0; x_N^0) \\ \vdots & \ddots & \ddots \\ G_\lambda(x_N^0; x_1^0) & \cdots & G_\lambda(x_N^0; x_N^0) \end{pmatrix}\,, \quad \tilde{C} := \begin{pmatrix} \tilde{C}_1 \\ \vdots \\ \tilde{C}_N \end{pmatrix}\,, \quad \mathbf{\Psi_0} := \begin{pmatrix} \Psi_{01} \\ \vdots \\ \Psi_{0N} \end{pmatrix}\,, \tag{3.16}$$

we can write the linear algebraic system (3.15) for $\tilde{C}_j$, with $j = 1,\ldots,N$, in matrix form as

$$\left(\frac{2}{a_g}\mathcal{G}_\lambda - I \right)\tilde{C} = \frac{2}{a_g}\mathcal{G}_\lambda \left(-\frac{\bar{\chi}}{\int_{-\infty}^{\infty} U_0^2\, dy} \int_{-\infty}^{\infty} U_0^2\mathbf{\Psi_0}\, dy \right)\,. \tag{3.17}$$

By combining (3.7) with (3.17), we obtain a vector nonlocal eigenvalue problem (NLEP) given by

$$\mathbf{\Psi_0''} - \mathbf{\Psi_0} + \bar{\chi}U_0\mathbf{\Psi_0} - \bar{\chi}U_0\frac{\int_{-\infty}^{\infty} U_0^2\mathcal{B}\mathbf{\Psi_0}\, dy}{\int_{-\infty}^{\infty} U_0^2\, dy} = \lambda_0\mathbf{\Psi_0}\,, \tag{3.18}$$

where, to leading order, we have $\mathbf{\Psi_0} \to 0$ as $|y| \to \infty$. Here $\mathcal{B}$ is the $N \times N$ matrix defined by

$$\mathcal{B} := \frac{2}{a_g}\left(\frac{2}{a_g}\mathcal{G}_\lambda - I \right)^{-1}\mathcal{G}_\lambda\,. \tag{3.19}$$

Next, we diagonalize the vector NLEP (3.18) by introducing the orthogonal eigenspace of $\mathcal{B}$ as

$$\mathcal{B}\mathbf{q}_j = \alpha_j\mathbf{q}_j\,, \qquad j = 1,\ldots,N\,. \tag{3.20}$$

13

Denoting Q as the matrix of eigenvectors $\mathbf{q}_j$ (as columns), we obtain $\mathcal{B} = Q \operatorname{diag}(\alpha_1, \ldots, \alpha_N)Q^{-1}$. By defining $\tilde{\Psi}_0 = Q^{-1}\Psi_0$, we obtain that (3.18) reduces to the following N-scalar NLEPs, where α is any eigenvalue of $\mathcal{B}$:

$$\Psi'' - \Psi + \bar{\chi}U_0\Psi - \alpha\bar{\chi}U_0\frac{\int_{-\infty}^{\infty} U_0^2\Psi\, dy}{\int_{-\infty}^{\infty} U_0^2\, dy} = \lambda_0\Psi, \qquad \Psi \to 0 \text{ as } |y| \to \infty. \tag{3.21}$$

Since $U_0 \gg \mathcal{O}(1)$ in the sub-inner region, we will transform (3.21) to the z-variable. Recall that in the jth sub-inner region, we have from Proposition 2.1 that

$$z = v_{\max 0}y, \qquad y = \epsilon^{-1}(x - x_j), \qquad U_0 \sim \frac{1}{2}\bar{\chi}v_{\max 0}^2 \operatorname{sech}^2\left(\frac{\bar{\chi}z}{2}\right). \tag{3.22}$$

By introducing the re-scaled coordinate $\bar{z} := \bar{\chi}z/2$, and defining

$$\bar{U}_0 := 2\operatorname{sech}^2(\bar{z}), \tag{3.23}$$

we readily derive from (3.21) that we must analyze, on $-\infty < \bar{z} < +\infty$, the approximating NLEP given by

$$\Psi_{\bar{z}\bar{z}} + \bar{U}_0\Psi - \alpha\bar{U}_0\frac{\int_{-\infty}^{\infty} \bar{U}_0^2\Psi\, d\bar{z}}{\int_{-\infty}^{\infty} \bar{U}_0^2\, d\bar{z}} = \frac{4}{\bar{\chi}^2v_{\max 0}^2}(\lambda_0 + 1)\Psi, \qquad \Psi \text{ bounded as } |\bar{z}| \to \infty. \tag{3.24}$$

3.1 Competition Instabilities: $\tau = 0$

From the NLEP (3.24), we now determine the conditions on $d_1 \in \mathcal{T}_e$, μ, $\bar{u}$ and N such that the N-spike equilibrium is linearly stable with respect to the large eigenvalues when $\tau = 0$. To do so, we must first determine explicit formulae for the eigenvalues of the matrix $\mathcal{B}$ in (3.19). Then, by analyzing the NLEP, we must calculate the critical threshold $\alpha_c > 0$ such that in the restricted subset for which $\lambda_0 \neq 0$, we can guarantee that when $\alpha < \alpha_c$ the principal eigenvalue of (3.24) has a positive real part, and that when $\alpha > \alpha_c$ it has a negative real part.

One can immediately conclude that when the minimum eigenvalue of matrix $\mathcal{B}$, labeled by α_{min}, satisfies $\alpha_{min} > \alpha_c$, the NLEP (3.24) with $\tau = 0$ has no eigenvalue with a positive real part in the subset for which $\lambda_0 \neq 0$. We will calculate the explicit range of parameter values $d_1 \in \mathcal{T}_e$, μ, $\bar{u}$ and N to ensure that the condition $\alpha_{min} > \alpha_c$ holds, which guarantees that the N-spike equilibrium is linearly stable with respect to the large eigenvalues when $\tau = 0$. Our results will be expressed in terms of a threshold value in the diffusivity d_1.

In Appendix B we show that when $d_1 \in \mathcal{T}_e$, the eigenvalues α_j of $\mathcal{B}$ when $\tau = 0$ are related to the eigenvalues σ_j of the Green's matrix $\mathcal{G}$ by

$$\alpha_j = \frac{2\sigma_j}{2\sigma_j - \sigma_1}, \qquad \text{for} \quad j = 1, \ldots, N, \tag{3.25}$$

where σ_j is defined in (B.8) upon setting $\tau = 0$. The minimum such eigenvalue is $\alpha_{min} = \alpha_N$.

Next, we focus on the computation of the critical threshold α_c. In fact, if we entirely follow the method in [56] to study (3.24), we readily obtain that $\alpha_c \sim 1$. However, the next order term in α_c is $\mathcal{O}(|\log \epsilon|^{-1})$ since it involves $v_{\max 0}$. This term is key for obtaining accurate predictions of the stability threshold when $\tau = 0$. To obtain this refined asymptotic formula of α_c, in Appendix C we transform the NLEP into an ODE that can be solved with the use of hypergeometric functions. We summarize our rigorous results in the following theorem:

Theorem 3.1. *Consider the following nonlocal eigenvalue problem (NLEP):*

$$\begin{cases} \Psi_{\bar{z}\bar{z}} + \bar{U}_0\Psi - \gamma_0\bar{U}_0\frac{\int_{-\infty}^{\infty} \bar{U}_0^2\Psi\, d\bar{z}}{\int_{-\infty}^{\infty} \bar{U}_0^2\, d\bar{z}} = \frac{4}{\bar{\chi}^2v_{\max 0}^2}(\lambda_0 + 1)\Psi, & -\infty < z < +\infty, \\ \Psi \text{ bounded as } |z| \to \infty. \end{cases} \tag{3.26}$$

Here $\gamma_0 \geq 0$ and $\bar{U}_0$ is given in (3.23). Let $\lambda_0 \neq 0$ be the eigenvalue of (3.26) with the largest real part. Then for $v_{\max 0} \gg 1$, we have $Re(\lambda_0) > 0$ when $\gamma_0 < \gamma_c := 1 - \frac{3}{2\bar{\chi}v_{\max 0}}$. Alternatively, we have $Re(\lambda_0) < 0$ when $\gamma_0 > \gamma_c$.

Proof. The proof of Theorem 3.1 is given in Appendix C. □

We observe from Theorem 3.1 that when $v_{\max 0}$ is sufficiently large, we have $\gamma_c \sim 1$, However, the correction term is needed to obtain an improved result. Since the minimum eigenvalue of $\mathcal{B}$ in (3.25) occurs when $j = N$, we use Theorem 3.1 to conclude for $\tau = 0$ and $d_1 \in \mathcal{T}_e$, that $\mathrm{Re}(\lambda_0) = 0$ when

$$\frac{2\sigma_N}{2\sigma_N - \sigma_1} = 1 - \frac{3}{2\bar{\chi}v_{\max 0}}, \tag{3.27}$$

where σ_1 and σ_N are given in (B.8) when $\tau = 0$. This yields that

$$\frac{\sigma_N}{\sigma_1} = \frac{e/(2f) + 1}{e/(2f) - \cos(\pi/N)} = \frac{1}{2} - \frac{\bar{\chi}v_{\max 0}}{3}, \tag{3.28}$$

where $e/(2f) = -\cos(2\theta/N)$ with $\theta = \sqrt{\frac{\mu\bar{u}}{d_1}}$ can be calculated from (B.6). By isolating $\cos(2\theta/N)$, we get

$$\cos\left(\frac{2\theta}{N}\right) = \frac{1 - a\cos(\pi/N)}{a + 1}, \quad \text{where} \quad a := \frac{\bar{\chi}v_{\max 0}}{3} - \frac{1}{2}.$$

Upon solving this expression for d_1, we can obtain a critical threshold in terms of μ, $\bar{u}$, $\bar{\chi}$ and N. In this way, owing to Theorem 3.1, we summarize our results for the case $\tau = 0$ as follows:

Proposition 3.1. *Assume that $d_1 \in \mathcal{T}_e$ and $\tau = 0$. Let $\lambda_0 \neq 0$ be the eigenvalue of (3.24) with the largest real part when $\tau = 0$. Then, for $N = 1, 2, \ldots$, $\mathrm{Re}(\lambda_0) < 0$ when*

$$d_1 < d_{1cN} := \frac{4\mu\bar{u}}{N^2(\arccos(\eta_N))^2}, \quad \text{where} \quad \eta_N := \frac{1 - a\cos(\pi/N)}{a + 1}, \quad a := \frac{\bar{\chi}v_{\max 0}}{3} - \frac{1}{2}. \tag{3.29}$$

Here $v_{\max 0}$ is determined by (2.32). Alternatively, when $d_1 > d_{1cN}$, we have $\mathrm{Re}(\lambda_0) > 0$. Since $d_{1c1} = \infty$ when $N = 1$, we conclude that a single interior spike is always linearly stable with respect to the large eigenvalues for any $d_1 = O(1)$ when $\tau = 0$.

Proposition 3.1 provides the stability criterion for an N-spike equilibrium with respect to the large eigenvalues when $\tau = 0$. To relate d_{1cN} to the thresholds d_{1pN} and d_{1Tm} of the admissible set $\mathcal{T}_e$, as defined in (2.35), we observe from (3.29) that since $v_{\max 0} \gg 1$, we have $\eta_N > 0$ for $N = 2$, and $\eta_N < 0$ for $N \geq 3$. Therefore, $0 < \arccos(\eta_2) < \pi/2$, while $\pi/2 < \arccos(\eta_N) < \pi$ for any $N \geq 3$. As a result, for $\epsilon \to 0$, we conclude that

$$d_{1p2} < d_{1T1} < d_{1c2}, \quad \text{for } N = 2; \qquad d_{1pN} < d_{1cN} < d_{1Tm}, \quad \text{for } N \geq 3 \text{ and } m \leq N/2. \tag{3.30}$$

However, since $v_{\max 0}$ depends weakly on d_1, the threshold d_{1cN} in (3.29) is a weakly nonlinear implicit expression that must be solved numerically. To illustrate our results, we chose $d_2 = 0.0004 = \epsilon^2$, $\bar{u} = 2$, $\mu = 1$ and $\bar{\chi} = 1$, and we calculate the thresholds d_{1cN} for $N = 2, 3, 4$ as

$$d_{1c2} \approx 2.36 \ (N = 2); \qquad d_{1c3} \approx 0.74 \ (N = 3); \qquad d_{1c4} \approx 0.39 \ (N = 4). \tag{3.31}$$

When $N \gg 1$, d_{1cN} has the limiting behavior $d_{1cN} \sim 4\mu\bar{u}N^{-2}/[\arccos(\eta_\infty)]^2$ where $\eta_\infty := (1 - a)/(1 + a)$. This limiting result is valid only for $N \ll 1/\epsilon$, owing to the fact that steady-state analysis in §2 requires that $d_1/\epsilon^2 \gg 1$.

In summary, our analysis has shown that a sufficiently large cellular diffusion rate d_1 will trigger a competition instability for an N-spike steady-state solution when $\tau = 0$, To partially confirm our theory, in Figure 2 we show full numerical results computed from (1.2) showing a competition instability for a two-spike quasi steady-state solution as d_1 slowly increases in time. This initial instability is found to lead to a nonlinear process that annihilates one of the two spikes. This observation suggests that competition instabilities for the KS model (1.2) are in fact subcritical, as is well-known for the 1D Gierer-Meinhardt RD model [29].
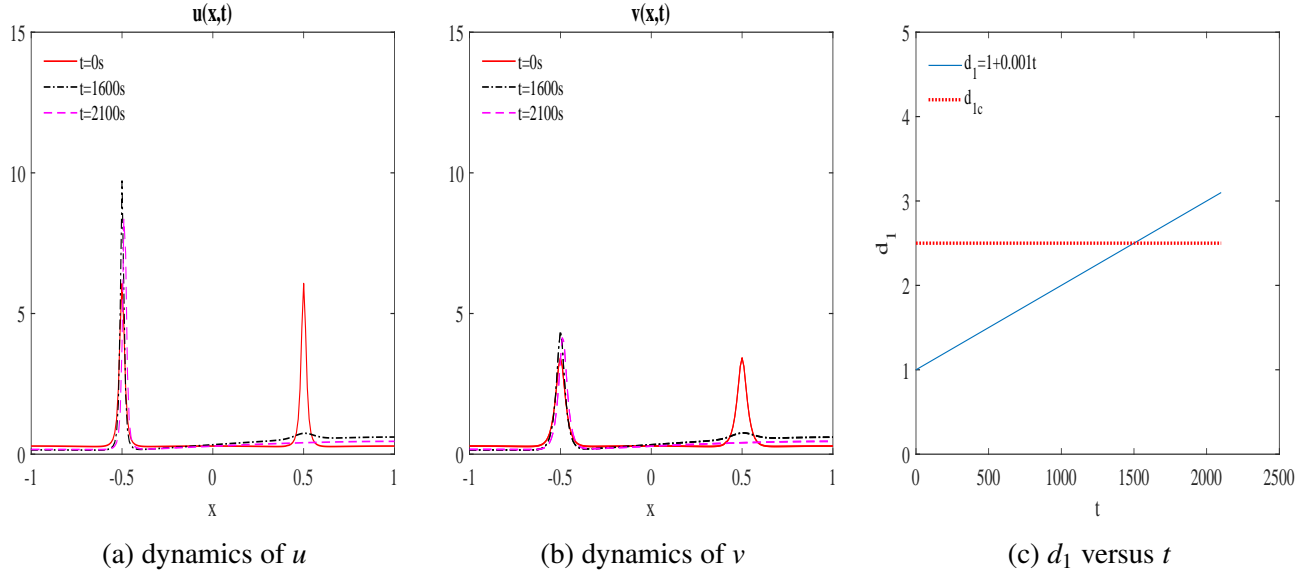
(a) dynamics of u (b) dynamics of v (c) d_1 versus t

Figure 2: *Full PDE simulations of (1.2) using FlexPDE7 [14] illustrating a competition instability of a two-spike steady-state when d_1 is increased slowly in time t. Left and Middle: snapshots of (u, v) at three times, showing the collapse of a spike, with $d_1 = \chi = 1$, $\bar{u} = 2$, $d_2 = 0.0004$ and $\mu = 1$; Right: the cellular diffusion d_1 versus time.* In subfigure (c), the dotted line d_{1c2} represents the stability threshold of large eigenvalues computed numerically and the solid line is the slow increasing ramp for d_1 versus t. Observe that $d_{1c2} \approx 2.5$ agrees rather well with the analytical results in (3.31) and (3.40).

3.1.1 Invertibility of the Jacobian Matrix for s_j

We now provide an alternative approach to estimate the competition instability threshold when $\tau = 0$. We will show that this threshold closely approximates a bifurcation point associated with the linearization of the coupled nonlinear algebraic system (2.27) that was derived in our analysis of quasi steady-state patterns.

We begin by writing (2.27) in the vector form $\boldsymbol{F}(s_1, \ldots, s_N) = 0$ with $\boldsymbol{F} = (F_1, \ldots, F_N)^T$. By differentiating F_i with respect to s_j we obtain, in terms of the Kronecker symbol δ_{ij}, that

$$\frac{\partial F_i}{\partial s_j}(s_1, \ldots, s_N) = \delta_{ij} - 2\epsilon \bar{\chi} v_{\max j}^2 v'_{\max j} G(x_i; x_j), \tag{3.32}$$

where from (D.4) of Appendix D we have that

$$v'_{\max j} := \frac{dv_{\max j}}{ds_j} \sim -\frac{\zeta_{\max j}}{\bar{\chi} s_j}, \qquad \zeta_{\max j} := \left(1 - \frac{2}{\bar{\chi} v_{\max j}}\right)^{-1}. \tag{3.33}$$

We now evaluate the Jacobian matrix $\mathcal{J} = \left(\frac{\partial F_i}{\partial s_j}\right)_{N \times N}$ at the equilibrium solution where $x_j = x_j^0$, $s_j = s_0$, $v_{\max j} = v_{\max 0}$, and $\zeta_{\max j} = \zeta_0 = (1 - 2/(\bar{\chi} v_{\max 0}))^{-1}$ for $j = 1, \ldots, N$ with x_j^0 and s_0 defined by (2.29) and (2.30). We seek to determine the largest value of d_1 in the admissible set $\mathcal{T}_e$ of (2.35) where the Jacobian matrix is not invertible. Upon substituting (3.33) into (3.32), and evaluating the resulting expression at the equilibrium solution, where we use $s_0 = 2\epsilon \bar{\chi} a_g v_{\max 0}^3 / 3$ from (2.30), we obtain that

$$\left.\frac{\partial F_i}{\partial s_j}(s_1, \ldots, s_N)\right|_{s_1 = \cdots = s_N = s_0} \sim \delta_{ij} - \left(\frac{3}{2 - \bar{\chi} v_{\max 0}}\right) \frac{G(x_i^0; x_j^0)}{a_g}. \tag{3.34}$$

In this way, the Jacobian matrix $\mathcal{J}$ at the equilibrium solution is given for $\epsilon \to 0$ by

$$\mathcal{J} \sim I - \left(\frac{3}{2 - \bar{\chi} v_{\max 0}}\right) \frac{\mathcal{G}}{a_g}. \tag{3.35}$$

16

Here $\mathcal{G}$ is the Green's matrix $\left(G(x_i^0; x_j^0)\right)_{N \times N}$ for $\tau = 0$, which is evaluated at the equilibrium spike locations.

When $d_1 \in \mathcal{T}_e$, it follows from (3.35) that the eigenvalues $\lambda_{\mathcal{J},j}$ of the Jacobian $\mathcal{J}$ are related to the eigenvalues σ_j of the Green's matrix $\mathcal{G}$, obtained by setting $\tau = 0$ in (B.8) of Appendix B, by

$$\lambda_{\mathcal{J},j} = 1 - \frac{3}{(2 - \bar{\chi} v_{\max 0})} \frac{\sigma_j}{\sigma_1}, \tag{3.36}$$

where we used $\sigma_1 = a_g$. The Jacobian matrix is singular when $\lambda_{\mathcal{J},j} = 0$ in (3.36), which yields the condition

$$\frac{\sigma_j}{\sigma_1} \sim \frac{2}{3} - \frac{\bar{\chi} v_{\max 0}}{3}. \tag{3.37}$$

The largest value of d_1 where the Jacobian is singular is obtained by setting $j = N$. By using (3.28) this yields

$$\frac{\sigma_N}{\sigma_1} = \frac{\cos(2\theta/N) - 1}{\cos(2\theta/N) + \cos(\pi/N)} \sim \frac{2}{3} - \frac{\bar{\chi} v_{\max 0}}{3}, \tag{3.38}$$

where $\theta = \sqrt{\mu \bar{u}/d_1}$. Upon solving this expression for d_1, we obtain the following critical threshold for d_1:

$$d_{1cN}^\star := \frac{4\mu\bar{u}}{N^2 \left[\arccos\left(\frac{1 - a_1 \cos(\pi/N)}{a_1 + 1}\right)\right]^2}, \quad N = 1, 2, \ldots, \quad \text{where} \quad a_1 := \frac{\bar{\chi} v_{\max 0}}{3} - \frac{2}{3}. \tag{3.39}$$

We remark that the leading order term for a_1 given in (3.39) is $\bar{\chi} v_{\max 0}/3$, which agrees precisely with the leading term of a defined in (3.29), as derived by analyzing the zero-eigenvalue crossing condition of the NLEP. This observation partially confirms our asymptotic results given in Proposition 3.1. For the parameter values $d_2 = 0.0004$, $\bar{u} = 2$, $\mu = 1$ and $\bar{\chi} = 1$, we use (3.39) to calculate $d_{1c1}^\star = \infty$ and

$$d_{1c2}^\star \approx 2.91 \ (N = 2); \qquad d_{1c3}^\star \approx 0.97 \ (N = 3); \qquad d_{1c4}^\star \approx 0.54 \ (N = 4). \tag{3.40}$$

3.2 Hopf Bifurcations: $\tau \neq 0$

In this subsection we focus on the possibility of an oscillatory instability in the amplitude of a single steady-state spike for (1.2) on the range $d_1 \in \mathcal{T}_e$ where $\tau \neq 0$. In particular, for the linearization of a one-spike steady-state solution we will show that there can be a Hopf bifurcation leading to an oscillatory instability in the spike amplitude. More specifically, by analyzing (3.24) we will compute the threshold $\tau = \tau_c > 0$ such that the principal eigenvalue of (3.24) has the form $\lambda_0 = i\lambda_H$ where $i := \sqrt{-1}$ and $\lambda_H > 0$ is real.

As shown in (C.7) of Appendix C, if we define $w = \sqrt{\bar{U}_0}$ we can transform (3.24) to

$$\Psi_{0\bar{z}\bar{z}} + w^2 \Psi_0 - \kappa \frac{\int_{-\infty}^{\infty} w^2 \Psi_0 \, d\bar{z}}{\int_{-\infty}^{\infty} w^4 \, d\bar{z}} w^2 = \Lambda \Psi_0; \qquad \kappa := \frac{\alpha(4 - \Lambda)}{2 + \alpha}, \qquad \Lambda := 4 \frac{(\lambda_0 + 1)}{\bar{\chi}^2 v_{\max 0}^2}. \tag{3.41}$$

By using the results in Appendix B for α, we obtain that the NLEP multiplier κ is

$$\kappa = 4\left(1 - \frac{\Lambda}{4}\right)\left(3 - \sqrt{1 - \frac{\tau\lambda_0}{\mu\bar{u}}} \frac{\tan\left(\theta\sqrt{1 - \frac{\tau\lambda_0}{\mu\bar{u}}}\right)}{\tan\theta}\right)^{-1}, \qquad \text{where} \qquad \theta = \sqrt{\frac{\mu\bar{u}}{d_1}},$$

and where we have taken the principal branch of $\sqrt{1 - \frac{\tau\lambda_0}{\mu\bar{u}}}$. Next, we transform (3.41) to an algebraic equation in terms of hypergeometric functions. By using (C.34) of Appendix C, we choose $\delta_1 = \sqrt{\Lambda}/2$ to get

$$
\begin{aligned}
\frac{4}{\kappa} =& (1 - \delta_1^2)^{-1} {}_4F_3(1, \frac{1}{2}, 2, 2; 2 - \delta_1, 2 + \delta_1, \frac{5}{2}; 1) \\
&+ \frac{A}{3}\left(\frac{3}{2}\right)^{1+\delta_1} \frac{\Gamma(1 + \delta_1)\Gamma(\frac{1}{2})}{\Gamma(\frac{3}{2} + \delta_1)} {}_3F_2(1 + \delta_1, \delta_1 - \frac{1}{2}, 1 + \delta_1; 2\delta_1 + 1, \frac{3}{2} + \delta_1; 1),
\end{aligned}
\tag{3.42}
$$

where $\sqrt{\Lambda}$ is taken as the principal branch. In terms of $\tau = \tau_c$ and $\lambda_0 = i\lambda_H$, (3.42) is a single complex algebraic equation that can be separated into real and imaginary parts to obtain a coupled algebraic system for τ_c and λ_H.

The results obtained by solving this system numerically are shown in Figure 3, where we set $\mu = 1$, $\bar{u} = 2$, $\bar{\chi} = 1$, and $d_2 = 0.0004$. Figure 3a shows that the spike will develop amplitude oscillations when τ increases passes through τ_c. The threshold τ_c is seen to be a decreasing function of the cellular diffusivity d_1. Figure 3b shows numerically that the transversality condition of the Hopf bifurcation is satisfied, as unstable eigenvalues enter $\text{Re}(\lambda_0) > 0$ when τ increases above τ_c.
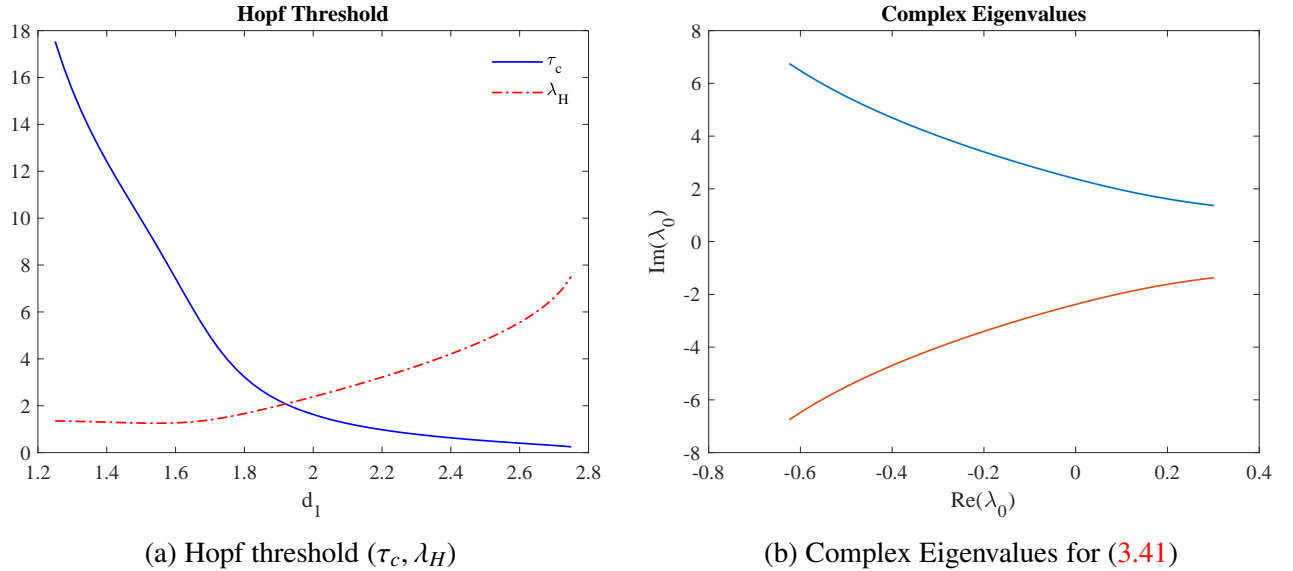

(a) Hopf threshold (τ_c, λ_H) (b) Complex Eigenvalues for (3.41)

Figure 3: *The Hopf bifurcation threshold (τ_c, λ_H) (left panel) and the path of the complex spectra of (3.41) as τ is increased above τ_c for the linearization of a single steady-state spike, as obtained by solving (3.42) numerically.* In (a), the solid blue line represents the Hopf threshold $\tau_c(d_1)$ and the dotted red line denotes the critical eigenvalues $i\lambda_H$. The left panel (a) shows that the Hopf threshold τ_c decreases as the cellular diffusivity d_1 increases. The right panel (b) shows the path of the complex spectra for $d_1 = 2$ as τ increases. We observe that for $\tau > \tau_c$ unstable eigenvalues enter $\text{Re}(\lambda_0) > 0$.

4 Analysis of the Small Eigenvalues

In §3 we analyzed the linear stability of an N-spike steady-state solution with respect to the large eigenvalues of the linearization. In this section, for $d_1 \in \mathcal{T}_e$, we will formulate a matrix problem for the small eigenvalues of order $O(\epsilon^3 v_{\max 0}^3)$ in the linearization, and we will calculate an explicit asymptotic formula for them.

To begin the analysis, we differentiate (1.3) for v to obtain

$$
L_\epsilon v_{ex} = -u_{ex}, \qquad \text{where} \quad L_\epsilon \psi := \epsilon^2 \psi_{xx} - \psi.
\tag{4.1}
$$

Our first goal is to obtain an approximate expression for (4.1) in terms of the inner coordinate near a spike. Focusing on the jth spike, we find from Proposition 2.1 that the composite expansion of the quasi-equilibrium solution u_q can be written near the jth spike as

$$u_q \sim s_j(x) e^{\bar{\chi}(V_0(y) - s_0)}, \quad y = \epsilon^{-1}(x - x_j), \quad j = 1, \dots, N.$$

Here $V_0(y)$ is the inner solution near the jth spike and

$$s_j(x) := \frac{2\bar{\chi}}{3} \epsilon \sum_{k=1}^{N} v_{\max k}^3(x) G(x; x_k), \quad j = 1, \dots, N. \tag{4.2}$$

Since $s_0 = o(1)$, we find $e^{-\bar{\chi} s_0} \sim 1$, so that

$$u_q \sim s_j(x) e^{\bar{\chi} V_0(y)}, \quad y = \epsilon^{-1}(x - x_j), \quad j = 1, \dots, N.$$

We differentiate u_q with respect to x to get for the jth spike that

$$u_{qx} \sim s_{jx}(x) e^{\bar{\chi} V_0} + \epsilon^{-1} \bar{\chi} s_j(x) e^{\bar{\chi} V_0} V_0', \tag{4.3}$$

and by differentiating (4.2) we obtain that

$$s_{jx}(x) = 2\bar{\chi} \epsilon \sum_{k=1}^{N} v_{\max k}^2(x) \left[\partial_x v_{\max k}(x) \right] G(x; x_k) + \frac{2\bar{\chi}}{3} \epsilon \sum_{k=1}^{N} v_{\max k}^3(x) G_x(x; x_k). \tag{4.4}$$

Noting from (D.5) of Appendix D that we can approximate

$$\partial_x v_{\max k}(x) \sim -\frac{\zeta_{\max k}}{\bar{\chi} s_k} \partial_x s_k(x), \qquad \zeta_{\max k} = \left(1 - \frac{2}{\bar{\chi} v_{\max k}}\right)^{-1}, \quad k = 1, \dots, N,$$

we obtain that (4.4) becomes

$$s_{jx}(x) \sim -2\epsilon \sum_{k=1}^{N} v_{\max k}^2(x) \zeta_{\max k} \frac{s_{kx}}{s_k} G(x; x_k) + \frac{2\bar{\chi}}{3} \epsilon \sum_{k=1}^{N} v_{\max k}^3(x) G_x(x; x_k).$$

At the steady-state, for which $x_j = x_j^0$, for $j = 1, \dots, N$, we have $v_{\max k}(x) = v_{\max}^0(x)$, $s_k(x) = s^0(x)$, and $\zeta_0 = \zeta_{\max k}$. Therefore, for the jth spike evaluated at the steady-state we have

$$s_x^0(x)\big|_{x_i = x_j^0} \sim \overbrace{-\frac{2s_x^0(x)}{s^0(x)} \epsilon [\zeta_0 (v_{\max}^0)^2(x)] \sum_{k=1}^{N} G(x_j^0; x_k^0)}^{I_1} + \overbrace{\frac{2\bar{\chi}}{3} \epsilon [(v_{\max}^0)^3(x)] \sum_{k=1}^{N} G_x(x_j^0; x_k^0)}^{I_2}. \tag{4.5}$$

Next, since $y = \epsilon^{-1}(x - x_j^0)$, we find from $S^0(y) := s^0(x_j^0 + \epsilon y)$ and $V_{\max}^0(y) := v_{\max}^0(x_j^0 + \epsilon y)$, where S^0 (resp. $V_{\max}^0$) is s^0 (resp. $v_{\max}^0$), that in terms of the y-variable

$$\partial_y S^0(y)\big|_{x_j = x_j^0} \sim \overbrace{-\frac{2\partial_y S^0(y)}{S^0(y)} \epsilon [\zeta_0 (V_{\max}^0)^2(y)] \sum_{k=1}^{N} G(\epsilon y + x_j^0; x_k^0)}^{I_1} + \overbrace{\frac{2\bar{\chi}}{3} \epsilon^2 [(V_{\max}^0)^3(y)] \sum_{k=1}^{N} G_x(\epsilon y + x_j^0; x_k^0)}^{I_2},$$

where for G we have $G_x(x; x_k^0) = G_x(\epsilon y + x_j^0; x_k^0)$. Then, at $x = x_j^0$, for $j = 1, \ldots, N$, we have $v_{\max}^0(x_j^0) = v_{\max 0}$ and $s^0(x_j^0) = s_0$. In this way, (4.5) becomes

$$s_x^0(x_j^0) = \overbrace{-\frac{2s_x^0(x_j^0)}{s_0}\epsilon\zeta_0 v_{\max 0}^2 \sum_{k=1}^{N} G(x_j^0; x_k^0)}^{II_1} + \overbrace{\frac{2\bar{\chi}}{3}\epsilon v_{\max 0}^3 \sum_{k=1}^{N} G_x(x_j^0; x_k^0)}^{II_2},$$

where we identify that $II_2 = u_{ox}(x_j^0)$ with $u_o(x)$ being the outer solution constructed previously. In the y-variable, we find as $|y| \to \infty$, that

$$\partial_y S^0 \to \overbrace{-\frac{2\partial_y S^0}{s_0}\epsilon\zeta_0 v_{\max 0}^2 \sum_{k=1}^{N} G(x_j^0; x_k^0)}^{II_1} + \overbrace{\frac{2\bar{\chi}}{3}\epsilon^2 v_{\max 0}^3 \sum_{k=1}^{N} G_x(x_j^0; x_k^0)}^{II_2}. \tag{4.6}$$

According to (4.3), we set $x_j = x_j^0$ to conclude for the jth spike region $x \in (x_j^0 - \epsilon, x_j^0 + \epsilon)$ that u_e satisfies

$$u_{ex} \sim s_x^0(x)e^{\bar{\chi} V_0} + \epsilon^{-1}\bar{\chi} s^0(x)e^{\bar{\chi} V_0} V_0',$$

where $V_0' = \partial_y V_0$. Finally, we use $y = \epsilon^{-1}(x - x_j^0)$ and transform u_{ex} to the y-variable to get

$$\partial_y U \sim \partial_y S^0(y)e^{\bar{\chi} V_0} + \bar{\chi} S^0(y)e^{\bar{\chi} V_0}\partial_y V_0,$$

where $U_j(y) = u_e(x_j^0 + \epsilon y)$. It follows from (4.1) that for x near x_j

$$L_\epsilon V_j' \sim -\partial_y S^0(y)e^{\bar{\chi} V_0} - \bar{\chi} S^0(y)e^{\bar{\chi} V_0}\partial_y V_0. \tag{4.7}$$

Next, we investigate the linearized eigenvalue problem (2.43). To obtain the jth inner solution, we expand

$$\Phi_j(y) = c_j\Phi_{0j} + \epsilon^2 c_j\Phi_{1j} + \ldots, \qquad \Psi_j(y) = c_j V_j' + \epsilon^2 c_j\Psi_{1j} + \ldots, \tag{4.8}$$

where $y = \epsilon^{-1}(x - x_j)$. Similarly as in §3, we substitute (4.8) into (2.43) to get

$$\Phi_{0j} = \bar{\chi} U_j V_j'. \tag{4.9}$$

Moreover, by using the fact that $\lambda = o(1)$, we conclude from (4.7) and (4.9) that the $\bar{\chi} U_j V_j'$ term in the ψ-equation (2.43b) is cancelled but the term $-\partial_y S^0(y)e^{\bar{\chi} V_0}$ remains. To eliminate this term, we need to formulate the matching condition between the inner and outer solutions.

Defining the outer solution by ϕ_o, we now derive the appropriate jump conditions across the jth spike for ϕ_0. To begin with, we observe that $\partial_y S(y)e^{\bar{\chi} V_0} \sim \partial_y S(y)$ for $|y|$ large. Moreover, since II_1 defined in (4.6) is expressed in terms of the Green's function G, we have that ϕ_o satisfies the following jump condition across x_j:

$$\left[\frac{d_1}{\mu}\phi_{ox}\right]_j = -\frac{2\epsilon\zeta_0 v_{\max 0}^2}{s_0}\langle\phi_o\rangle_j, \quad j = 1, \ldots, N, \tag{4.10}$$

where $\langle f\rangle_j$ and $[f]_j$ are defined as $\langle f\rangle_j := [f(x_j^+) + f(x_j^-)]/2$ and $[f]_j := f(x_j^+) - f(x_j^-)$, respectively. The coefficient in (4.10) can be simplified by eliminating s_0 by using (2.31). In addition, we find as $\epsilon \to 0$ that

$$2U_0 c_j\Phi_{0j} \sim \frac{2\bar{\chi} c_j}{3}\epsilon^2 v_{\max j}^3 \delta'(x - x_j). \tag{4.11}$$

20

Upon defining $\phi_o := \epsilon^2 \bar{\phi}_o$, and dropping the overbar notation, we combine (4.10) and (4.11) to obtain the following leading order outer problem for ϕ_o with jump conditions across the jth spike:

$$\frac{d_1}{\mu}\phi_{oxx} + \bar{u}\phi_o \sim \frac{2\bar{\chi}}{3}v_{\text{max}\,0}^3 \sum_{j=1}^{N} c_j \delta'(x - x_j) - \frac{3\zeta_0}{\bar{\chi}a_g v_{\text{max}\,0}} \sum_{j=1}^{N} \langle\phi_o\rangle_j \delta(x - x_j). \tag{4.12}$$

Our next aim is to establish the solvability condition that provides the matrix eigenvalue problem for the small eigenvalues. To do so, we substitute (4.8) into (2.43b) and multiply it by V_j'. Upon integrating the resulting expression over $-1 < x < 1$, we drop some asymptotically negligible terms to get

$$\sum_{i=1}^{N}\left(c_j L_\epsilon V_i', V_j'\right) + \epsilon^2 \sum_{i=1}^{N}\left(c_i L_\epsilon \Psi_{1i}, V_j'\right) + \sum_{i=1}^{N}\left(c_i \Phi_{0i}, V_j'\right) + \epsilon^2\left(\bar{\phi}_o, V_j'\right) + \epsilon^2 \sum_{i=1}^{N}\left(c_i \Phi_{1i}, V_j'\right) \sim \lambda \sum_{i=1}^{N}\left(c_i V_i', V_j'\right), \tag{4.13}$$

for each $j = 1, \ldots, N$. Here the inner product (f, g) is defined as $(f, g) := \int_{-1}^{1} fg\, dx$. Since V_j decays exponentially as $|y| \to \infty$, we collect the dominant terms to simplify (4.13) as

$$c_j\left(V_j', L_\epsilon V_j' + \Phi_{0j}\right) + \epsilon^2 c_j\left(V_j', L_\epsilon \Psi_{1j} + \Phi_{1j}\right) + \epsilon^2\left(\phi_o, V_j'\right) \sim \lambda c_j\left(V_j', V_j'\right), \quad j = 1, \ldots, N. \tag{4.14}$$

Noting that L_ϵ is self-adjoint, we integrate by parts on the second term of (4.14). Expressing the integrals in terms of $y = \epsilon^{-1}(x - x_j)$ we get in terms of $u_o = u_o(x_j + \epsilon y)$ and $\phi_o = \phi_o(x_j + \epsilon y)$ that

$$-\epsilon^2 c_j \int_{-\infty}^{\infty} V_j' u_{ox}\, dy + \epsilon^3 \int_{-\infty}^{\infty} \phi_o V_j'\, dy \sim \lambda c_j \epsilon \int_{-\infty}^{\infty}\left(V_j'\right)^2 dy, \quad j = 1, \ldots, N. \tag{4.15}$$

Next, we analyze the left-hand side of (4.15) by expanding u_o and ϕ_o in one-sided Taylor series. In this way, the left-hand side of (4.15) becomes

$$-\epsilon^2 c_j \int_{-\infty}^{\infty} V_j' u_{ox}\, dy + \epsilon^3 \int_{-\infty}^{\infty} \phi_o V_j'\, dy = \epsilon^4 \langle\phi_{ox}\rangle_j \int_{-\infty}^{\infty} y V_j'\, dy - \epsilon^3 \langle u_{oxx}\rangle c_j \int_{-\infty}^{\infty} y V_j'\, dy. \tag{4.16}$$

By using $\langle u_{oxx}\rangle_j = -\frac{\bar{u}\mu}{d_1}\langle u_o\rangle_j$, we further simplify (4.16) as

$$-\epsilon^2 c_j \int_{-\infty}^{\infty} V_j' u_{ox}\, dy + \epsilon^3 \int_{-\infty}^{\infty} \phi_o V_j'\, dy = \epsilon^4 \langle\phi_{ox}\rangle_j \int_{-\infty}^{\infty} y V_j'\, dy + \epsilon^3 \frac{s_0 c_j \bar{u}\mu}{d_1} \int_{-\infty}^{\infty} y V_j'\, dy. \tag{4.17}$$

After rewriting the outer problem (4.12) in terms of jump conditions, we combine (4.15) and (4.17) to obtain the following characterization for the small eigenvalues:

Proposition 4.1. *For $d_1 \in \mathcal{T}_e$, the eigenvalues λ of (2.43) of order $O(\epsilon^3 v_{\text{max}\,0}^2)$ satisfy*

$$\lambda c_j \int_{-\infty}^{\infty}\left(V_j'\right)^2 dy \sim \epsilon^3\left(\langle\phi_{ox}\rangle_j + \frac{s_0 c_j \bar{u}\mu}{\epsilon d_1}\right) \int_{-\infty}^{\infty} y V_j'\, dy, \quad j = 1, \ldots, N, \tag{4.18}$$

where $s_0 = O(\epsilon v_{\text{max}\,0}^3)$, and where $\langle\phi_{ox}\rangle_j$ is determined by the solution to the BVP

$$\frac{d_1}{\mu}\phi_{oxx} + \bar{u}\phi_o = 0, \quad -1 < x < 1, \quad x \neq x_j^0, \ j = 1, \ldots, N; \quad \phi_{ox}(\pm 1) = 0, \tag{4.19}$$

which satisfies the following jump conditions across each spike:

$$\left[\frac{d_1}{\mu}\phi_o\right]_j = \frac{2\bar{\chi}c_j}{3}v_{\text{max}\,0}^3\epsilon, \quad \left[\frac{d_1}{\mu}\phi_{ox}\right]_j = -\frac{3\zeta_0}{\bar{\chi}a_g v_{\text{max}\,0}}\langle\phi_o\rangle_j, \quad \zeta_0 := \left(1 - \frac{2}{\bar{\chi}v_{\text{max}\,0}}\right)^{-1}. \tag{4.20}$$

21

4.1 Formulation of the Matrix Problem

We will now solve (4.18) for $d_1 \in \mathcal{T}_e$ so as to derive a matrix eigenvalue problem for the small eigenvalues. To do so, we let m_k, for $k = 1, \ldots, N$, be constants to be found and we write the solution to (4.19) in the form

$$\phi_o = \frac{2\bar{\chi}}{3} v_{\max 0}^3 \sum_{k=1}^{N} c_k g(x; x_k) + \sum_{k=1}^{N} m_k G(x; x_k) \,. \tag{4.21}$$

Here, for $d_1 \in \mathcal{T}_e$, the Green's function G satisfies (2.24), while the dipole Green's function g satisfies

$$\frac{d_1}{\mu} g_{xx} + \bar{u} g = \delta'(x - x_j)\,, \quad -1 < x < 1\,; \quad g_x(\pm 1; x_j) = 0\,; \quad \left[\frac{d_1}{\mu} g\right]_j = 1\,, \quad [g']_j = 0\,. \tag{4.22}$$

Upon defining $\boldsymbol{m} := (m_1, \ldots, m_N)^T$, we use the jump condition in (4.20) to obtain from (4.21) that $\boldsymbol{m}$ satisfies

$$\boldsymbol{m} = -\frac{3\zeta_0}{\bar{\chi} a_g v_{\max 0}} \left(\mathcal{G} \boldsymbol{m} + \frac{2\bar{\chi}}{3} v_{\max 0}^3 \mathcal{P}_g \boldsymbol{c} \right), \tag{4.23}$$

where $\mathcal{G}$ is the Green's matrix and where $\mathcal{P}_g$ and $\boldsymbol{c}$ are defined as

$$\mathcal{P}_g := \begin{pmatrix} \langle g(x_1; x_1) \rangle_1 & \cdots & g(x_1; x_N) \\ \vdots & \ddots & \ddots \\ g(x_N; x_1) & \cdots & \langle g(x_N; x_N) \rangle_N \end{pmatrix}, \quad \boldsymbol{c} := \begin{pmatrix} c_1 \\ \vdots \\ c_N \end{pmatrix}. \tag{4.24}$$

Upon solving (4.23) for $\boldsymbol{m}$ we get

$$\boldsymbol{m} = -\frac{2 v_{\max 0}^2 \zeta_0}{a_g} \left(I + \frac{3\zeta_0}{\bar{\chi} a_g v_{\max 0}} \mathcal{G} \right)^{-1} \mathcal{P}_g \boldsymbol{c} \,. \tag{4.25}$$

Next, we use (4.21) to calculate $\langle \phi_{ox} \rangle_j$, for $j = 1, \ldots, N$, in the form

$$\langle \boldsymbol{\phi_{ox}} \rangle = \frac{2\bar{\chi}}{3} v_{\max 0}^3 \mathcal{G}_g \boldsymbol{c} + \mathcal{P} \boldsymbol{m} \,, \tag{4.26}$$

where $\langle \boldsymbol{\phi_{ox}} \rangle := (\langle \phi_{ox} \rangle_1, \ldots, \langle \phi_{ox} \rangle_N)^T$ and $\boldsymbol{m}$ is given by (4.25). Here $\mathcal{P}$ and $\mathcal{G}_g$ are defined by

$$\mathcal{P} := \begin{pmatrix} \langle G_x(x_1; x_1) \rangle_1 & \cdots & G_x(x_1; x_N) \\ \vdots & \ddots & \ddots \\ G_x(x_N; x_1) & \cdots & \langle G_x(x_N; x_N) \rangle_N \end{pmatrix}, \quad \mathcal{G}_g := \begin{pmatrix} g_x(x_1; x_1) & \cdots & g_x(x_1; x_N) \\ \vdots & \ddots & \ddots \\ g_x(x_1; x_N) & \cdots & g_x(x_N; x_N) \end{pmatrix}. \tag{4.27}$$

By substituting (4.25) and (4.26) into (4.18) of Proposition 4.1, we obtain that

$$\lambda \boldsymbol{c} \sim -\epsilon^3 \beta_0 \mathcal{M} \boldsymbol{c} \,, \quad \text{where} \quad \beta_0 := -\frac{\int_0^\infty y V_0' \, dy}{\int_0^\infty \left(V_0' \right)^2 dy} > 0 \,. \tag{4.28}$$

Here V_0 is the common leading order core solution, and $\mathcal{M}$ is defined for $d_1 \in \mathcal{T}_e$ by

$$\mathcal{M} := \frac{2\bar{\chi}}{3} v_{\max 0}^3 \mathcal{G}_g - \frac{2 v_{\max 0}^2 \zeta_0}{a_g} \mathcal{P} \left(I + \frac{3\zeta_0}{\bar{\chi} a_g v_{\max 0}} \mathcal{G} \right)^{-1} \mathcal{P}_g + \frac{s_0 \bar{u} \mu}{\epsilon d_1} I \,. \tag{4.29}$$

This result shows that λ and $\boldsymbol{c}$ are related to eigenpairs of the matrix $\mathcal{M}$. As a result, the analysis of the linear stability properties of the small eigenvalues in (2.43) when $d_1 \in \mathcal{T}_e$ is reduced to the problem of analyzing the eigenvalues of the matrix $\mathcal{M}$ and determining conditions on the parameters for which $\mathrm{Re}(\lambda) < 0$.

An important relationship between the existence of $\mathcal{M}$ and the invertibility of the Jacobian associated with the nonlinear algebraic system of quasi-equilibria, as studied in §3.1.1, is summarized as follows:

22

Remark 4.1. *Recalling that $a_g = \sigma_1$, the inverse $\left(I + \frac{3\zeta_0}{\bar{\chi} a_g v_{\max 0}}\mathcal{G}\right)^{-1}$ appearing in $\mathcal{M}$ of (4.29) does not exist when*

$$\frac{\sigma_j}{\sigma_1} = -\frac{\bar{\chi} v_{\max 0}}{3\zeta_0} = -\frac{\bar{\chi} v_{\max 0}}{3}\left(1 - \frac{2}{\bar{\chi} v_{\max 0}}\right) = \frac{2}{3} - \frac{\bar{\chi} v_{\max 0}}{3}, \tag{4.30}$$

where σ_j for $j = 1, \dots, N$ are the eigenvalues of $\mathcal{G}$ when $\tau = 0$ and $d_1 \in \mathcal{T}_e$. As a result, the non-existence of the small eigenvalues coincides, by using (3.37), with the non-invertibility of the Jacobian matrix of the linearization of the quasi-equilibrium solution around the steady-state. By setting $j = N$ in (4.30), we obtain $d_1 = d_{1cN}^\star$, as given in (3.39), which approximates the competition instability threshold for an N-spike steady state solution when $\tau = 0$ (see Proposition 3.1).

To analyze $\mathcal{M}$, we must calculate the matrix spectrum of the dipole Green's matrix $\mathcal{G}_g$ given in (4.27) when $d_1 \in \mathcal{T}_e$. As shown in Appendix E, when $d_1 \in \mathcal{T}_e$ the inverse matrix of $\mathcal{G}_g$ is readily identified as being proportional to the inverse of a $N \times N$ symmetric tridiagonal matrix, labeled by $\mathcal{D}_g$, and defined in (E.5) as

$$\mathcal{G}_g = \frac{\mu\theta}{d_1}\mathcal{D}_g^{-1}. \tag{4.31}$$

The matrix spectrum of $\mathcal{D}_g$ for $d_1 \in \mathcal{T}_e$, is readily calculated as in [24], and is summarized as follows:

Proposition 4.2. *The eigenvalues ξ_j and the normalized eigenvectors $v_j = (v_{1,j}, \dots, v_{N,j})^T$ of $\mathcal{D}_g$ are*

$$\xi_1 = 2\cot\left(\frac{2\theta}{N}\right) + 2\csc\left(\frac{2\theta}{N}\right) = 2\cot\left(\frac{\theta}{N}\right), \quad v_1 = \frac{1}{\sqrt{N}}\left(1, -1, \dots, 1, \dots, (-1)^{N+1}\right)^T, \tag{4.32a}$$

$$\xi_j = 2\cot\left(\frac{2\theta}{N}\right) - 2\csc\left(\frac{2\theta}{N}\right)\cos\left(\frac{\pi(j-1)}{N}\right), \quad v_{l,j} = \sqrt{\frac{2}{N}}\sin\left(\frac{\pi(j-1)}{N}(l-\frac{1}{2})\right), \quad j = 2, \dots, N, \tag{4.32b}$$

for $l = 1, \dots, N$, where $\theta = \sqrt{\mu\bar{\mu}/d_1}$. When $d_1 \in \mathcal{T}_e$, i.e. $\theta < \pi N/2$, we have the ordering $\xi_2 < \dots < \xi_N < \xi_1$.

By using the key Proposition 4.2, in Appendix F we show how to diagonalize $\mathcal{M}$ and compute its spectrum. This leads to the following explicit asymptotic result for the small eigenvalues, valid as $\epsilon \to 0$:

Proposition 4.3. *For $d_1 \in \mathcal{T}_e$ and $d_1 < d_{1cN}^\star$, the small eigenvalues λ_j satisfying (4.28) are given explicitly for $\epsilon \to 0$ by*

$$\lambda_j \sim -\frac{2\epsilon^3\beta_0}{3}\bar{\chi} v_{\max 0}^3\left(\frac{\mu\theta}{d_1\xi_j} - \frac{3\zeta_0}{\bar{\chi} a_g v_{\max 0}}\frac{\omega_j}{\xi_j} + \frac{\bar{u}\mu}{d_1}a_g\right), \quad j = 1, \dots, N, \tag{4.33}$$

where ξ_j are the matrix eigenvalues in (4.32) and $\zeta_0 = (1 - 2/(\bar{\chi} v_{\max 0}))^{-1}$. Here a_g and ω_j, as defined in (2.30) and (F.10), respectively, are given by

$$a_g = \frac{1}{2}\sqrt{\frac{\mu}{d_1\bar{\mu}}}\cot\left(\frac{\theta}{N}\right); \quad \omega_1 = 0, \quad \omega_j = \frac{\mu^2}{d_1^2}\csc^2\left(\frac{2\theta}{N}\right)\frac{\sin^2\left(\frac{(j-1)}{N}\pi\right)}{\left(-\xi_j + \frac{3\zeta_0}{\bar{\chi} a_g v_{\max 0}}\sqrt{\frac{\mu}{d_1\bar{u}}}\right)}, \quad j = 2, \dots, N, \tag{4.34}$$

where $\theta = \sqrt{\mu\bar{\mu}/d_1}$. The associated eigenvectors c are simply the eigenvectors of $\mathcal{G}_g$ as given in (4.32).

As shown below in §5.1, the stability threshold of an N-spike steady-state for the small eigenvalues can also be obtained by first deriving a DAE system for slow spike dynamics and then linearizing this DAE system about the equilibrium spike locations.

4.2 Stability Thresholds for the Small Eigenvalues

In this subsection, we examine the explicit formulae (4.33) for the small eigenvalues on the range $d_1 \in \mathcal{T}_e$ but with $d_1 < d_{1cN}^\star$ as given in (3.39). This latter inequality is needed to ensure that the steady-state is linearly stable with respect to the large eigenvalues when $\tau = 0$. To this end, we write (4.33) in the more convenient form

$$\lambda_j = -\frac{2\epsilon^3 \beta_0}{3} \bar{\chi} v_{\max 0}^3 h_j, \qquad \text{where} \quad h_j := \frac{1}{\xi_j} \left(\frac{\mu\theta}{d_1} - \frac{3\zeta_0 \omega_j}{\bar{\chi} a_g v_{\max 0}} \right) + \frac{\bar{u}\mu}{d_1} a_g, \quad j = 1, \dots, N, \tag{4.35}$$

where ω_j and a_g are defined in (4.34). If on the range $d_1 \in \mathcal{T}_e$, but with $d_1 < d_{1cN}^\star$, we have $h_j > 0$ for each $j = 1, \dots, N$, we conclude from (4.35) that the N-spike steady-state solution is linearly stable with respect to both the small and large eigenvalues when $\tau = 0$. Alternatively, if for some $j \in \{1, \dots, N\}$, we have $h_j < 0$ on some range of $d_1 \in \mathcal{T}_e$, but with $d_1 < d_{1cN}^\star$, it follows that the N-spike steady-state is unstable to the small eigenvalues on this range but is linearly stable to the large eigenvalues when $\tau = 0$.

For any $N \geq 1$, we first establish the sign of h_1 in (4.35) when $d_1 \in \mathcal{T}_e$. By using $\theta = \sqrt{\mu\bar{u}/d_1}$ together with (4.34) and (4.32a) for a_g and ξ_1, respectively, we use the fact that $\omega_1 = 0$ in (4.35) to obtain

$$h_1 = \frac{\theta^3}{2\bar{u}} \left[\tan\left(\frac{\theta}{N}\right) + \cot\left(\frac{\theta}{N}\right) \right] = \frac{\theta^3}{\bar{u}} \csc\left(\frac{2\theta}{N}\right). \tag{4.36}$$

When $d_1 \in \mathcal{T}_e$, we have $d_1 > d_{1pN}$ and so we require that $\theta < N\pi/2$. As $d_1 \to d_{1pN}$ from above, or equivalently as $\theta \to N\pi/2$ from below, h_1 has a vertical asymptote with $h_1 \to +\infty$. However, for $\theta < N\pi/2$, we observe from (4.36) that $h_1 > 0$, and so this mode is always stable for the small eigenvalues. This leads to the following result:

Proposition 4.4. *For $d_1 > d_{1p1} = 4\mu\bar{u}/\pi^2$, and in the limit $\epsilon \to 0$, a one-spike steady-state solution for (1.1) is always linearly stable with respect to the small eigenvalue.*

To examine the other mode functions h_j for $j = 2, \dots, N$, it is convenient to write h_j in (4.35) in terms of $\theta = \sqrt{\bar{u}\mu/d_1}$ rather than d_1. To do so, we substitute (4.34) into (4.35), and observe that $a_g = \theta(2\bar{u})^{-1} \cot(\theta/N)$ and $v_{\max 0}\bar{\chi}(6\zeta_0)^{-1} = (v_{\max 0}\bar{\chi} - 2)/6$ upon recalling that $\zeta_0 = (1 - 2/(\bar{\chi} v_{\max 0}))^{-1}$. In this way, we obtain after some algebra that h_j can be written explicitly in terms of θ as

$$h_j = \frac{\theta^3}{2\bar{u}} \cot\left(\frac{\theta}{N}\right) \hat{h}_j, \qquad \hat{h}_j := \frac{1}{\hat{\xi}_j} \left(2 + \hat{\xi}_j - 2\frac{\csc^2(2\theta/N)\sin^2(\pi(j-1)/N)}{1 - a_1\hat{\xi}_j/2} \right), \tag{4.37a}$$

where we have defined $\hat{\xi}_j$ and re-introduced a_1 (see (3.39)) as

$$a_1 := \frac{1}{3}(v_{\max 0}\bar{\chi} - 2), \qquad \hat{\xi}_j := \xi_j \cot\left(\frac{\theta}{N}\right). \tag{4.37b}$$

Next, we determine the algebraic sign, the asymptotes, and the continuity properties of h_j for the modes $j = 2, \dots, N$. By using (4.32b) of Proposition 4.32 for ξ_j for $j = 2, \dots, N$, we readily determine the following two equivalent identities for $\hat{\xi}_j$, as defined in (4.37b):

$$\hat{\xi}_j = \csc^2\left(\frac{\theta}{N}\right)\left[\cos\left(\frac{2\theta}{N}\right) - \cos\left(\frac{\pi(j-1)}{N}\right)\right] = -2 + 2\sin^2\left(\frac{\pi(j-1)}{2N}\right)\csc^2\left(\frac{\theta}{N}\right), \quad j = 2, \dots, N. \tag{4.38}$$

For $d_1 \in \mathcal{T}_e$ we have that $\theta < \theta_N := N\pi/2$ but with $\theta \neq \theta_m := m\pi/2$ for $m = 1, \dots, N-1$. For any $m = 1, \dots, N-1$, when $d_1 \to d_{1Tm}$, or equivalently when $\theta \to \theta_m$, we conclude from the first identity in (4.38) that $\hat{\xi}_{m+1}$ vanishes. As a result, we observe from (4.37a) that $\hat{h}_{m+1}$ has an apparent singularity as $\theta \to \theta_m$, which will require the evaluation of a singular $0/0$ limit. However, by a further analytical simplification of $\hat{h}_j$, as summarized below in Lemma 4.1, we can show that this singularity at $\theta = \theta_m$ is removable.

Lemma 4.1. *On the range $\theta < \theta_N := N\pi/2$, we have for $j = 2, \ldots, N$ that $\lambda_j = -2\epsilon^3\beta_0\bar{\chi}v_{\max 0}^3 h_j/3$, where h_j is given explicitly by*

$$h_j = \frac{\theta^3}{\bar{u}}\csc\left(\frac{2\theta}{N}\right)\sin^2\left(\frac{\pi(j-1)}{2N}\right)\frac{[1 - a_1 - (1 + a_1)\cos(2\theta/N)]}{[1 + a_1\cos(\pi(j-1)/N) - (1 + a_1)\cos(2\theta/N)]}. \tag{4.39}$$

It follows that $\lambda_j \to -\infty$ as $\theta \to \theta_N^-$. In addition, for all $j = 2, \ldots, N$, we have $\lambda_j < 0$ on the range $\theta_{sN} < \theta < \theta_N$, where the simultaneous zero-crossing threshold θ_{sN} satisfies

$$\theta_{sN} := \frac{N}{2}\arccos\left(\frac{1 - a_1}{a_1 + 1}\right), \quad \text{where} \quad a_1 = \frac{1}{3}(\bar{\chi}v_{\max 0} - 2). \tag{4.40}$$

Finally, λ_j is continuous and satisfies $\lambda_j > 0$ for all $j = 2, \ldots, N$ on the range $\theta_{cN} < \theta < \theta_{sN}$, where

$$\theta_{cN} := \frac{N}{2}\arccos\left(\frac{1 - a_1\cos(\pi/N)}{a_1 + 1}\right). \tag{4.41}$$

This threshold θ_{cN} is the value of θ for which $\hat{h}_N$ has a vertical asymptote. As θ is decreased below θ_N, it is the mode $j = N$ that first has a vertical asymptote. Written in terms of d_1, this vertical asymptote is equivalent to the approximation $d_{1cN}^\star$, given in (3.39), for the competition instability threshold associated with the large eigenvalues when $\tau = 0$.

Proof. We first derive (4.39). In the proof it is convenient to label $\varphi := \theta/N$ and $b := \pi(j-1)/(2N)$, so on $0 < \theta < \theta_N$, and for $j = 2, \ldots, N$, we have $0 < \varphi < \pi/2$ and $0 < b < \pi/2$. In terms of φ and b, (4.38) becomes

$$\hat{\xi}_j = \frac{[\cos(2\varphi) - \cos(2b)]}{\sin^2(\varphi)} = -2 + \frac{2\sin^2(b)}{\sin^2(\varphi)}; \qquad 1 - \hat{\xi}_j\frac{a_1}{2} = \frac{1}{\sin^2(\varphi)}\left[\sin^2(\varphi) - \frac{a_1}{2}(\cos(2\varphi) - \cos(2b))\right]. \tag{4.42}$$

By substituting (4.42) into (4.37a), we obtain that

$$\hat{h}_j = \frac{2\sin^2(\varphi)\sin^2(b)}{[\cos(2\varphi) - \cos(2b)]}\frac{\left[2 - \hat{\xi}_j a_1 - 2\sin^2(\varphi)\sin^2(2b)/\left(\sin^2(2\varphi)\sin^2(b)\right)\right]}{\left[2\sin^2(\varphi) - a_1(\cos(2\varphi) - \cos(2b))\right]}.$$

Next, we use $\sin(2\omega)/\sin\omega = 2\cos\omega$ to simplify the trigonometric ratio in the numerator of $\hat{h}_j$ to get

$$\hat{h}_j = \frac{2\sin^2(\varphi)\sin^2(b)}{\cos^2(\varphi)[\cos(2\varphi) - \cos(2b)]}\frac{\left[2\left(\cos^2(\varphi) - \cos^2(b)\right) - \hat{\xi}_j a_1\cos^2(\varphi)\right]}{\left[2\sin^2(\varphi) - a_1(\cos(2\varphi) - \cos(2b))\right]}.$$

Upon using $\cos^2(\varphi) - \cos^2(b) = [\cos(2\varphi) - \cos(2b)]/2$ together with the first identity for $\hat{\xi}_j$ in (4.42), we can cancel the common factor $\cos(2\varphi) - \cos(2b)$ from the numerator and denominator of $\hat{h}_j$, which leaves

$$\hat{h}_j = \frac{2\sin^2(b)\left[\sin^2(\varphi) - a_1\cos^2(\varphi)\right]}{\cos^2(\varphi)\left[2\sin^2(\varphi) - a_1(\cos(2\varphi) - \cos(2b))\right]} = \frac{\sin^2(b)}{\cos^2(\varphi)}\frac{[1 - a_1 - (a_1 + 1)\cos(2\varphi)]}{[1 + a_1\cos(2b) - (a_1 + 1)\cos(2\varphi)]}. \tag{4.43}$$

Finally, we substitute (4.43) into (4.37a) and use $\sin^2(b)\cot(\varphi)/\cos^2(\varphi) = 2\sin^2(b)/\sin(2\varphi)$. Upon recalling the definition of φ and b we readily obtain the explicit result (4.39).

Next, we let $\theta \to \theta_N^-$ for which $\cos(2\theta/N) \to -1$ and $\csc(2\theta/N) \to +\infty$. It readily follows from (4.39) that for each $j = 2, \ldots, N$, we have $h_j \to +\infty$ as $\theta \to \theta_N^-$ when $a_1 > 0$. Since $v_{\max 0} \gg 1$ when $\epsilon \ll 1$, $a_1 > 0$ must hold. This implies that $\lambda_j \to -\infty$ as $\theta \to \theta_N^-$. Finally, the zero-eigenvalue crossing threshold (4.40) and the value of θ for the mode $j = N$ that yields the first vertical asymptote (4.41) as θ is decreased, are both readily identified from the numerator and denominators in (4.39), respectively. □

25

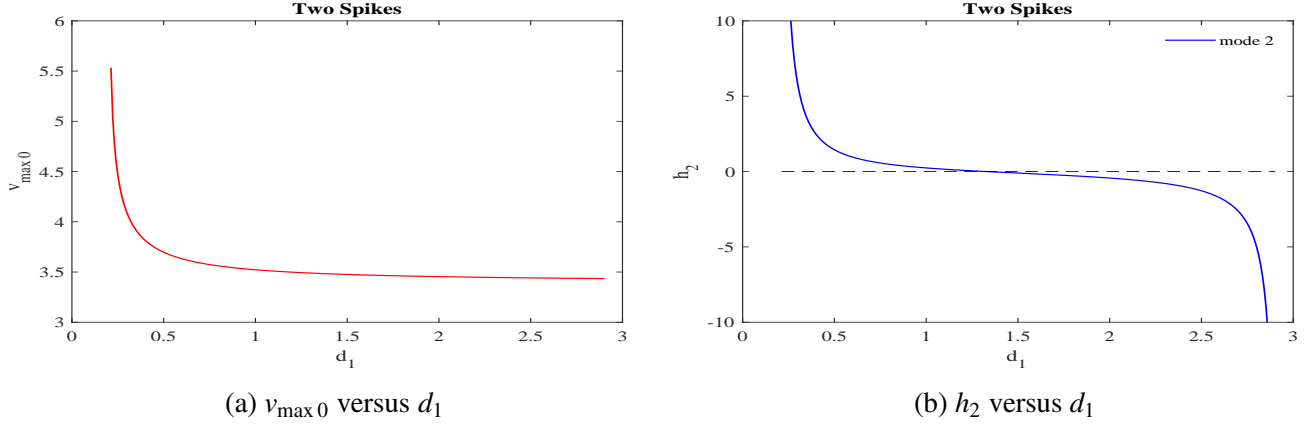(a) $v_{\max 0}$ versus d_1 (b) h_2 versus d_1

Figure 4: *Numerically computed results for $v_{\max 0}$ and h_2 on the range $d_{1p2} < d_1 < d_{1c2}^{\star}$ when $N = 2$, $\bar{\chi} = 1$, $\bar{u} = 2$, $d_2 = 0.0004 = \epsilon^2$, and $\mu = 1$. Here $d_{1p2} \approx 0.2$ and $d_{1c2}^{\star} \approx 2.91$. Left: $v_{\max 0}$ is monotone decreasing in d_1. Right: h_2 slowly decreases and crosses zero at $d_1 \approx d_{1s2} \approx 1.61$.*

To illustrate the implication of Lemma 4.1 for $N = 2$ as d_1 is varied, in the left and right panels of Figure 4 we plot $v_{\max 0}$ and h_2 versus d_1 as computed from (2.32) and (4.39), respectively. We conclude from Figure 4 that the two-spike steady-state is unstable with respect to the small eigenvalue with mode $m = 2$ when $1.61 \approx d_{1s2} < d_1 < d_{1c2}^{\star} \approx 2.91$, but is linearly stable on the range $0.20 \approx d_{1p2} < d_1 < d_{1s2} \approx 1.61$. Similar results are shown in Figure 5 for $N = 3$ for the same parameter set. We conclude that a three-spike steady-state is unstable with respect to the small eigenvalue modes $j = 2$ and $j = 3$ on the range $0.70 \approx d_{1s3} < d_1 < d_{1c3}^{\star} \approx 0.97$. On the range $0.09 \approx d_{1p3} < d_1 < d_{1s3} \approx 0.70$, the three-spike steady-state is linearly stable for all the small eigenvalues.
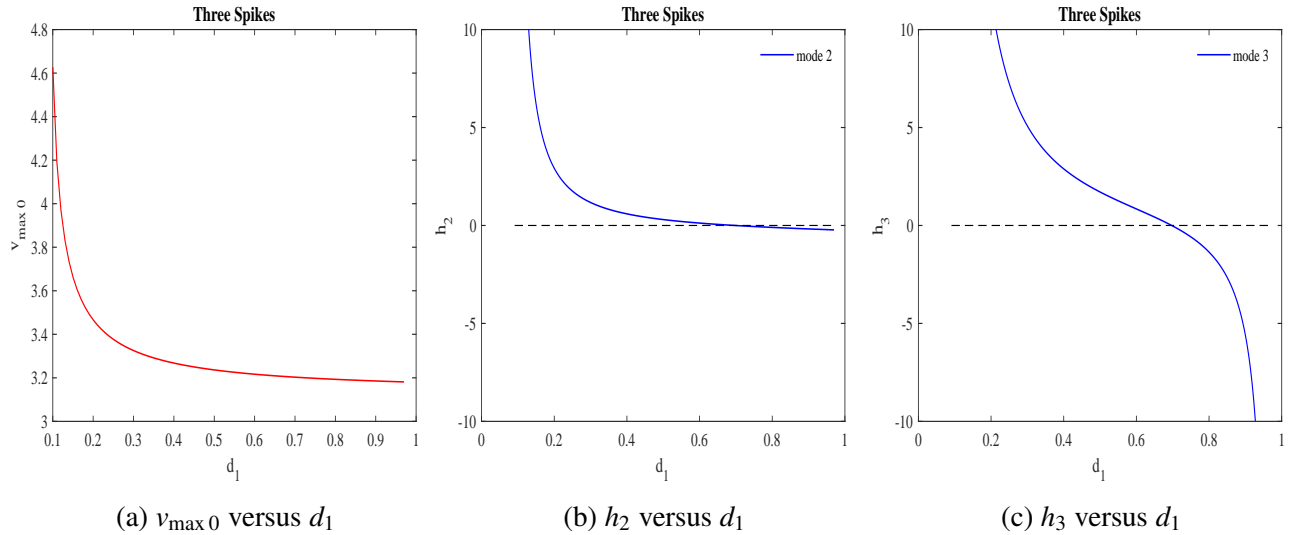

(a) $v_{\max 0}$ versus d_1 (b) h_2 versus d_1 (c) h_3 versus d_1

Figure 5: *Numerically computed results for $v_{\max 0}$, h_2, and h_3 on the range $d_{1p3} < d_1 < d_{1c3}^{\star}$ when $N = 3$, $\bar{\chi} = 1$, $\bar{u} = 2$, $d_2 = 0.0004 = \epsilon^2$, and $\mu = 1$. Here $d_{1p3} \approx 0.09$ and $d_{1c3}^{\star} \approx 0.97$. Left: $v_{\max 0}$ is monotone decreasing in d_1. Middle and Right: h_2 and h_3 slowly decrease as d_1 increases and the simultaneous zero crossing occurs at $d_{1s3} \approx 0.70$.*

In summary, in terms of d_1, Lemma 4.1 shows that an N-spike steady-state solution loses translation stability to $N - 1$ possible modes when d_1 increases above a critical threshold d_{1sN}. In this way, we obtain our main linear stability result for N-spike steady-state solutions of (1.2).

Proposition 4.5. *For $\tau = 0$ and $\epsilon \to 0$, an N-spike steady-state solution of (1.2) is linearly stable to both the*

large and small eigenvalues of the linearization when

$$d_{1pN} < d_1 < d_{1sN}, \quad where \quad d_{1pN} = \frac{4\mu\bar{u}}{N^2\pi^2}, \quad d_{1sN} := \frac{4\mu\bar{u}}{N^2\left(\arccos\left(\frac{1-a_1}{1+a_1}\right)\right)^2}. \tag{4.44}$$

Here a_1 is defined in (4.40). The steady-state is unstable to $N-1$ modes of instability for the small eigenvalues, but is linearly stable with respect to the large eigenvalues when $d_{1sN} < d_1 < d_{1cN}^{\star}$. Finally, when $d_1 > d_{1cN}^{\star}$, the steady-state is unstable with respect to both the large and small eigenvalues.

In Appendix G we show that the simultaneous zero-eigenvalue crossing threshold θ_{sN} for the small eigenvalues occurs precisely at the critical threshold where asymmetric steady-state solutions bifurcate from the symmetric steady-state solution branches constructed in §2.
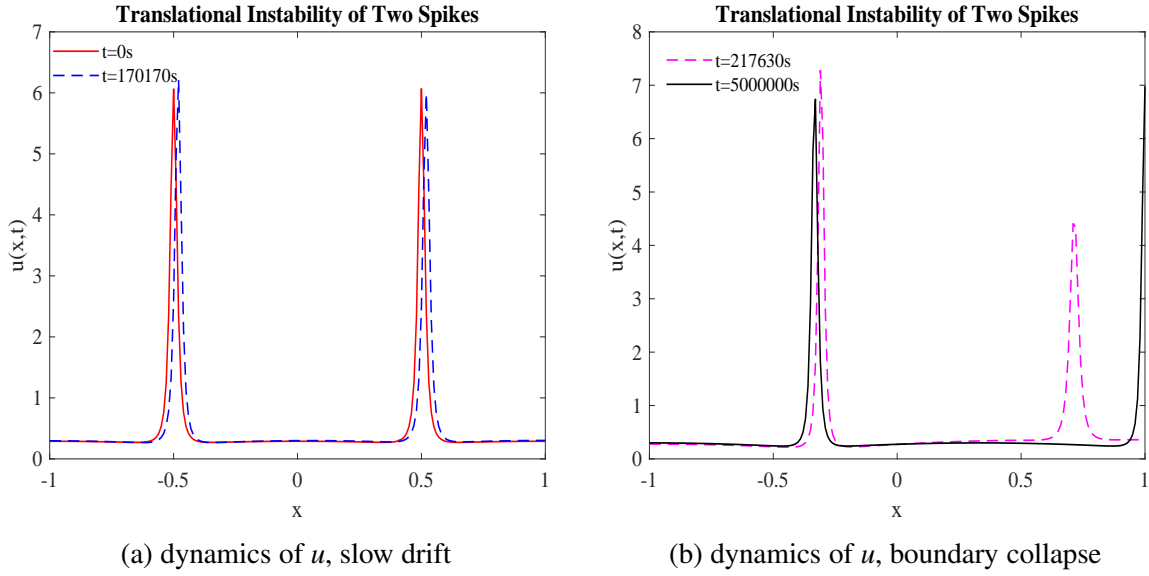

(a) dynamics of u, slow drift   (b) dynamics of u, boundary collapse

Figure 6: *Full PDE simulations of (1.2) using FlexPDE7 [14] illustrating a translational instabilitiy of a two-spike steady-state when $d_1 = 1.6$, and the long-time behavior for $\bar{\chi} = 1$, $\bar{u} = 2$, $d_2 = 0.0004$ and $\mu = 1$. Left: snapshots of u at two times showing the initial slow motion of a two-spike quasi-equilibrium. Right: long time dynamics leads to a final steady-state with an interior and a boundary spike.*

In Figure 6 we show FlexPDE7 simulations of (1.2) that illustrates a translation instability for a two-spike pattern when d_1 is on the range $d_{1s} < d_1 < d_{1c2}^{\star}$ for the parameter set in the caption of Figure 4. For these values, the interior two-spike steady-state is unstable to the mode $j = 2$ small eigenvalue. The resulting long-time dynamics leads to a final steady-state that has an interior and a boundary spike.

Finally, for an otherwise identical parameter set, in Figure 7 we show FlexPDE7 numerical results for (1.2) for an initial two-spike quasi-steady state solution as the cellular diffusivity d_1 is slowly decreased in time below the threshold d_{1p2} for which the base-state is unstable to a Turing instability. This figure illustrates that the instability of the base state leads to the nucleation of boundary spikes at each endpoint together with the creation of a new interior spike. The analysis of this spike nucleation behavior is beyond the scope of this paper.

5   Slow Dynamics of N-Spike Quasi-Equilibria

Next, we analyze the slow dynamics of an N-spike quasi-equilibrium pattern for (1.2), denoted by (u_q, v_q). Over a long time-scale, this analysis will characterize how the spike locations tend to their steady-state values. Similar
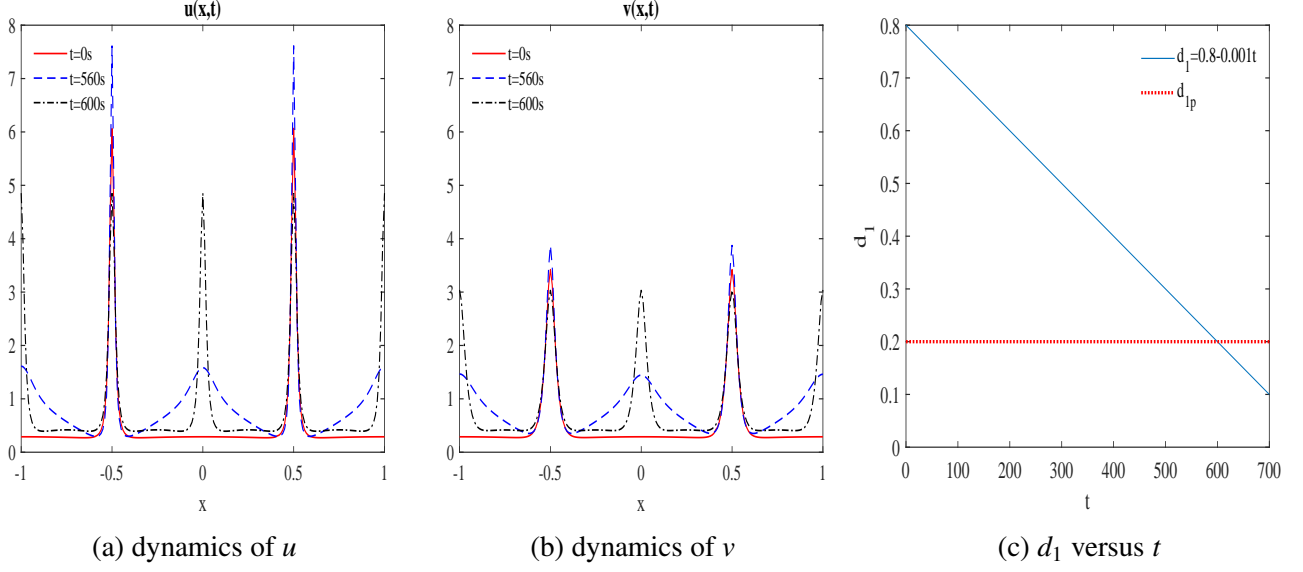
Figure 7: *Full PDE simulations of (1.2) using FlexPDE7 [14] illustrating nucleation behavior for an initial two-spike quasi steady-state when d_1 is decreased slowly in time.* Left and Middle: snapshots of (u, v) at three times, showing the spike nucleation behavior, with $\bar{\chi} = 1$, $\bar{u} = 2$, $d_2 = 0.0004$ and $\mu = 1$; Right: the diffusivity d_1 versus t. As d_1 decreases below $d_{1p2} \approx 0.20$, a new spike is nucleated between the two initial spikes and two new boundary spikes are created.

slow motion spike dynamics have been derived for other RD systems such as the GM and Gray-Scott models ([23], [8], [12]). However, there have been no previous such analyses for chemotaxis-type RD systems that exhibit slow spike dynamics over algebraically long time-scales of order $\mathcal{O}(\epsilon^{-p})$ for some $p > 0$. In our analysis, we will implicitly assume that the quasi-equilibrium pattern is linearly stable on $\mathcal{O}(1)$ time-scales, and that the base-state between spikes is linearly stable in the sense that (2.36) holds.

Recall that the spatial profile of the N-spike quasi-equilibrium pattern is characterized as in Proposition 2.1. In this result, we will now allow the spike locations to depend slowly on time in that $x_j = x_j(T)$ where $T = \epsilon^3 t$ is the long time-scale and with $d_2 = \epsilon^2$ in (1.2b). In the jth inner region, we introduce the local variables

$$y = \epsilon^{-1}[x - x_j(T)], \qquad U(y, T) = u\left(x_j + \epsilon y, \epsilon^{-3} T\right) \qquad V(y, T) = v\left(x_j + \epsilon y, \epsilon^{-3} T\right),$$

and we expand the inner solution to (1.2) as

$$U(y, T) = U_{0j}[y, x_j(T)] + \epsilon^2 U_{1j}(y, T) + \dots, \qquad V(y, T) = V_{0j}[y, x_j(T)] + \epsilon^2 V_{1j}(y, T) + \dots. \qquad (5.1)$$

Upon substituting (5.1) into (1.2), we obtain from the leading order problem that (U_{0j}, V_{0j}) satisfy the core problem (2.2). Moreover, we obtain from collecting $\mathcal{O}(\epsilon^2)$ terms that, on $-\infty < y < \infty$, U_{1j} and V_{1j} satisfy

$$U_{1j}'' - \bar{\chi}(U_{0j}V_{1j}')' - \bar{\chi}(U_{1j}V_{0j}')' + \frac{\mu}{d_1}U_{0j}(\bar{u} - U_{0j}) = 0, \qquad V_{1j}'' - V_{1j} + U_{1j} = -V_{0j}'\dot{x}_j(T), \qquad (5.2)$$

where $\dot{x}_j(T) := \frac{d}{dT}x_j(T)$ and $\bar{\chi} = \chi/d_1$. The imposition of a solvability condition for (5.2) will yield $\dot{x}_j$.

To this end, we decompose U_{1j} and V_{1j} into even and odd parts with respect to y in the form

$$U_{1j} = U_{1jE} + U_{1jO}, \qquad V_1 = V_{1jE} + V_{1jO}, \qquad (5.3)$$

where U_{1jE} (resp. V_{1jE}) and U_{1jO} (resp. V_{1jO}) satisfy homogeneous Neumann and Dirichlet boundary conditions at $y = 0$, respectively. From substituting (5.3) in (5.2), we obtain two problems, each defined on $-\infty < y < \infty$:

$$U_{1jE}'' - \bar{\chi}(U_{0j}V_{1jE}')' - \bar{\chi}(U_{1jE}V_{0j}')' + \frac{\mu}{d_1}U_{0j}(\bar{u} - U_{0j}) = 0; \qquad U_{1jE}'(0) = 0, \qquad (5.4a)$$

$$V_{1jE}'' - V_{1jE} + U_{1jE} = 0; \qquad V_{1jE}'(0) = 0, \qquad (5.4b)$$

and

$$U''_{1jO} - \bar{\chi}(U_{0j}V'_{1jO})' - \bar{\chi}(U_{1jO}V'_{0j})' = 0; \qquad U_{1jO}(0) = 0, \tag{5.5a}$$

$$V''_{1jO} - V_{1jO} + U_{1jO} = -V'_{0j}\dot{x}_j(T); \qquad V_{1jO}(0) = 0. \tag{5.5b}$$

Upon defining the functions g_{1jE} and g_{1jO} by

$$g_{1jE} = \frac{U_{1jE}}{U_{0j}} - \bar{\chi}V_{1jE}, \qquad g_{1jO} = \frac{U_{1jO}}{U_{0j}} - \bar{\chi}V_{1jO}, \tag{5.6}$$

we can more conveniently rewrite (5.4) and (5.5) on $-\infty < y < \infty$ as

$$(U_{0j}g'_{1jE})' + \frac{\mu}{d_1}U_{0j}(\bar{u} - U_{0j}) = 0, \quad V'_{jE}(0) = 0; \qquad V''_{1jE} - V_{1jE} + U_{1jE} = 0, \quad g'_{1jE}(0) = 0. \tag{5.7}$$

and

$$(U_{0j}g'_{1jO})' = 0, \quad V_{1jO}(0) = 0; \qquad V''_{1jO} - V_{1jO} + U_{1jO} = -V'_{0j}\dot{x}_j(T), \quad g_{1jO}(0) = 0. \tag{5.8}$$

By solving the g-equation in (5.7), we have for $y \in (0, \infty)$ that

$$g_{1jE} = \frac{\mu}{d_1} \int_0^y \frac{1}{U_{0j}(\rho)} \left(\int_0^\rho U_{0j}(\xi)(\bar{u} - U_{0j}(\xi))\,d\xi \right) d\rho + g_{1jE}(0), \tag{5.9}$$

where $g_{1jE}(0)$ is an unknown constant. In this way, the V-equation in (5.7) becomes

$$V''_{1jE} - V_{1jE} + U_{0j}g_{1jE} + \bar{\chi}U_{0j}V_{1jE} = 0, \quad -\infty < y < \infty; \qquad V'_{1jE}(0) = 0. \tag{5.10}$$

Similarly, we can solve the g-equation in (5.8) to get

$$g_{1jO} = \bar{C}_j \int_0^y \frac{1}{U_{0j}}\,d\xi, \tag{5.11}$$

where the constant $\bar{C}_j > 0$ is undetermined. Then, V_{1jO} in (5.8) satisfies

$$V''_{1jO} - V_{1jO} + U_{0j}g_{1jO} + \bar{\chi}U_{0j}V_{1jO} = -V'_{0j}\dot{x}_j(T), \quad -\infty < y < \infty; \qquad V_{1jO}(0) = 0. \tag{5.12}$$

By adding (5.10) and (5.12), we obtain that the problem for V_1 can be written in terms of an operator $\mathcal{L}$ as

$$\mathcal{L}V_{1j} + U_{0j}g_{1jO} + U_{0j}g_{1jE} = -V'_{0j}\dot{x}_j, \qquad \text{where} \quad \mathcal{L}V_{1j} := V''_{1j} - V_{1j} + \bar{\chi}U_{0j}V_{1j}. \tag{5.13}$$

Here g_{1jE} and g_{1jO} are given by (5.9) and (5.11), respectively.

To derive our solvability condition for (5.13), we multiply (5.13) by V'_{0j} and integrate the resulting expression over $(-\rho, \rho)$ with ρ large. This yields that

$$\lim_{\rho \to +\infty} \left(\int_{-\rho}^\rho V'_{0j}\mathcal{L}V_{1j}\,dy + \int_{-\rho}^\rho U_{0j}g_{1jO}V'_{0j}\,dy + \int_{-\rho}^\rho U_{0j}g_{1jE}V'_{0j}\,dy \right) = -\dot{x}_j \lim_{\rho \to +\infty} \int_{-\rho}^\rho \left(V'_{0j} \right)^2 dy. \tag{5.14}$$

To simplify (5.14), we invoke Green's second identity in the form

$$\lim_{\rho \to +\infty} \left(\int_{-\rho}^\rho V'_{0j}\mathcal{L}V_{1j}\,dy - \int_{-\rho}^\rho V_{1j}\,\mathcal{L}V'_{0j}\,dy \right) = \lim_{\rho \to +\infty} V'_{1j}V'_{0j}\Big|_{-\rho}^\rho - \lim_{\rho \to +\infty} V''_{0j}V_{1j}\Big|_{-\rho}^\rho. \tag{5.15}$$

29

Since V'_{0j} and V''_{0j} are exponentially small as $|y| \to \infty$, while $\mathcal{L}V'_{0j} = 0$, we conclude from (5.15) that

$$\lim_{\rho \to +\infty} \int_{-\rho}^{\rho} V'_{0j}\mathcal{L}V_{1j}\, dy = 0 . \tag{5.16}$$

Moreover, since U_{0j} and g_{1jE} are even, while V'_{0j} is odd, we get that $\int_{-\rho}^{\rho} U_{0j}g_{1jE}V'_{0j}\, dy = 0$. By using this result together with (5.16) in (5.14) and letting $\rho \to \infty$, we obtain from (5.11) the solvability condition

$$\dot{x}_j = \bar{C}_j\beta_j , \qquad \text{where} \quad \beta_j := -\frac{\int_0^\infty U_{0j}V'_{0j}\left(\int_0^y \frac{1}{U_{0j}}\, d\xi\right) dy}{\int_0^\infty \left(V'_{0j}\right)^2 dy} . \tag{5.17}$$

This expression determines the speed $\dot{x}_j$ of the spike in terms of the, as yet, undetermined constant $\bar{C}_j$.

Our final step in the analysis is to formulate a matching condition between the inner and outer solutions so as to determine $\bar{C}_j$. To do so, we find from (5.6) and (5.11), and together with the relation $U'_{0j} = \bar{\chi}U_{0j}V'_{0j}$ from the core problem (2.2), that the odd part of the inner solution in the jth region satisfies

$$U_{0j}g'_{1jO} = U'_{1jO} - \bar{\chi}(U_{0j}V'_{1jO}) - \bar{\chi}\left(U_{1jO}V'_{0j}\right) = \bar{C}_j . \tag{5.18}$$

Owing to the exponential decay of V'_{0j} and U'_{0j} as $y \to \pm\infty$, as shown in §2, we obtain that the far-field behavior of the derivative of the odd part of the inner solution must satisfy

$$U'_{1jO} \sim V'_{1jO} \sim \bar{C}_j , \quad \text{as} \quad y \to \pm\infty . \tag{5.19}$$

In the outer region we have, as a result of the slow time dependence, that the outer solution satisfies $u_o \sim w_o$, where w_o was given in (2.26) of §2 in our analysis of the quasi-equilibrium pattern. From (2.26), we have that

$$u_o \sim w_o \sim \frac{2\bar{\chi}}{3}\epsilon \sum_{k=1}^{N} v_{\text{max}\,k}^3 G(x; x_k) = \frac{2\bar{\chi}}{3}\epsilon \sum_{k \neq j} v_{\text{max}\,k}^3 G(x; x_k) + \frac{2\bar{\chi}}{3}\epsilon v_{\text{max}\,j}^3 G(x; x_j) ,$$

where $G(x; x_k)$ is the Helmholtz Green's function of (2.25).

To proceed, it is convenient to decompose $G(x; x_k)$ globally on $-1 < x < 1$ as

$$G(x; x_k) = K(|x - x_k|) + R(x; x_k) , \quad \text{where} \quad K := \frac{\mu}{2d_1}|x - x_k| . \tag{5.20}$$

Here K is the singular part of G, while R is the smooth regular part. By expanding $G(x; x_k)$ as $x \to x_j$, we get

$$G(x; x_k) \sim \begin{cases} G(x_j; x_k) + G_x(x_j; x_k)(x - x_j) , & j \neq k , \\ K(|x - x_k|) + R(x_k; x_k) + R_x(x_k; x_k)(x - x_k) , & j = k . \end{cases} \tag{5.21}$$

Upon using (5.21), we obtain that the limiting behavior of $u_{ox} \sim w_{ox}$ as we approach the jth spike is

$$u_{ox} \sim w_{ox} \sim \frac{2\bar{\chi}}{3}\epsilon \sum_{k \neq j} v_{\text{max}\,k}^3 G_x(x_j; x_k) + \frac{2\bar{\chi}}{3}\epsilon v_{\text{max}\,j}^3 R_x(x_j; x_j) + \frac{2\bar{\chi}}{3}\epsilon v_{\text{max}\,j}^3 K_x^{\pm}(x_j; x_j) , \quad \text{as} \quad x \to x_j^{\pm} , \tag{5.22}$$

where $K_x^{\pm} := \pm\frac{\mu}{2d_1}$. To find $\bar{C}_j$, we use the matching condition that $\epsilon^2 U'_{1j0}$ as $y \to \pm\infty$ must agree with ϵu_{ox} as $x \to x_j$, when we include only the first two terms on the right-hand side of (5.22). This determines $\bar{C}_j$ as

$$\bar{C}_j = \frac{2\bar{\chi}}{3}\sum_{k \neq j}^{N} v_{\text{max}\,k}^3 G_x(x_j; x_k) + \frac{2\bar{\chi}}{3}v_{\text{max}\,j}^3 R_x(x_j; x_j) . \tag{5.23}$$

30

Since U'_{1jE} is an odd function, the last term in (5.22) must match with the far-field behavior of $\epsilon^2 U'_{1jE}$. However, since this explicit matching requirement does not affect our solvability condition, it is not performed here.

Upon substituting (5.23) into (5.17), we obtain a coupled nonlinear ODE system for the spike locations in the quasi-equilibrium pattern. In our ODE system, $v_{\max j}$ and β_j must be calculated by using the nonlinear algebraic system (2.28) for C_j, s_j and $v_{\max j}$. This leads to a differential algebraic system (DAE) of ODE's characterizing slow spike dynamics for (1.2), which we summarize in the following formal proposition.

Proposition 5.1. *For (1.2) with $d_2 = \epsilon^2 \ll 1$ and where $d_1 \in \mathcal{T}_e$, as defined in (2.35), assume that the quasi-equilibrium pattern is linearly stable with respect to the large eigenvalues and that (2.36) holds. Then, the slow dynamics of a collection $x_1, \ldots, x_N$ of spikes satisfies the DAE system:*

$$\frac{dx_j}{dt} \sim \frac{2\bar{\chi}}{3}\epsilon^3\beta_j\left(\sum_{k\neq j}^{N} v_{\max k}^3 G_x(x_j; x_k) + v_{\max j}^3 R_x(x_j; x_j)\right), \qquad \begin{cases} C_k e^{\bar{\chi}s_k} - s_k = 0, \\ -\frac{1}{2}v_{\max k}^2 + \frac{1}{2}s_k^2 + \frac{C_k}{\bar{\chi}}e^{\bar{\chi}v_{\max k}} - \frac{s_k}{\bar{\chi}} = 0, \\ s_k = \frac{2\bar{\chi}}{3}a_g v_{\max k}^3 \epsilon, \end{cases} \quad (5.24)$$

where $j = 1, \ldots, N$. Here β_j is defined in (5.17) with the asymptotics (5.26). The Green's functions $G(x; x_k)$ and its regular part R_x can be found explicitly from (2.25). In particular, the locations x_j^0, for $j = 1, \ldots, N$, of the N-spike true steady-state solution, are the equilibrium point of the slow dynamics and satisfy

$$\sum_{k\neq j}^{N} G_x(x_j^0; x_k^0) + R_x(x_j^0; x_j^0) = 0, \quad j = 1, \ldots, N. \quad (5.25)$$

Proposition 5.1 characterizes the slow dynamics of an N-spike quasi-equilibrium solution on the long $O\left(\epsilon^{-3}\right)$ time-scale. We remark that this time-scale is longer than the $O\left(\epsilon^{-2}\right)$ time-scale of slow spike dynamics for the GM and Gray-Scott models ([23], [8], [12]), where there are no chemotactic effects.

In Appendix H, we show that β_j, as given in (5.17), can be calculated asymptotically by retaining only the contribution from the sub-inner solution. In particular, in Appendix H we provide the leading order estimate

$$\beta_j \sim \frac{2}{v_{\max j}}, \qquad \text{for } v_{\max j} \gg 1. \quad (5.26)$$

Moreover, in Appendix H we show at the steady-state spike locations that $\beta_j = \beta_0 \ \forall j$, with β_0 given in (4.28).

To illustrate our results, we now compare the dynamics computed from the DAE system (5.24) with corresponding numerical results computed from the full PDE system (1.2) using FLEXPDE7 [14]. In our comparison, we computed the integrals defining β_j numerically from (5.17). The results for a one- and two-spike dynamics are shown in Figure 8 for the parameter values in the figure caption. In Figure 8a, where we chose the initial condition $x_1(0) = -0.1$, the asymptotic and numerical spike trajectories are favorably compared for a one-spike quasi-equilibrium pattern. In Figure 8b a similar favorable comparison is shown for the case of two-spike dynamics starting from the initial condition $x_1(0) = -0.6$ and $x_2(0) = 0.6$.

5.1 Computation of Jacobian Matrix for Balancing Conditions

In this subsection, and as remarked in §4, we show that when $d_1 \in \mathcal{T}_e$ the matrix $\mathcal{M}$ in (4.29) arises from the linearization of the DAE dynamics (5.24) in Proposition 5.1 about the steady-state spike locations. Our approach below is inspired by a related analysis for the GM model in [58].

To this end, we use the Green's function in (2.24) together with its decomposition in (5.20) to define

$$\partial_{x_j} G(x_j; x_k) := \begin{cases} \frac{\partial R}{\partial x}(x; x_j)|_{x=x_j}, & j = k, \\ \frac{\partial G}{\partial x}(x; x_k)|_{x=x_j}, & j \neq k, \end{cases} \qquad \partial_{x_j}\partial_{x_k} G(x_j; x_k) = \begin{cases} \frac{\partial}{\partial x}|_{x=x_j}\frac{\partial}{\partial y}|_{y=x_k} R(x; y), & j = k, \\ \partial_{x_j}\partial_{x_k} G(x_j; x_k), & j \neq k. \end{cases} \quad (5.27)$$
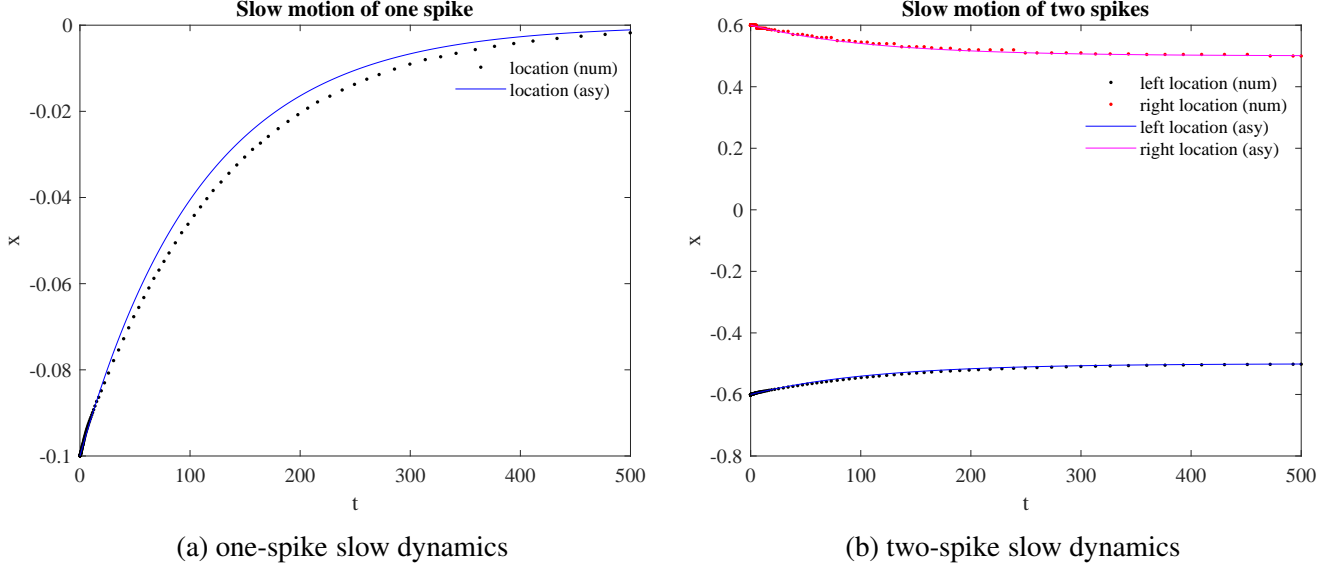
(a) one-spike slow dynamics **(b) two-spike slow dynamics**

Figure 8: *Slow dynamics of one- and two-spike quasi-equilibria for* (1.2) *with different parameter values. Left:* $d_1 = \chi = 1$, $\bar{u} = 2$, $d_2 = 0.02 = \epsilon^2$ *and* $\mu = 0.25$; *Right:* $d_1 = \chi = 1$, $\bar{u} = 2$, $d_2 = 0.005 = \epsilon^2$, $\mu = 1$. *The solid curves are the results from the asymptotic DAE system* (5.24). *The dotted curves are the results obtained from the full numerical PDE simulation of* (1.2) *using* [14]. *In the numerical results, the center of the spike is chosen as the maximum of* u *on the computational grid. Observe the slow dynamics towards the equilibrium spike locations.*

Here R is the smooth regular part of G as defined in (5.20). Next, we denote the $N \times N$ matrices $\nabla \mathcal{G}$, $(\nabla \mathcal{G})^T$, and $\nabla^2 \mathcal{G}$ evaluated at the steady-state spike locations by

$$\nabla \mathcal{G} := (\partial_{x_j} G(x_j^0; x_k^0))_{N \times N}, \qquad (\nabla \mathcal{G})^T := (\partial_{x_k} G(x_j^0; x_k^0))_{N \times N}, \qquad \nabla^2 \mathcal{G} := (\partial_{x_j} \partial_{x_k} G(x_j^0; x_k^0))_{N \times N}. \qquad (5.28)$$

The relationship between these matrices and the matrices $\mathcal{P}$, $\mathcal{P}_g$, and $\mathcal{G}_g$, as defined in (4.27), (4.24), and (4.27), respectively, that were used in our analysis of the small eigenvalues in §4, is clarified in Appendix I.

In our analysis, it is convenient to write the DAE system (5.24) in the form

$$\frac{dx_j}{dt} = \frac{2\bar{\chi}}{3}\epsilon^3 \beta_j \mathcal{F}_j, \qquad \text{where} \qquad \mathcal{F}_j := \sum_{k=1}^{N} v_{\max k}^3 \partial_{x_j} G(x_j; x_k), \qquad j = 1, \dots, N. \qquad (5.29)$$

Our goal below is to compute the Jacobian matrix $\mathcal{J} := \left(\frac{\partial \mathcal{F}_j}{\partial x_i}\right)_{N \times N}$ that arises by linearizing the DAE system (5.24) around the steady-state spike locations. More specifically, if we introduce the perturbation

$$x_j = x_j^0 + c_j e^{\lambda t}, \qquad j = 1, \dots, N,$$

into (5.29), the linearization of the DAE system yields the matrix eigenvalue problem

$$\lambda \boldsymbol{c} = -\epsilon^3 \beta_0 \tilde{\mathcal{M}} \boldsymbol{c}, \qquad \tilde{\mathcal{M}} := -\frac{2\bar{\chi}}{3} \mathcal{J}, \qquad \text{where} \qquad \mathcal{J} := \left(\frac{\partial \mathcal{F}_j}{\partial x_i}\right)_{N \times N}, \qquad (5.30)$$

where $\boldsymbol{c} := (c_1, \dots, c_N)^T$. From an explicit calculation of $\mathcal{J}$ given below, we will show via (5.30) that $\tilde{\mathcal{M}}$ is identical to the matrix $\mathcal{M}$ as given in (4.29), which was derived in our analysis of the small eigenvalues.

To calculate the Jacobian, we first differentiate $\mathcal{F}_j$ in (5.29) with respect to x_i to obtain

$$\frac{\partial \mathcal{F}_j}{\partial x_i} = \sum_{k=1}^{N} 3v_{\max k}^2 (\partial_{x_i} v_{\max k}) \partial_{x_j} G(x_j; x_k) + \sum_{k=1}^{N} v_{\max k}^3 \partial_{x_i} \left[\partial_{x_j} G(x_j; x_k)\right], \qquad j = 1, \dots, N. \qquad (5.31)$$

By using the nonlinear algebraic system in (5.24), in (D.5) of Appendix D we calculate $\partial_{x_i} v_{\max k}$, so as to obtain

$$\frac{\partial \mathcal{F}_j}{\partial x_i} \sim -3 \sum_{k=1}^N \frac{v_{\max k}^2 \zeta_{\max k}}{\bar{\chi} s_k} (\partial_{x_i} s_k) \partial_{x_j} G(x_j; x_k) + \sum_{k=1}^N v_{\max k}^3 \partial_{x_i} \left[\partial_{x_j} G(x_j; x_k) \right], \qquad j = 1, \ldots, N, \tag{5.32}$$

where $\zeta_{\max k} = (1 - 2/(\bar{\chi} v_{\max k}))^{-1}$. To determine $\partial_{x_i} s_j$, as needed in (5.32), we differentiate (2.27) in x_i to get

$$\partial_{x_i} s_j = \frac{2 \bar{\chi} \epsilon}{3} \sum_{k=1}^N \left[3 v_{\max k}^2 (\partial_{x_i} v_{\max k}) G(x_j; x_k) + v_{\max k}^3 \partial_{x_i} G(x_j; x_k) \right]. \tag{5.33}$$

By using (D.5) of Appendix D to estimate $\partial_{x_i} v_{\max k}$, we obtain for $\epsilon \to 0$ that

$$\partial_{x_i} s_j \sim -2\epsilon \sum_{k=1}^N \frac{v_{\max k}^2 \zeta_{\max k}}{s_k} (\partial_{x_i} s_k) G(x_j; x_k) + \frac{2\bar{\chi}\epsilon}{3} \sum_{k=1}^N v_{\max k}^3 \partial_{x_i} G(x_j; x_k), \quad j = 1, \ldots, N. \tag{5.34}$$

Then, by calculating the second term in (5.34), we get

$$\partial_{x_i} s_j \sim -2\epsilon \sum_{k=1}^N \frac{v_{\max k}^2 \zeta_{\max k}}{s_k} (\partial_{x_i} s_k) G(x_j; x_k) + \begin{cases} \frac{2\bar{\chi}\epsilon}{3} v_{\max i}^3 \partial_{x_i} G(x_j; x_i), & i \neq j, \\ \frac{2\bar{\chi}\epsilon}{3} v_{\max i}^3 \partial_{x_i} G(x_j; x_i) + \frac{2\bar{\chi}\epsilon}{3} \sum_{k=1}^N v_{\max k}^3 \partial_{x_i} G(x_j; x_k), & i = j. \end{cases} \tag{5.35}$$

Next, we evaluate (5.35) at the equilibrium solution where $x_j = x_j^0$, for which $s_k = s_0$, $v_{\max k} = v_{\max 0}$, and $\zeta_{\max k} = \zeta_0$, where $s_0 = 2\bar{\chi} a_g v_{\max 0}^3 \epsilon/3$. Moreover, at the steady-state, we use the equilibrium condition (5.25) to eliminate the last sum in (5.35) that holds when $i = j$. In this way, (5.35) reduces to

$$\partial_{x_i} s_j \sim -\frac{3\zeta_0}{\bar{\chi} a_g v_{\max 0}} \sum_{k=1}^N (\partial_{x_i} s_k) G(x_j^0; x_k^0) + \frac{s_0}{a_g} \partial_{x_i} G(x_j^0; x_i^0), \quad i, j = 1, \ldots, N, \tag{5.36}$$

when evaluated at the steady-state. By introducing $\boldsymbol{s} := (s_1, \ldots, s_N)^T$ and $\nabla := (\partial_{x_1}, \ldots, \partial_{x_N})$, (5.36) can be written in matrix form as

$$\nabla \boldsymbol{s} \sim \frac{s_0}{a_g} \left(I + \frac{3\zeta_0}{\bar{\chi} a_g v_{\max 0}} \mathcal{G} \right)^{-1} (\nabla \mathcal{G})^T, \qquad \text{where} \quad \nabla \boldsymbol{s} := (\nabla s_1, \ldots, \nabla s_N)^T |_{x_j = x_j^0, \, j=1, \ldots, N}. \tag{5.37}$$

Here $\mathcal{G} := (G(x_j^0; x_k^0))_{N \times N}$ is the Green's matrix at the steady-state and $(\nabla \mathcal{G})^T$ is defined in (5.28). By using (5.37), the first term on the right-hand side of (5.32), when evaluated at the steady-state, is the matrix product

$$-\frac{3}{\bar{\chi} s_0} v_{\max 0}^2 \zeta_0 \left(\sum_{k=1}^N \partial_{x_j} G(x_j^0; x_k^0) (\partial_{x_i} s_k) \right)_{N \times N} \sim -\frac{3}{\bar{\chi} s_0} v_{\max 0}^2 \zeta_0 \, \nabla \mathcal{G} \, \nabla \boldsymbol{s} = -\frac{3}{\bar{\chi} a_g} v_{\max 0}^2 \zeta_0 \, \nabla \mathcal{G} \left(I + \frac{3\zeta_0}{\bar{\chi} a_g v_{\max 0}} \mathcal{G} \right)^{-1} (\nabla \mathcal{G})^T. \tag{5.38}$$

Next, we focus on the second sum in (5.32), which is equivalent to

$$\sum_{k=1}^N v_{\max k}^3 \partial_{x_i} [\partial_{x_j} G(x_j; x_k)] = \begin{cases} v_{\max i}^3 \partial_{x_i} \partial_{x_j} G(x_j; x_i), & i \neq j, \\ \sum_{k \neq j}^N v_{\max k}^3 \partial_{x_j}^2 G(x_j; x_k) + v_{\max j}^3 \frac{\partial}{\partial y}|_{y=x_j} \frac{\partial}{\partial x}|_{x=x_j} R(x; y), & i = j. \end{cases} \tag{5.39}$$

From the BVP (2.24) satisfied by $G(x; x_k)$, we conclude that $\partial^2_{x_j} G(x_j; x_k) = -\frac{\bar{u}\mu}{d_1} G(x_j; x_k)$ for $j \neq k$, so that

$$\sum_{k=1}^{N} v^3_{\max k} \partial_{x_i}[\partial_{x_j} G(x_j; x_k)] = \begin{cases} v^3_{\max i} \partial_{x_i} \partial_{x_j} G(x_j; x_i), & i \neq j, \\ -\frac{\bar{u}\mu}{d_1} \sum_{k \neq j}^{N} v^3_{\max k} G(x_j; x_k) + v^3_{\max j} \frac{\partial}{\partial y}|_{y=x_j} \frac{\partial}{\partial x}|_{x=x_j} R(x; y), & i = j. \end{cases} \tag{5.40}$$

To evaluate the last term in (5.40), we use the chain rule on the regular part $R(x; y)$ to get

$$\frac{\partial}{\partial y}|_{y=x_j} \frac{\partial}{\partial x}|_{x=x_j} R(x; y) = -R_{xx}(x_j; x_j) + \partial_{x_j}\left(\frac{\partial R}{\partial x}(x; x_j)|_{x=x_j}\right). \tag{5.41}$$

By using (5.27) to identify the second term on the right-hand side of (5.41), and by calculating $R_{xx}(x_j; x_j)$ from (I.5) of Appendix I, we conclude that

$$\frac{\partial}{\partial y}|_{y=x_j} \frac{\partial}{\partial x}|_{x=x_j} R(x; y) = -\frac{\bar{u}\mu}{d_1} G(x_j; x_j) + \partial^2_{x_j} G(x_j; x_j). \tag{5.42}$$

Upon substituting (5.42) into (5.40) we obtain

$$\sum_{k=1}^{N} v^3_{\max k} \partial_{x_i}[\partial_{x_j} G(x_j; x_k)] = \begin{cases} v^3_{\max i} \partial_{x_i} \partial_{x_j} G(x_j; x_i), & i \neq j, \\ -\frac{\bar{u}\mu}{d_1} \sum_{k=1}^{N} v^3_{\max k} G(x_j; x_k) + v^3_{\max j} \partial^2_{x_j} G(x_j; x_j), & i = j. \end{cases} \tag{5.43}$$

Finally, we evaluate (5.43) at the steady-state solution where $x_j = x^0_j$ and $v_{\max j} = v_{\max 0}$ for $j = 1, \ldots, N$, and where we recall that $a_g = \sum_{k=1}^{N} G(x^0_j; x^0_k)$. Upon writing the resulting expression in matrix form, we get

$$\left(\sum_{k=1}^{N} v^3_{\max 0} \partial_{x_i}[\partial_{x_j} G(x_j; x_k)]\right)_{N \times N} = -\frac{\bar{u}\mu}{d_1} v^3_{\max 0} a_g I + v^3_{\max 0} \nabla^2 \mathcal{G}, \tag{5.44}$$

where $\nabla^2 \mathcal{G}$ was defined in (5.28). By substituting (5.44) and (5.38) in (5.31), we calculate the Jacobian as

$$\mathcal{J} := \left(\frac{\partial \mathcal{F}_i}{\partial x_j}\right)_{N \times N} = -\frac{3v^2_{\max 0} \zeta_0}{\bar{\chi} a_g} \nabla \mathcal{G}\left(I + \frac{3\zeta_0}{\bar{\chi} a_g v_{\max 0}} \mathcal{G}\right)^{-1} (\nabla \mathcal{G})^T + v^3_{\max 0} \nabla^2 \mathcal{G} - \frac{\bar{u}\mu a_g}{d_1} v^3_{\max 0} I, \tag{5.45}$$

where $\nabla \mathcal{G}$, $(\nabla \mathcal{G})^T$ and $\nabla^2 \mathcal{G}$ were given in (5.28). Then, by evaluating the matrix $\tilde{\mathcal{M}}$ in (5.30) that arises in the linearization of the DAE system around the steady-state spike locations, we get

$$\tilde{\mathcal{M}} = \frac{2v^2_{\max 0} \zeta_0}{a_g} \nabla \mathcal{G}\left(I + \frac{3\zeta_0}{\bar{\chi} a_g v_{\max 0}} \mathcal{G}\right)^{-1} (\nabla \mathcal{G})^T - \frac{2\bar{\chi}}{3} v^3_{\max 0} \nabla^2 \mathcal{G} + \frac{2\bar{u}\mu\bar{\chi} a_g}{3d_1} v^3_{\max 0} I. \tag{5.46}$$

Finally, upon using $s_0 = 2\bar{\chi} a_g v^3_{\max 0} \epsilon / 3$ to simplify the coefficient of the identity matrix in (5.46), and by using the key relations

$$\nabla \mathcal{G} = \mathcal{P}, \qquad (\nabla \mathcal{G})^T = -\mathcal{P}_g, \qquad \nabla^2 \mathcal{G} = -\mathcal{G}_g, \tag{5.47}$$

as derived in Appendix I, we conclude upon comparing (5.46) and (4.29) that $\tilde{\mathcal{M}} = \mathcal{M}$.

In summary, our analysis establishes that the small eigenvalues associated with the linearization of the steady-state solution are precisely the same eigenvalues that are associated with linearizing the DAE system of slow spike dynamics about the steady-state spike locations.

6 Discussion

In this concluding section, we first discuss how our analysis of 1D spike patterns in the KS model (1.2) in the limit $d_2 \ll 1$ shares some common features with a related analysis of localized spike patterns for the GM model (cf. [24], [23], [55], [58]). We also mention a few open problems that warrant further investigation.

6.1 Comparison with the GM System

We first make some remarks on an interesting connection between the analysis of spike patterns for the KS model (1.2) in the limit $d_2 = \epsilon^2 \ll 1$ and that for the GM model

$$A_t = d_a A_{xx} - A + A^p/H^q, \qquad \tau H_t = D H_{xx} - \mu H + A^r/H^s, \tag{6.1}$$

in the limit $d_a \ll 1$ of small activator diffusivity. In this context, A and H are the activator and inhibitor fields, respectively. Moreover, $\tau > 0$, $D > 0$, and $\mu > 0$ are constants and the GM exponents (p, q, r, s) satisfy the usual conditions $p > 1$, $q > 0$, $r > 0$, $s \geq 0$, and $(p-1)/q < r/(s+1)$.

In [24], steady-state 1D spike patterns in which A is spatially localized with spike-width $O(\sqrt{d_a})$ were constructed for (6.1) in the limit $d_a \ll 1$ using the method of matched asymptotic expansions. For this class of solutions, the spike profile is characterized by the homoclinic solution of $w_{yy} - w + w^p = 0$, where $y = d_a^{-1/2}(x - x_j)$. In the outer region between spikes where $A \approx 0$, the interaction between steady-state spikes is mediated by the inhibitor diffusion field with the term A^r/H^s being approximated by Dirac masses concentrated at the spike locations. As a result, when $d_a \ll 1$, the activator A behaves like a linear combination of discrete spikes on the domain, while H is well-approximated by a superposition of translates of the reduced-wave Green's function.

In comparison, we observe from our steady-state analysis of the KS model (1.2) in the limit $d_2 \ll 1$ given in §2 that the chemoattractant v and the cellular population density u share a similar asymptotic structure to A and H, respectively, in (6.1). In our analysis, the spike profile for v is represented by a homoclinic solution (2.3), while the outer solution for u is well-approximated by a superposition of translates of the Helmholtz Green's functions (2.26). Moreover, in the limit $d_2 \ll 1$, the background constant $s_0 \ll 1$ in (2.30) plays the same role as the locally constant inhibitor field in the core of a spike for (6.1).

With regards to the NLEP linear stability analysis, the approximating NLEP (3.24) that arises from our sub-inner layer analysis in §3 is rather similar in form to the NLEP for the GM model that occurs for the exponents $p = 3$ and $s = 0$. This connection results from the explicit form given in (3.22) for the sub-inner solution. As a result, by adapting the NLEP linear stability analysis given in [24], [55], and [58], we are able to calculate parameter thresholds corresponding to either zero-eigenvalue crossings as d_1 is varied, or Hopf bifurcations as τ is increased. In particular, although in minimal KS models, without the logistic term, spike amplitude temporal oscillations are not expected, our NLEP linear stability analysis in the presence of the logistic source term has shown that a sufficiently large reaction time $\tau > 0$ in (2.43) can trigger such spike oscillations for a one-spike steady-state. The mechanism for these oscillations, being a sufficiently large diffusive time-delay between the two components in (1.2), is qualitatively the same as that studied in [55] for the GM model.

With regards to the analysis of the small eigenvalues, which characterize possible translational instabilities of the spike locations, the reduced multi-point BVP derived in Proposition 4.1 is very similar in form to that derived for the GM model in §4 of [24]. As a result, the detailed framework for the GM matrix analysis in §4 of [24] was employed for obtaining Proposition 4.3 for the small eigenvalues, which lead to the explicit result in Lemma 4.1. As qualitatively similar to that for the GM model (cf. [24]), we showed for our N-spike steady-sate solution that there are $N - 1$ simultaneous zero-crossings for the small eigenvalues that occur at the same critical value of d_1. For the GM model, these simultaneous crossings occur at a common value of D, and this threshold provides the critical value of D for which branches of asymmetric spike equilibria, corresponding to spikes of different height, bifurcate from the symmetric steady-state branch (cf. [54]). Finally, the slow DAE dynamics of spike quasi-equilibria, as characterized by Proposition 5.1 in terms of gradients of the Helmholtz Green's function, is rather similar to that derived for the GM model in [23].

One novel feature of our analysis has been to use distinctly different approaches to both calculate and verify linear stability thresholds resulting from our detailed asymptotic analysis. In particular, in §3.1.1, the non-invertibility of the Jacobian matrix that resulted from the steady-state analysis for fixed spike locations closely approximates the NLEP linear stability threshold when $\tau = 0$. Moreover, the linearization of the steady-state

of the DAE slow spike dynamics (5.24) was found in §5.1 to correspond identically to our asymptotic result in Proposition 5.1 for the small eigenvalues. Finally, our zero-eigenvalue crossing condition for the small eigenvalues in (4.40) was shown in Appendix G to correspond to the bifurcation point where asymmetric equilibria emerge from the symmetric steady-state solution branch.

Next, we discuss some key differences between our analysis of spike patterns for the KS model (1.2) and that for the GM model in [24]. Firstly, owing to the different Green's functions mediating the spike interactions for (1.2) and for (6.1), for the GM model there is no analogue of the positivity and resonance conditions of (2.35) discussed in Remark 2.1. Secondly, the competition and translational stability thresholds for symmetric spike equilibria for the GM model (6.1) are given by explicit critical values for the inhibitor diffusivity D. In our analysis of the KS model, these two thresholds are characterized by weakly nonlinear algebraic equations in the cellular diffusivity d_1. This distinction arises, in part, to the existence of an intricate sub-inner structure of the spike profile for the KS model (1.2) that has no counterpart in the GM model (6.1). Finally, for the KS model, the numerical results shown in Figure 7 suggest that spike nucleation behavior can occur from the midpoint of the background state between neighboring spikes as d_1 is decreased below the positivity threshold d_{1pN} in (2.35). Such nucleation behavior does not occur for the GM model (6.1).

6.2   Further Directions

In the limit of small diffusivity $d_2 = \epsilon^2 \ll 1$ for the chemotactic concentration field, we have developed a hybrid asymptotic-numerical approach to analyze the existence, linear stability, and slow dynamics of 1D spike patterns for (1.2). The study of pattern forming properties for (1.2) when $d_2 \ll 1$ is distinctly different than that based on the usual approach of considering the large chemotactic drift limit, i.e. $\chi \gg 1$ in (1.2), as was done in most previous analyses and numerical simulations of localized patterns (cf. [34], [33], [25], [51]). In the limit $d_2 \ll 1$, we have shown that the analysis of localized 1D spike patterns is rather closely related to that for the GM model.

We now discuss a few open problems related to our study. From a mathematical viewpoint, the analytical tractability of our quasi steady-state and linear stability analysis has relied to a large extent on the availability of certain explicit formulae for the spike profile that exists in the sub-inner region of a spike. More specifically, our explicit but approximate analysis is based on the asymptotically large spike height $v_{\max} \gg 1$ limit. However, since $v_{\max} = \mathcal{O}(-\log \epsilon)$ is only rather large when ϵ is extremely small, our asymptotic results for steady-states and for the linear stability thresholds provide only a moderately decent prediction of corresponding full numerical results when $\epsilon = 0.01$ is only fairly small. One theoretical open challenge is to provide a rigorous steady-state and linear stability analysis for multi-spike patterns that is based on the full inner problem (2.3) and the corresponding NLEP (3.21), which does not exploit the large $v_{\max}$ limit.

One important open problem from the viewpoint of global bifurcation theory is to numerically compute solution branches of localized 1D steady-state spike patterns for (1.2) as d_1, d_2 and χ are varied. This would clarify how solution branches of spike equilibria differ when either $d_2 \ll 1$ or when $\chi \gg 1$. The observation of spike nucleation behavior as shown in [19, 44] for certain parameter sets, and hinted at in Figure 7 as d_1 is decreased below the positivity threshold in (2.35) of Remark 2.1 should be investigated. For chemotaxis models of urban crime, spike nucleation events for the emergence of hotspots have been shown to occur near saddle-node bifurcation points of branches of spike equilibria (cf. [48]). In contrast, for (1.2) when $d_1 = \mathcal{O}(1)$, $d_2 = \mathcal{O}(1)$ and $\chi = \mathcal{O}(1)$ they appear to arise from Turing bifurcations of the base state (cf. [19, 44]). Two other possible extensions of our 1D analysis are to analyze the existence and linear stability of asymmetric spike equilibria for (1.2) and to analyze steady-state patterns for variants of (1.2) that incorporate other cellular population growth models and possible nonlinear mechanisms that couple the cellular density to the chemoattractant concentration.

It would also be worthwhile to extend our 1D analysis to analyze the existence, linear stability, and slow dynamics of localized patterns for (1.1) when $d_2 \ll 1$ in a 2D bounded domain. One such direction would be to analyze the linear stability properties of a localized stripe in a 2D rectangular domain that results from a trivial

extension of the 1D spike in the transverse direction. Numerical results in [44] suggest that, in marked contrast to the well-known instability behavior of homoclinic stripes for the GM model (cf. [30]), a localized stripe for a coupled chemotaxis system may be linearly stable to breakup into spots. As a result, it would be interesting to theoretically investigate the possibility of varicose or transverse instabilities of such localized stripes. A second interesting direction is motivated by the numerical simulations reported in [25] that suggest that localized 2D spot patterns for (1.1) should exist in the singular limit $d_2 \ll 1$. Given the rather close correspondence between the analysis of localized patterns for (1.1) in the limit $d_2 \ll 1$ and the GM model in the limit of a small activator diffusivity, the framework for a 2D steady-state and linear stability analysis of (1.1) for spot patterns would likely rely somewhat on the approach developed for the 2D GM model, as summarized in [59].

Acknowledgments

A   Solvability of the Outer Problem: Turing Instability of the Base State

In this appendix, we relate the solvability of the outer problem (2.22) to Turing bifurcation points in the parameter d_1 for the spatially uniform base state $u = v = 0$ of (1.2). This analysis will motivate Remark 2.1.

On an interval of length L, with homogeneous Neumann conditions for u and v, we linearize (1.2) around $u = v = 0$ by setting $u = e^{\lambda t + ikx}\Phi$ and $v = e^{\lambda t + ikx}N$, where $k = m\pi/L$ with $m = 1, 2, \ldots$. We readily obtain that

$$\begin{pmatrix} -d_1 k^2 + \mu\bar{u} - \lambda & 0 \\ 1 & -\epsilon^2 k^2 - 1 - \lambda \end{pmatrix} \begin{pmatrix} \Phi \\ N \end{pmatrix} = \mathbf{0}, \tag{A.1}$$

which has a nontrivial solution if and only if $\lambda = -1 - \epsilon^2 k^2$ or $\lambda = -d_1 k^2 + \mu\bar{u}$. As such, with $k = m\pi/L$, there is a zero-eigenvalue crossing associated with the spatially uniform state $u = v = 0$ at the critical values

$$d_1 = \frac{\mu\bar{u}L^2}{m^2\pi^2}, \quad m = 1, 2, \ldots. \tag{A.2}$$

This base-state is linearly stable on a domain of length L when $d_1 > \mu\bar{u}L^2/\pi^2$. Setting $L = 2$, consistent with (1.2), we conclude that (A.2) coincides precisely with the "resonant" values of d_1 in (2.23) for the outer problem.

However, in our construction of N-spike steady-state patterns for (1.2), the spatially uniform base state approximates the outer solution w_o only on intervals of length $2/N$. Upon setting $L = 2/N$ in (A.2), this observation suggests that the outer solution for an N-spike steady-state should be linearly stable when $d_1 > 4\mu\bar{u}/(N^2\pi^2)$. This latter threshold also has the alternative interpretation that it is the smallest value of d_1 for which the outer solution w_o is always positive in $|x| < 1$. In particular, for an N-spike steady-state, it is easy to verify that this positivity condition for w_o holds when $d_1 > d_{1pN} := \bar{u}\mu/\lambda_1$, where $\lambda_1 := N^2\pi^2/4$ is the first non-zero eigenvalue of the negative Neumann Laplacian $-d^2/dx^2$ on $(-1/N, 1/N)$. We remark that for quasi-equilibrium patterns with unequally spaced spikes, this positivity threshold must be modified to (2.36).

Next, we verify that the outer problem (2.22) is solvable for an N-spike steady-state pattern when $d_1 = d_{1Tm}$, where d_{1Tm} is one of the "resonant" values in (2.23) with $m = 1, \ldots, N - 1$. For the steady-state problem, where $v_{\max k} = v_{\max 0}$ and where $x_k = x_k^0$, with x_k^0 as given in (2.29), (2.22) is solvable at $d_1 = d_{1Tm}$ if and only if

$$\int_{-1}^{1} w_{oh}\mathcal{L}_0 w_o \, dx = \frac{2\bar{\chi}\epsilon}{3}v_{\max 0}^3 \sum_{k=1}^{N} \int_{-1}^{1} w_{oh}(x)\,\delta(x - x_k^0)\,dx = \frac{2\bar{\chi}\epsilon}{3}v_{\max 0}^3 \sum_{k=1}^{N} \cos\left(\frac{m\pi}{2}\frac{(2k - 1)}{N}\right) = 0. \tag{A.3}$$

The trigonometric sum in (A.3) can be readily evaluated for $m = 1, \ldots, N - 1$ with the result

$$\sum_{k=1}^{N} \cos\left(\frac{m\pi}{2} \frac{(2k-1)}{N}\right) = \frac{\sin(m\pi)}{2 \sin(m\pi/N)} = 0. \tag{A.4}$$

As a consequence, (2.22) is solvable for an N-spike steady-state even when $d_1 = \mathcal{T}_e$ (see (2.35)).

Finally, we remark that when $d_1 = 4\mu\bar{u}/(m^2\pi^2)$, for some $m = 1, \ldots, N-1$, a solution (non-unique) to (2.22) for an N-spike steady-state can be represented as $u_o \sim w_o = \frac{2}{3}\bar{\chi}\epsilon v_{\max 0}^3 \sum_{k=1}^{N} G_m(x; x_k^0)$. Here, with the operator $\mathcal{L}_0$ of (2.22), the modified Green's function $G_m(x; \xi)$ satisfies

$$\mathcal{L}_0 G_m = \delta(x - \xi) - w_{oh}(\xi)w_{oh}(x), \quad |x| \le 1; \qquad G_{mx}(\pm 1; \xi) = 0. \tag{A.5}$$

Although G_m can be found analytically, for simplicity we have restricted our analysis only to when $d_1 \in \mathcal{T}_e$.

B Calculation of $\mathcal{G}_\lambda$ and $\mathcal{P}$

In this appendix, we show how to determine the matrix spectrum of $\mathcal{G}_\lambda$, as defined in (3.16) of §3. Moreover, we calculate $\mathcal{P}$, as defined in (4.27) of §4. To do so, we introduce an auxiliary problem for $y = y(x)$, given by

$$\frac{d_1}{\mu}y'' + \hat{u}y = 0, \quad -1 < x < 1; \quad y'(\pm 1) = 0; \quad [y]_j = 0, \quad \left[\frac{d_1}{\mu}y'\right]_j = b_j, \tag{B.1}$$

for $j = 1, \ldots, N$, where $[y]_j := y(x_j^+) - y(x_j^-)$ and $x_j = x_j^0$ is given by (2.29). Here $\hat{u} := \bar{u} - \tau\lambda_0/\mu$. This problem is solvable when $d_1 \ne 4\mu\hat{u}/(m^2\pi^2)$ for $m = 1, 2, \ldots$. When $\tau = 0$, (B.1) is always solvable when $d_1 \in \mathcal{T}_e$.

With the exception of this restricted set for d_1, the solution to (B.1) can be represented in terms of the Green's function $G_\lambda(x; x_k)$, satisfying (3.13), as $y = \sum_{k=1}^{N} b_k G_\lambda(x; x_k)$. Upon defining $\boldsymbol{y} := (y_1, \ldots, y_N)^T$, $\langle \boldsymbol{y'} \rangle := (y_1', \ldots, y_N')^T$ and $\boldsymbol{b} := (b_1, \ldots, b_N)^T$, where $y_j = y(x_j)$ and $\langle y' \rangle_j = (y'(x_j^+) + y'(x_j^-))/2$, we identify the eigenvalue-dependent Green's matrix $\mathcal{G}_\lambda$ of (3.16) and $\mathcal{P}$ of (4.27) as

$$\boldsymbol{y} = \mathcal{G}_\lambda \boldsymbol{b}, \qquad \langle \boldsymbol{y'} \rangle = \mathcal{P}\boldsymbol{b}. \tag{B.2}$$

Next, we show how to represent $\mathcal{G}_\lambda$ and $\mathcal{P}$ in terms of tridiagonal matrices. By solving (B.1) on each subinterval, and enforcing the continuity conditions $[y]_j = 0$ for $j = 1, \ldots, N$, we get

$$y = \begin{cases} y_1 \frac{\cos[\theta_\lambda(1+x)]}{\cos[\theta_\lambda(1+x_1)]}, & -1 < x < x_1, \\ y_j \frac{\sin[\theta_\lambda(x_{j+1}-x)]}{\sin[\theta_\lambda(x_{j+1}-x_j)]} + y_{j+1}\frac{\sin[\theta_\lambda(x-x_j)]}{\sin[\theta_\lambda(x_{j+1}-x_j)]}, & x_j < x < x_{j+1}, \quad j = 1, \ldots, N-1, \\ y_N \frac{\cos[\theta_\lambda(1-x)]}{\cos[\theta_\lambda(1-x_N)]}, & x_N < x < 1. \end{cases} \tag{B.3}$$

Then, upon satisfying the jump conditions in (B.1) we can write $\boldsymbol{b}$ as

$$\boldsymbol{b} = \frac{d_1\theta_\lambda}{\mu}\mathcal{D}\boldsymbol{y}, \qquad \text{where} \quad \theta_\lambda := \sqrt{\frac{\mu}{d_1}\left(\bar{u} - \frac{\tau\lambda_0}{\mu}\right)}. \tag{B.4}$$

Here, for $d_1 \ne 4\mu\hat{u}/(m^2\pi^2)$ with $m = 1, 2, \ldots$, $\mathcal{D}$ is the invertible tridiagonal matrix defined by

$$\mathcal{D} = \begin{pmatrix} d & f & 0 & \cdots & 0 & 0 & 0 \\ f & e & f & \cdots & 0 & 0 & 0 \\ 0 & f & e & \ddots & 0 & 0 & 0 \\ \vdots & \vdots & \ddots & \ddots & \ddots & \vdots & \vdots \\ 0 & 0 & 0 & \ddots & e & f & 0 \\ 0 & 0 & 0 & \cdots & f & e & f \\ 0 & 0 & 0 & \cdots & 0 & f & d \end{pmatrix}. \tag{B.5}$$

The matrix entries of $\mathcal{D}$, for which the identity $d = f + e$ holds, are

$$d \equiv \tan(\theta_\lambda/N) - \cot(2\theta_\lambda/N)\,, \quad e \equiv -2\cot(2\theta_\lambda/N)\,, \quad f \equiv \csc(2\theta_\lambda/N)\,. \tag{B.6}$$

By combining (B.4) with the first equation in (B.2), we conclude for $d_1 \neq 4\mu\hat{u}/(m^2\pi^2)$ for $m = 1, 2, \ldots$ that

$$\mathcal{G}_\lambda = \sqrt{\frac{\mu}{d_1\hat{\mu}}}\,\mathcal{D}^{-1}\,, \quad \text{with} \quad \hat{u} = \bar{u} - \frac{\tau\lambda_0}{\mu}\,. \tag{B.7}$$

When $\tau = 0$, we remark that (B.7) holds when $d_1 \in \mathcal{T}_e$.

Since $\mathcal{D}$ is a tridiagonal matrix with a constant row sum, its eigenpairs κ_j and $\mathbf{q}_j$ for $j = 1, \ldots, N$ can be calculated explicitly (see [24]), with the following result:

Proposition B.1. *The eigenvalues κ_j and the normalized eigenvectors of $\mathcal{D}$ are*

$$\begin{cases} \kappa_1 = e + 2f\,; \quad \kappa_j = e + 2f\cos\left(\pi(j-1)/N\right)\,, & j = 2, \ldots, N, \\ \mathbf{q}_1 = \frac{1}{\sqrt{N}}(1, \ldots, 1)^T\,, \quad q_{l,j} = \sqrt{\frac{2}{N}}\cos\left(\frac{\pi(j-1)}{N}\left(l - \frac{1}{2}\right)\right)\,, & j = 2, \ldots, N\,, \ l = 1, \ldots, N, \end{cases}$$

where $\mathbf{q}_j = (q_{1,j}, \ldots, q_{N,j})^T$ and d, e and f are given by (B.6). By using (B.7), the eigenvalues σ_j of $\mathcal{G}_\lambda$ when $d_1 \neq 4\mu\hat{u}/(m^2\pi^2)$ for $m = 1, 2, \ldots$, are

$$\sigma_j = \sqrt{\frac{\mu}{d_1\hat{u}}}\left[e + 2f\cos\left(\frac{\pi(j-1)}{N}\right)\right]^{-1}\,, \quad j = 1, \ldots, N\,. \tag{B.8}$$

By setting $\lambda_0 = 0$, we use (B.7) and Proposition B.1 to calculate a_g, as defined in (2.30). For $d_1 \in \mathcal{T}_e$, we get

$$a_g = \sum_{k=1}^{N} G(x_j^0; x_k^0) = \sqrt{\frac{\mu}{d_1\bar{u}}}\mathcal{D}^{-1}\sqrt{N}\mathbf{q}_1 = \sqrt{\frac{\mu}{d_1\bar{u}}}\frac{1}{(e+2f)} = \frac{1}{2}\sqrt{\frac{\mu}{d_1\bar{u}}}\cot\left(\frac{\theta}{N}\right)\,, \quad \theta = \sqrt{\frac{\mu\bar{u}}{d_1}}\,. \tag{B.9}$$

To determine $\mathcal{P}$ when $\lambda_0 = 0$, we use (B.3) to write $\langle y'\rangle$ in terms of $\mathbf{y}$ as $\langle y'\rangle = -(\theta/2)\csc\left(2\theta/N\right)C^T\mathbf{y}$, where $\theta = \sqrt{\mu\bar{u}/d_1}$ and C is the tridiagonal matrix defined by

$$C := \begin{pmatrix} 1 & 1 & 0 & \cdots & 0 & 0 & 0 \\ -1 & 0 & 1 & \cdots & 0 & 0 & 0 \\ 0 & -1 & 0 & \ddots & 0 & 0 & 0 \\ \vdots & \vdots & \ddots & \ddots & \ddots & \vdots & \vdots \\ 0 & 0 & 0 & \ddots & 0 & 1 & 0 \\ 0 & 0 & 0 & \cdots & -1 & 0 & 1 \\ 0 & 0 & 0 & \cdots & 0 & -1 & -1 \end{pmatrix}\,. \tag{B.10}$$

By combining the second equation in (B.2) with this result, we conclude for $d_1 \in \mathcal{T}_e$ that

$$\mathcal{P} = -\frac{\mu}{2d_1}\csc\left(\frac{2\theta}{N}\right)C^T\mathcal{D}^{-1}\,. \tag{B.11}$$

C   Proof of Theorem 3.1

For convenience, we drop the overbars in (3.24) to rewrite the NLEP as

$$\Psi_{0zz} + U_0\Psi_0 - \alpha U_0 \frac{\int_{-\infty}^{\infty} U_0{}^2\Psi_0\,dz}{\int_{-\infty}^{\infty} U_0{}^2\,dz} = \Lambda\Psi_0, \quad -\infty < z < +\infty; \qquad \Psi_0 \text{ bounded as } |z| \to \infty. \tag{C.1}$$

Here $U_0 = 2\mathrm{sech}^2 z$, $\Lambda := \delta^2(\lambda_0 + 1)$ with $\delta := 2/(\bar{\chi}v_{\max 0})$. It is well-known [32] that the homoclinic solution to $w_{zz} - w + w^3 = 0$ on $-\infty < z < \infty$ with $w(0) > 0$, $w'(0) = 0$ and $w \to 0$ as $|z| \to \infty$ is $w = \sqrt{2}\mathrm{sech}(y)$. Therefore, we have $U_0 = w^2$ and the NLEP (C.1) becomes

$$\Psi_{0zz} + w^2\Psi_0 - \alpha w^2 \frac{\int_{-\infty}^{\infty} w^4\Psi_0\,dz}{\int_{-\infty}^{\infty} w^4\,dz} = \Lambda\Psi_0, \quad -\infty < z < +\infty; \qquad \Psi_0 \text{ bounded as } |z| \to \infty. \tag{C.2}$$

There is a standard approach [56] to study (C.2). Firstly, we focus on the following local eigenvalue problem:

$$\Psi_{0zz} + w^2\Psi_0 = \lambda\Psi_0, \quad -\infty < z < \infty; \qquad \Psi_0 \text{ bounded as } |z| \to \infty. \tag{C.3}$$

As shown in [32], the principal eigenvalue of (C.3) is $\lambda = 1$ and the corresponding eigenfunction is $\Psi_0 = w$. Next, we transform (C.2) into a form more amenable for analysis. To this end, we observe from the ODE $w'' - w + w^3 = 0$ that w^2 satisfies

$$(w^2)_{zz} - 4w^2 + 3w^4 = 0, \quad -\infty < z < +\infty; \qquad w \to 0 \quad \text{as} \quad |z| \to \infty. \tag{C.4}$$

Therefore, upon multiplying the Ψ_0-equation in (C.2) by w^2 and integrating it over $(-\infty, \infty)$ by parts, we get

$$\int_{-\infty}^{\infty} (w^2)_{zz}\Psi_0\,dz + \int_{-\infty}^{\infty} w^4\Psi_0\,dz - \alpha\int_{-\infty}^{\infty} w^4\Psi_0\,dz = \Lambda\int_{-\infty}^{\infty} w^2\Psi_0\,dz. \tag{C.5}$$

Next, upon substituting (C.4) into (C.5), we obtain

$$(4 - \Lambda)\int_{-\infty}^{\infty} w^2\Psi_0\,dz = (2 + \alpha)\int_{-\infty}^{\infty} w^4\Psi_0\,dz. \tag{C.6}$$

Then, by using (C.6), we transform the NLEP in (C.2) into the following form, as written in (3.41):

$$\Psi_{0zz} + w^2\Psi_0 - \kappa\frac{\int_{-\infty}^{\infty} w^2\Psi_0\,dz}{\int_{-\infty}^{\infty} w^4\,dz}w^2 = \Lambda\Psi_0, \qquad \kappa := \frac{\alpha(4 - \Lambda)}{(2 + \alpha)}, \tag{C.7}$$

Next, we test (C.7) against the conjugate Ψ_0^* and by integrating the resulting expression by parts we get

$$\int_{-\infty}^{\infty} |\Psi_{0z}|^2\,dz - \int_{-\infty}^{\infty} w^2|\Psi_0|^2\,dz + \Lambda\int_{-\infty}^{\infty} |\Psi_0|^2\,dz = -\frac{\alpha(4 - \Lambda)\left|\int_{-\infty}^{\infty} w^2\Psi_0\,dz\right|^2}{(2 + \alpha)\int_{-\infty}^{\infty} w^4\,dz}. \tag{C.8}$$

We first claim that Λ is real-valued when α is real-valued. To show this, the imaginary part of (C.8) yields

$$\mathrm{Im}(\Lambda)\int_{-\infty}^{\infty} |\Psi_0|^2\,dz = \frac{\alpha\,\mathrm{Im}(\Lambda)\left|\int_{-\infty}^{\infty} w^2\Psi_0\,dz\right|^2}{2 + \alpha}\frac{}{\int_{-\infty}^{\infty} w^4\,dz}. \tag{C.9}$$

Then, upon invoking the Cauchy-Schwartz inequality, we obtain

$$\frac{\alpha}{2+\alpha} \frac{\left| \int_{-\infty}^{\infty} w^2 \Psi_0 \, dz \right|^2}{\int_{-\infty}^{\infty} w^4 dz} \leq \frac{\alpha}{2+\alpha} \int_{-\infty}^{\infty} |\Psi_0|^2 \, dz \, . \tag{C.10}$$

Upon substituting this inequality into (C.9), we conclude that $\text{Im}(\Lambda) = 0$. This completes the proof of our claim. It immediately follows that (C.8) is also real-valued when α is real-valued.

The next step is to study the sign of Λ in (C.7). We claim that

$$\int_{-\infty}^{\infty} |\Psi_{0z}|^2 \, dz - \int_{-\infty}^{\infty} w^2 |\Psi_0|^2 \, dz \geq -\frac{\left| \int_{-\infty}^{\infty} w^2 \Psi_0 \, dz \right|^2}{\int_{-\infty}^{\infty} w^2 \, dz} \, .$$

Similarly as the proof of Lemma 5 in [32], this claim is established if we can equivalently show that the real eigenvalues υ of the following NLEP are non-positive:

$$\Delta \Psi_0 + w^2 \Psi_0 - w^2 \frac{\int_{-\infty}^{\infty} w^2 \Psi_0 dz}{\int_{-\infty}^{\infty} w^2 dz} = \upsilon \Psi_0 \, . \tag{C.11}$$

We first observe that if $\Psi_0 \equiv 1$, then $\upsilon = 0$. Next, we observe that (C.11) is equivalent to solving

$$(L_0 - \upsilon)\Psi_0 = w^2 \, , \qquad \int_{-\infty}^{\infty} w^2 \Psi_0 \, dz = \int_{-\infty}^{\infty} w^2 \, dz = 4 \, . \tag{C.12}$$

As such, we define Ξ as

$$\Xi(\upsilon) := \int_{-\infty}^{\infty} w^2 (L_0 - \upsilon)^{-1} w^2 \, dz - 4 \, .$$

Since the operator is self-adjoint and $L_0(1) = w^2$, we obtain that $\Xi(0) = 0$. By differentiating in Ξ we get

$$\Xi'(\upsilon) = \int_{-\infty}^{\infty} w^2 (L_0 - \upsilon)^{-2} w^2 \, dz = \int_{-\infty}^{\infty} [(L_0 - \upsilon)^{-1} w^2]^2 \, dz > 0 \, .$$

Noting that L_0 admits a single positive eigenvalue at $\upsilon = 1$, it follows that Ξ has a single pole at $\upsilon = 1$ and that there are no other poles for $\upsilon > 0$. On the other hand, as $\upsilon \to +\infty$, we have

$$\Xi(\upsilon) \sim -\frac{1}{\upsilon} \int_{-\infty}^{\infty} w^4 \, dz \to 0^- \, .$$

To summarize, $\Xi(\upsilon)$ has a vertical asymptote at $\upsilon = 1$; $\Xi(0) = 0$, $\Xi \to 0^-$ as $\upsilon \to \infty$ and Ξ is increasing for $\upsilon > 0$. It follows that $\Xi(\upsilon) \neq 0$ for all $\upsilon > 0$, which proves our claim.

Next, from (C.8), we conclude that when $\Lambda \geq 4/(\bar{\chi}^2 v_{\max 0}^2)$ we have

$$-1 + \Lambda \frac{\int_{-\infty}^{\infty} w^2 \, dz}{\int_{-\infty}^{\infty} w^4 \, dz} \leq -\frac{\alpha(4 - \Lambda)}{2 + \alpha} \frac{\int_{-\infty}^{\infty} w^2 \, dz}{\int_{-\infty}^{\infty} w^4 \, dz} \, . \tag{C.13}$$

By using the identity $4 \int_{-\infty}^{\infty} w^2 \, dz = 3 \int_{-\infty}^{\infty} w^4 \, dz$, (C.13) implies that $\alpha \leq 1 - 3\Lambda/4$. By observing that the condition $\Lambda \geq 4/(\bar{\chi}^2 v_{\max 0}^2)$ holds when $\lambda_0 < 0$, we conclude that $\lambda_0 < 0$ when

$$\alpha \leq 1 - 3\bar{\chi}^{-2} v_{\max 0}^{-2} \, . \tag{C.14}$$

41

Similarly as in [56], we find when $\alpha = 1$, $\Psi_0 \equiv 1$ is an eigenfunction such that (C.2) admits the zero eigenvalue. If $\alpha > 1$, we claim there exists a positive real eigenvalue of (C.2). In fact, assume that some Λ satisfies $\Lambda \geq 0$. Then, one obtains that (C.2) can be written as the equivalent form

$$\Psi_0 = \alpha \frac{\int_{-\infty}^{\infty} w^4 \Psi_0 \, dz}{\int_{-\infty}^{\infty} w^4 \, dz} (L_0 - \Lambda)^{-1} w^2 \,, \quad \text{where} \quad L_0 \Psi_0 = \Psi_{0zz} + w^2 \Psi_0 \,,$$

and where α satisfies $\int_{-\infty}^{\infty} w^4 \, dz = \alpha \int_{-\infty}^{\infty} \left[(L_0 - \Lambda)^{-1} w^2 \right] w^4 \, dz$. Then, we define $R(\Lambda)$ as

$$R(\Lambda) := \int_{-\infty}^{\infty} w^4 \, dz - \alpha \int_{-\infty}^{\infty} \left[(L_0 - \Lambda)^{-1} w^2 \right] w^4 \, dz \,.$$

Since $R(0) = (1 - \alpha) \int_{-\infty}^{\infty} w^4 \, dz < 0$ and $R(\Lambda) \to +\infty$ as $\Lambda \to 1^-$, we conclude that there exists a positive $\Lambda \in (0, 1)$ such that $R(\Lambda) = 0$. This finishes the proof of our claim.

By comparing this result and (C.14), it follows that there is still a gap region between $1 - 3\bar{\chi}^{-2} v_{\max 0}^{-2}$ and 1. To eliminate this gap, and obtain a refined prediction of the threshold α_c, we shall rewrite the solution to (C.7) in terms of the hypergeometric function and perform a detailed asymptotic expansion of it similar to that in [57].

To do so, we first recall the definition and some properties of generalized hypergeometric functions [47]. The generalized hypergeometric functions $_pF_q(a_1, \cdots, a_p; b_1, \cdots, b_q; z)$ are defined by the following series:

$$_pF_q(a_1, \cdots, a_p; b_1, \cdots, b_q; z) = 1 + \frac{a_1 \cdots a_p}{b_1 \cdots b_q} \frac{z}{1!} + \frac{(a_1 + 1) \cdots (a_p + 1)}{(b_1 + 1) \cdots (b_q + 1)} \frac{z^2}{2!} + \cdots \,. \tag{C.15}$$

Their derivatives satisfy a recursion formula, given by

$$\frac{d}{dz} {}_pF_q(a_1, \cdots, a_p; b_1, \cdots, b_q; z) = \frac{\Pi_{i=1}^{P} a_i}{\Pi_{i=1}^{q} b_i} {}_pF_q(a_1 + 1, \cdots, a_p + 1; b_1 + 1, \cdots, b_q + 1; z) \,. \tag{C.16}$$

In addition, the relationship between $_{p+1}F_{q+1}(a_1, \cdots, a_p; b_1, \cdots, b_q; z)$ and $_pF_q(a_1, \cdots, a_p; b_1, \cdots, b_q; z)$ is

$$_{p+1}F_{q+1}(a_1, \cdots, a_p, a_{p+1}; b_1, \cdots, b_q, b_{q+1}; z)$$
$$= \frac{\Gamma(b_{q+1})}{\Gamma(a_{p+1})\Gamma(b_{q+1} - a_{p+1})} \int_0^1 t^{a_{p+1}-1} (1 - t)^{b_{q+1} - a_{p+1} - 1} {}_pF_q(a_1, \cdots, a_p; b_1, \cdots, b_q; tz) \, dt \,, \tag{C.17}$$

where Γ is the Gamma function $\Gamma(z) := \int_0^{\infty} t^{z-1} e^{-t} dt$. In particular, when $p = 2$ and $q = 1$, (C.15) becomes the ordinary hypergeometric function, which satisfies

$$_2F_1(a_1, a_2; b_1; 1) = \frac{\Gamma(b_1)\Gamma(b_1 - a_2 - a_1)}{\Gamma(b_1 - a_1)\Gamma(b_1 - a_2)} \,, \qquad b_1 > a_1 + a_2 \,. \tag{C.18}$$

In addition, for $|z| < 1$, $_2F_1(a_1; b_1, b_2; z)$ has the following recursion formula:

$$_2F_1(a_1, a_2; b_1; z) = (1 - z)^{b_1 - a_2 - a_1} {}_2F_1(b_1 - a_1; b_1 - a_2, b_1; z) \,, \qquad b_1 < a_1 + a_2 \,. \tag{C.19}$$

With this preliminary background, we return to the NLEP (C.7) and use generalized hypergeometric functions to calculate the critical value of α, labeled by α_c, for which $\lambda_0 = 0$ is an eigenvalue. This implies that $\Lambda = \delta^2$ in (C.7). By defining $\bar{z} := 2z$, (C.7) can be written when $\lambda_0 = 0$ and $\Lambda = \delta^2$ as

$$\Psi_{0\bar{z}\bar{z}} + \frac{w^2}{4} \Psi_0 - \frac{\bar{\kappa}}{4} \frac{\int_{-\infty}^{\infty} w^2 \Psi_0 \, d\bar{z}}{\int_{-\infty}^{\infty} w^2 \, d\bar{z}} w^2 = \frac{\delta^2}{4} \Psi_0 \,, \qquad \bar{\kappa} := \frac{\alpha(4 - \Lambda)}{2 + \alpha} \frac{\int_{-\infty}^{\infty} w^2 \, d\bar{z}}{\int_{-\infty}^{\infty} w^4 \, d\bar{z}} \,. \tag{C.20}$$

42

To use the standard results in [57], we define $\bar{w} := \frac{3}{2}\text{sech}^2(\bar{z}/2)$ and $\delta_1 := \delta/2$, so that (C.20) becomes

$$\Psi_{0\bar{z}\bar{z}} + \frac{\bar{w}}{3}\Psi_0 - \frac{\bar{\kappa}}{3}\frac{\int_{-\infty}^{\infty}\bar{w}\Psi_0\,d\bar{z}}{\int_{-\infty}^{\infty}\bar{w}\,d\bar{z}}\bar{w} = \delta_1^2\Psi_0. \tag{C.21}$$

Next, as was shown in [57], (C.21) can be transformed into a local problem with an integral constraint:

$$\Psi_{0\bar{z}\bar{z}} + \frac{\bar{w}}{3}\Psi_0 = \delta_1^2\Psi_0 + \bar{w}, \qquad \int_0^{\infty}\bar{w}\Psi_0\,d\bar{z} = \frac{3}{\bar{\kappa}}\int_0^{\infty}\bar{w}\,d\bar{z}. \tag{C.22}$$

Upon defining G by $\Psi_0 = \bar{w}^{\delta_1}G$, we substitute this relation into (C.22) to obtain

$$G_{\bar{z}\bar{z}} - 2\delta_1\frac{\bar{w}_{\bar{z}}}{\bar{w}}G_{\bar{z}} + \left[\frac{1}{3} - \frac{\delta_1}{3}(1 + 2\delta_1)\right]\bar{w}G = \bar{w}^{1-\delta_1}. \tag{C.23}$$

We next define $\tilde{z} := 2\bar{w}/3$ and rewrite (C.23) as

$$\tilde{z}(1-\tilde{z})G_{\tilde{z}\tilde{z}} + [c - (a+b+1)\tilde{z}]G_{\tilde{z}} - abG = \left(\frac{3}{2}\right)^{1-\delta_1}\tilde{z}^{-\delta_1}, \tag{C.24}$$

where we have labeled a, b, and c by $a = \delta_1 + 1$, $b = \delta_1 - 1/2$ and $c = 1 + 2\delta_1$.

With this reformulation, we now solve (C.24) in terms of hypergeometric functions. To begin, we recall from [32] that the two linear independent solutions to the homogeneous counterpart of (C.24) are

$$_2F_1(a, b; c; \tilde{z}), \qquad \tilde{z}^{1-c}\,_2F_1(a - c + 1, b - c + 1; 2 - c; \tilde{z}). \tag{C.25}$$

As such, we need only find a particular solution, labeled by G_1, of (C.24). To do so, we write G_1 in the form $G_1(\tilde{z}) = \tilde{z}^i\sum_{k=0}^{\infty}c_k\tilde{z}^k$, where the constants i and c_k need to be determined. Upon substituting this infinite series into (C.24), we solve the resulting recursion equations for i and c_k to get

$$G_1 = \left(\frac{3}{2}\right)^{1-\delta_1}(1 - \delta_1^2)^{-1}\tilde{z}^{1-\delta_1}\,_3F_2\left(1, \frac{1}{2}, 2; 2 - \delta_1, 2 + \delta_1; \tilde{z}\right). \tag{C.26}$$

It is verify that $\Psi_0 = \bar{w}^{\delta_1}G_1 \to 0$ as $\bar{z} \to +\infty$. However, we must have $\Psi_{0\bar{z}}(0) = 0$ since Ψ_0 is even. To enforce this condition, we write Ψ_0 as a linear combination of G_1 and the first homogeneous solution G_2 in (C.25) as

$$\Psi_0 = \bar{w}^{\delta_1}(G_1 + AG_2), \qquad \text{where} \quad G_2 := {}_2F_1\left(\delta_1 + 1, \delta_1 - \frac{1}{2}; 2\delta_1 + 1; \tilde{z}\right), \tag{C.27}$$

where the constant A will be determined below. To determine A, we apply (C.16) on (C.26) to get

$$\frac{dG_1}{d\tilde{z}} = \left(\frac{3}{2}\right)^{1-\delta_1}(1 - \delta_1^2)^{-1}\,_3F_2\left(2, \frac{3}{2}, 3; 3 - \delta_1, 3 + \delta_1; \tilde{z}\right).$$

By using (C.17), together with (C.18) and (C.19), we further calculate for $|\tilde{z}| \to 1^-$, that

$$\frac{dG_1}{d\tilde{z}} \sim \left(\frac{3}{2}\right)^{1-\delta_1}\frac{(1-\tilde{z})^{-1/2}}{4}\,_2F_1\left(1, \frac{3}{2}; 3; 1\right) \sim \left(\frac{3}{2}\right)^{1-\delta_1}(1-\tilde{z})^{-1/2}. \tag{C.28}$$

Similarly, from (C.16), (C.18) and (C.19), we get that the asymptotic behavior of G_2 in (C.27) as $|\tilde{z}| \to 1^-$ is

$$\frac{dG_2}{d\tilde{z}} \sim \frac{(1 + \delta_1)(\delta_1 - \frac{1}{2})}{2\delta_1 + 1}(1 - \tilde{z})^{-\frac{1}{2}}\frac{\Gamma(2\delta_2 + 2)\Gamma(\frac{1}{2})}{\Gamma(2\delta_1 + 1)\Gamma(\delta_1 + \frac{1}{2})}. \tag{C.29}$$

Upon combining (C.28) and (C.29), we conclude that $\Psi_{0\bar{z}}(0) = 0$ holds when

$$A = \left(\frac{3}{2}\right)^{1-\delta_1} \frac{\Gamma(1+\delta_1)\Gamma(\frac{1}{2}+\delta_1)}{(\frac{1}{2}-\delta_1)\Gamma(1+2\delta_1)\Gamma(\frac{1}{2})}. \tag{C.30}$$

This gives us an explicit form for Ψ_0 in (C.27).

Next, we focus on the integral constraint in (C.22). To begin, we calculate for $\delta_1 \ll 1$ that

$$\int_0^\infty \bar{w}^{1+\delta_1} G_1 \, d\bar{z} = -\frac{3}{2}\int_0^1 \bar{w}^{1+\delta_1} \frac{G_1}{\bar{w}_{\bar{z}}} \, d\bar{z} = \left(\frac{3}{2}\right)^2 (1-\delta_1^2)^{-1} \frac{\Gamma(2)\Gamma(\frac{1}{2})}{\Gamma(\frac{5}{2})} {}_4F_3\left(1,\frac{1}{2},2,2;2-\delta_1,2+\delta_1,\frac{5}{2};1\right)$$

$$\sim 3(1-\delta_1^2)^{-1}, \tag{C.31}$$

and

$$\int_0^\infty \bar{w}^{1+\delta_1} G_2 \, d\bar{z} = -\frac{3}{2}\int_0^1 \bar{w}^{1+\delta_1} \frac{G_2}{\bar{w}_{\bar{z}}} \, d\bar{z}$$

$$= \left(\frac{3}{2}\right)^{1+\delta_1} (1-\delta_1^2)^{-1} \frac{\Gamma(1+\gamma_1)\Gamma(\frac{1}{2})}{\Gamma(\frac{3}{2})} {}_3F_2\left(1+\delta_1,\delta_1-\frac{1}{2},1+\delta_1;2\delta_1+1,\frac{3}{2}+\delta_1;1\right). \tag{C.32}$$

Moreover, we calculate that

$$\int_0^\infty \bar{w} \, d\bar{z} = -\frac{3}{2}\int_0^1 \frac{\bar{w}}{\bar{w}_{\bar{z}}} \, d\bar{z} = \frac{3}{2}\int_0^1 \frac{1}{\sqrt{1-\bar{z}}} \, d\bar{z} = 3. \tag{C.33}$$

Upon collecting (C.31), (C.32) and (C.33), we use the constraint in (C.22), with A as in (C.30), to obtain

$$(1-\delta_1^2)^{-1} {}_4F_3\left(1,\frac{1}{2},2,2;2-\delta_1,2+\delta_1,\frac{5}{2};1\right)$$

$$+ \frac{A}{3}\left(\frac{3}{2}\right)^{1+\delta_1} \frac{\Gamma(1+\delta_1)\Gamma(\frac{1}{2})}{\Gamma(\frac{3}{2}+\delta_1)} {}_3F_2\left(1+\delta_1,\delta_1-\frac{1}{2},1+\delta_1;2\delta_1+1,\frac{3}{2}+\delta_1;1\right) = \frac{3}{\bar{\kappa}}. \tag{C.34}$$

As a partial verification of our computation, if we let $\delta_1 = 0$ then (C.34) yields that $\bar{\kappa} = 1$. This agrees precisely with our leading order threshold $\alpha_c \sim 1$. To seek a refined approximation of this threshold, as obtained by the next order term of α_c, we expand (C.34) up to $O(\delta_1)$. To do so, we use the standard result in [6] to find

$${}_3F_2\left(1+\delta_1,\delta_1-\frac{1}{2},1+\delta_1;2\delta_1+1,\frac{3}{2}+\delta_1;1\right) = \frac{\Gamma(b_1)\Gamma(b_2)}{\Gamma(a_3)\Gamma(a_1+1)\Gamma(a_2+1)} {}_3F_2\left(\delta_1,\frac{1}{2},1;2+\delta_1,\frac{1}{2}+\delta_1;1\right), \tag{C.35}$$

where $a_1 = 1+\delta_1$, $a_2 = \delta_1 - 1/2$, $a_3 = 1+\delta_1$, $b_1 = 2\delta_1 + 1$, and $b_2 = \delta_1 + 3/2$.

Next, we expand

$$\frac{\Gamma(b_1)\Gamma(b_2)}{\Gamma(a_3)\Gamma(a_1+r)\Gamma(a_2+r)} = \frac{\Gamma(1+2\delta_1)\Gamma(\frac{3}{2}+\delta_1)}{\Gamma(1+\delta_1)\Gamma(2+\delta_1)\Gamma(\frac{1}{2}+\delta_1)} = \frac{\frac{1}{2}+\delta_1}{1+\delta_1} + O(\delta_1^2), \tag{C.36a}$$

$${}_3F_2\left(\delta_1,\frac{1}{2},1;2+\delta_1,\frac{1}{2}+\delta_1;1\right) = 1 + \delta_1 + O(\delta_1^2). \tag{C.36b}$$

Upon substituting (C.36) into (C.35), we conclude that

$${}_3F_2\left(1+\delta_1,\delta_1-\frac{1}{2},1+\delta_1;2\delta_1+1,\frac{3}{2}+\delta_1;1\right) = \frac{1}{2}\left[1+2\delta_1+O(\delta_1^2)\right] = \frac{1}{2}+\delta_1+O(\delta_1^2). \tag{C.37}$$

Then, by using the identity $\Gamma^2(1 + \delta_1)/\Gamma(1 + 2\delta_1) = 1 + O(\delta_1^2)$. we substitute (C.37) into (C.34), and recall that $\delta_1 = \delta/2$ where $\delta = 2/(v_{\max 0}\bar\chi)$. This yields

$$\bar\kappa = 1 - \delta_1 + O(\delta_1^2) = 1 - \frac{\delta}{2} + O(\delta^2) = 1 - \frac{1}{\bar\chi v_{\max 0}} + O(v_{\max 0}^{-2}). \tag{C.38}$$

Finally, by relating $\bar\kappa$ to α using (C.20), and noting the identity $4 \int_{-\infty}^{\infty} w^2 \, d\bar z = 3 \int_{-\infty}^{\infty} w^4 \, d\bar z$, we conclude that (C.38) provides the following refined threshold at which $\lambda_0 = 0$, which completes the proof of Theorem 3.1:

$$\alpha_c \sim 1 - \frac{3}{2\bar\chi v_{\max 0}}. \tag{C.39}$$

D   Computation of Partial Derivatives for Quasi-Equilibria

In this appendix, we derive an approximation for $dv_{\max j}/ds_j$ from our quasi-equilibrium construction, and we calculate some related partial derivatives that are needed in our analysis. From (2.28), $v_{\max j}$ and C_j satisfy

$$v_{\max j}^2 = \frac{2C_j}{\bar\chi}e^{\bar\chi v_{\max j}} - \frac{2s_j}{\bar\chi} + s_j^2, \qquad C_j e^{\bar\chi s_j} = s_j. \tag{D.1}$$

Upon differentiating the equation for $v_{\max j}$ with respect to s_j, and labeling $v'_{\max j} := dv_{\max j}/ds_j$, we get

$$2v_{\max k}v'_{\max j} = (2e^{-\bar\chi s_j} - 2\bar\chi s_j e^{-\bar\chi s_j})\frac{e^{\bar\chi v_{\max j}}}{\bar\chi} + 2s_j e^{-\bar\chi s_j}e^{\bar\chi v_{\max j}}v'_{\max j} - \frac{2}{\bar\chi} + 2s_j, \tag{D.2}$$

We solve for $v'_{\max j}$ in (D.2), while eliminating C_j in (D.1). After some algebra we obtain

$$v'_{\max j} = \frac{\left(v_{\max j}^2/s_j - \bar\chi v_{\max j}^2 + \bar\chi s_j^2 - s_j\right)}{2v_{\max j} - \bar\chi v_{\max j}^2 - 2s_j + \bar\chi s_j^2}. \tag{D.3}$$

Since $s_j = O(\epsilon|\log\epsilon|^3)$ and $v_{\max j} = O(|\log\epsilon|)$, we obtain upon retaining only the first term in the numerator and the first two terms in the denominator that for $\epsilon \to 0$

$$v'_{\max j} = \frac{dv_{\max j}}{ds_j} \sim -\frac{\zeta_{\max j}}{\bar\chi s_j}, \qquad \zeta_{\max j} := \left(1 - \frac{2}{\bar\chi v_{\max j}}\right)^{-1}. \tag{D.4}$$

This result (D.4) is needed in (3.34) for analyzing the Jacobian of the quasi-equilibrium construction.

In a similar way, by taking the partial derivative of $v_{\max k}$ with respect to the location x_i of the ith spike in the quasi-equilibrium pattern, we readily derive the following result for $\epsilon \to 0$ that is needed in (5.32) and (5.34):

$$\partial_{x_i} v_{\max k} \sim -\frac{\zeta_{\max k}}{\bar\chi s_k}\partial_{x_i} s_k, \qquad \zeta_{\max k} = \left(1 - \frac{2}{\bar\chi v_{\max k}}\right)^{-1}. \tag{D.5}$$

E   Calculation of $\mathcal{G}_g$ and $\mathcal{P}_g$

In this appendix, for $d_1 \in \mathcal{T}_e$, we calculate the matrix spectrum of $\mathcal{G}_g$, as given in (4.27), as well as the matrix $\mathcal{P}_g$ that was defined in (4.24). To do so, for $d_1 \in \mathcal{T}_e$, we introduce the auxiliary BVP

$$\frac{d_1}{\mu}y'' + \bar u y = 0, \quad 1 < x < 1; \quad y'(\pm 1) = 0; \quad \left[\frac{d_1}{\mu}y\right]_j = b_j, \quad \left[\frac{d_1}{\mu}y'\right]_j = 0, \tag{E.1}$$

for $j = 1, \ldots, N$. Here $[y]_j := y(x_j^+) - y(x_j^-)$ with $x_j = x_j^0$ as given by (2.29). The solution to (E.1) is $y = \sum_{k=1}^{N} b_k g(x; x_k)$, where the dipole Green's function $g(x; x_k)$ satisfies (4.22). Upon defining $\mathbf{y}' := \left(y_1', \ldots, y_N'\right)^T$, $\langle \mathbf{y} \rangle := (\langle y \rangle_1, \ldots, \langle y \rangle_N)^T$, and $\mathbf{b} := (b_1, \ldots, b_N)^T$, where $y_j' = y'(x_j)$ and $\langle y \rangle_j = (y(x_j^+) + y(x_j^-))/2$, we conclude that

$$\mathbf{y}' = \mathcal{G}_g \mathbf{b} \,, \qquad \langle \mathbf{y} \rangle = \mathcal{P}_g \mathbf{b} \,. \tag{E.2}$$

The inverses of $\mathcal{G}_g$ and $\mathcal{P}_g$ exist and are tridiagonal when $d_1 \in \mathcal{T}_e$. To show this, we solve (E.1) on each subinterval where we impose the continuity conditions on y' across x_j. This yields that

$$y = \begin{cases} -\dfrac{y_1'}{\theta} \dfrac{\cos[\theta(1+x)]}{\sin[\theta(1+x_1)]} \,, & -1 < x < x_1 \,, \\[2mm] \dfrac{y_j'}{\theta} \dfrac{\cos[\theta(x_{j+1}-x)]}{\sin[\theta(x_{j+1}-x_j)]} - \dfrac{y_{j+1}'}{\theta} \dfrac{\cos[\theta(x-x_j)]}{\sin[\theta(x_{j+1}-x_j)]} \,, & x_j < x < x_{j+1} \,, \quad j = 1, \ldots, N-1 \,, \\[2mm] \dfrac{y_N'}{\theta} \dfrac{\cos[\theta(1-x)]}{\sin[\theta(1-x_N)]} \,, & x_N < x < 1 \,, \end{cases} \tag{E.3}$$

where $\theta = \sqrt{\mu \bar{u}/d_1}$. By using (E.3), we satisfy the jump conditions in (E.1) to get

$$\mathcal{D}_g \mathbf{y}' = \frac{\mu \theta}{d_1} \mathbf{b} \,, \qquad \mathcal{G}_g = \frac{\mu \theta}{d_1} \mathcal{D}_g^{-1} \,. \tag{E.4}$$

Here, for $d_1 \in \mathcal{T}_e$, $\mathcal{D}_g$ is the invertible tridiagonal matrix defined by

$$\mathcal{D}_g = \begin{pmatrix} d_g & f_g & 0 & \cdots & 0 & 0 & 0 \\ f_g & e_g & f_g & \cdots & 0 & 0 & 0 \\ 0 & f_g & e_g & \ddots & 0 & 0 & 0 \\ \vdots & \vdots & \ddots & \ddots & \ddots & \vdots & \vdots \\ 0 & 0 & 0 & \ddots & e_g & f_g & 0 \\ 0 & 0 & 0 & \cdots & f_g & e_g & f_g \\ 0 & 0 & 0 & \cdots & 0 & f_g & d_g \end{pmatrix} . \tag{E.5}$$

where $d_g = \cot(2\theta/N) + \cot(\theta/N)$, $e_g = 2\cot(2\theta/N)$ and $f_g = -\csc(2\theta/N)$, for which the identity $d_g = e_g - f_g$ holds. When $d_1 \in \mathcal{T}_e$ (see (2.35)), i.e. $2\theta/N < \pi$, we see that e_g, d_g and f_g are well-defined.

Similarly, we rewrite $\langle \mathbf{y} \rangle$ in terms of $\mathbf{y}'$ as $\langle \mathbf{y} \rangle = -(2\theta)^{-1} \csc(2\theta/N) \mathcal{C} \mathbf{y}'$. where $\mathcal{C}$ was defined in (B.10). By combining the second equation in (E.2) with this result we obtain for $d_1 \in \mathcal{T}_e$ that

$$\mathcal{P}_g = -\frac{\mu}{2d_1} \csc\left(\frac{2\theta}{N}\right) \mathcal{C} \mathcal{D}_g^{-1} \,. \tag{E.6}$$

The matrix spectrum of the tridiagonal matrix $\mathcal{D}_g$, labeled by $\mathcal{D}_g \mathbf{v} = \xi \mathbf{v}$ where $\mathbf{v} = (v_1, \ldots, v_N)^T$, is readily calculated as in [24] and the result is summarized in Proposition 4.2.

Finally, when $\lambda_0 = 0$, we establish a key identity

$$\mathcal{P}^T = -\mathcal{P}_g \,, \tag{E.7}$$

which relates (4.27) for $\mathcal{P}$ when $\lambda_0 = 0$ to (4.24). One way to derive this identity is to observe from (B.6) that when $\lambda_0 = 0$, we have $e_g = -e$, $f_g = -f$, and $d_g = -e + f$. By using these expressions in (E.5) a direct matrix multiplication yields the identity $\mathcal{C} \mathcal{D}_g = -\mathcal{D} \mathcal{C}$, where $\mathcal{D}$ and $\mathcal{C}$ are defined in (B.5) and (B.10), respectively. The result (E.7) follows by comparing (E.6) and (B.11), and noting that $\mathcal{D}$ and $\mathcal{D}_g$ are symmetric.

F Diagonalization of the Matrix $\mathcal{M}$ for the Small Eigenvalues

In this appendix, when $d_1 \in \mathcal{T}_e$, we show how to diagonalize the matrix $\mathcal{M}$ in (4.29) to obtain the result given in Proposition 4.3 for the small eigenvalues. From (4.29), the matrix for the small eigenvalues is

$$\mathcal{M} = \frac{2\bar{\chi}}{3} v_{\max 0}^3 \mathcal{G}_g - \frac{2v_{\max 0}^2 \zeta_0}{a_g} \mathcal{P} \left(I + \frac{3\zeta_0}{\bar{\chi} a_g v_{\max 0}} \mathcal{G} \right)^{-1} \mathcal{P}_g + \frac{s_0 \bar{u} \mu}{\epsilon d_1} I, \qquad \zeta_0 := \left(1 - \frac{2}{\bar{\chi} v_{\max 0}} \right)^{-1}. \tag{F.1}$$

We begin by focusing on the middle term in $\mathcal{M}$. We first introduce the matrix decomposition of $\mathcal{D}$ by $\mathcal{D} = Q\mathcal{K}Q^T$, where $\mathcal{K} = \text{diag}(\kappa_1, \ldots, \kappa_N)$ and Q is the orthogonal matrix formed from the eigenvectors $\boldsymbol{q}_j$ in Proposition B.1 when $\tau = 0$. For $\tau = 0$, the eigenvalues κ_j of $\mathcal{D}$ are related to the eigenvalues ξ_j of $\mathcal{D}_g$ by

$$\kappa_1 = 2\tan(\theta/N), \quad \kappa_j = -\xi_j = -2\cot(2\theta/N) + 2\csc(2\theta/N)\cos(\pi(j-1)/N), \quad j = 2, \ldots, N. \tag{F.2}$$

By using (B.7) with $\lambda_0 = 0$, we obtain that $\mathcal{G} = \sqrt{\frac{\mu}{d_1 \bar{u}}} Q\mathcal{K}^{-1}Q^T$, which yields

$$\mathcal{P} \left(I + \frac{3\zeta_0}{\bar{\chi} a_g v_{\max 0}} \mathcal{G} \right)^{-1} \mathcal{P}_g = \mathcal{P}Q \left(I + \frac{3\zeta_0}{\bar{\chi} a_g v_{\max 0}} \sqrt{\frac{\mu}{\bar{u} d_1}} \mathcal{K}^{-1} \right)^{-1} Q^T \mathcal{P}_g. \tag{F.3}$$

Next, we use (E.6) and (B.11) to conclude that $\mathcal{P}\mathcal{D} = \left(\mathcal{P}_g \mathcal{D}_g \right)^T$ so that

$$\mathcal{P} = \left(\mathcal{P}_g \mathcal{D}_g \right)^T \mathcal{D}^{-1} = \left(\mathcal{P}_g \mathcal{D}_g \right)^T Q\mathcal{K}^{-1}Q^T. \tag{F.4}$$

By combining (F.4) and (F.3), and using $QQ^T = I$, we get

$$\mathcal{P} \left(I + \frac{3\zeta_0}{\bar{\chi} a_g v_{\max 0}} \mathcal{G} \right)^{-1} \mathcal{P}_g = \mathcal{R}\mathcal{D}_g^{-1}, \qquad \text{where} \quad \mathcal{R} := \left(\mathcal{P}_g \mathcal{D}_g \right)^T Q\mathcal{H}Q^T \left(\mathcal{P}_g \mathcal{D}_g \right). \tag{F.5}$$

Here $\mathcal{R}$ is defined in terms of a diagonal matrix $\mathcal{H}$ given by

$$\mathcal{H} := \left(\frac{3\zeta_0}{\bar{\chi} a_g v_{\max 0}} \sqrt{\frac{\mu}{\bar{u} d_1}} I + \mathcal{K} \right)^{-1} = \text{diag}(h_1, \ldots, h_N). \tag{F.6}$$

Therefore, by using $\mathcal{G}_g = \frac{\mu \theta}{d_1} \mathcal{D}_g^{-1}$ from (E.4), together with (F.5), we can write (F.1) as

$$\mathcal{M} = \left(\frac{2\bar{\chi}}{3} v_{\max 0}^3 \frac{\mu \theta}{d_1} I + \frac{s_0 \bar{u} \mu}{\epsilon d_1} \mathcal{D}_g - \frac{2v_{\max 0}^2 \zeta_0}{a_g} \mathcal{R} \right) \mathcal{D}_g^{-1}. \tag{F.7}$$

Next, we must focus on analyzing the matrix $\mathcal{R}$ defined by (F.5). By using (E.6), we obtain

$$\left(\mathcal{P}_g \mathcal{D}_g \right)^T = -\frac{\mu}{2d_1} \csc \left(\frac{2\theta}{N} \right) C,$$

where C is given in (B.10). In this way, it is convenient to write $\mathcal{R}$ as

$$\mathcal{R} = \frac{\mu^2}{4d_1^2} \csc^2 \left(\frac{2\theta}{N} \right) C^T Q\mathcal{H}Q^T C = \frac{\mu^2}{4d_1^2} \csc^2 \left(\frac{2\theta}{N} \right) Q_g Q_g^T C^T Q\mathcal{H}Q^T C Q_g Q_g^T,$$

where Q_g are the normalized eigenvectors of $\mathcal{D}_g$ (see Proposition 4.2), arising in the matrix decomposition

$$\mathcal{D}_g = Q_g \mathcal{K}_g Q_g^T, \qquad \mathcal{K}_g = \text{diag}(\xi_1, \ldots, \xi_N), \tag{F.8}$$

where ξ_j are the eigenvalues of $\mathcal{D}_g$ as given in Proposition 4.2. In this way, we can write $\mathcal{R}$ as

$$\mathcal{R} = Q_g \Sigma Q_g^T, \qquad \text{where} \quad \Sigma := \frac{\mu^2}{4d_1^2} \csc^2\left(\frac{2\theta}{N}\right) \mathcal{S}\mathcal{H}\mathcal{S}^T, \quad \mathcal{S} := Q_g^T C^T Q. \tag{F.9}$$

The key step in the analysis is the calculation of Σ in (F.9) using the explicit forms for the matrices Q_g, C, and Q, as was done in section 4.2 of [24]. This calculation in [24] showed that Σ is a diagonal matrix given by

$$\Sigma = \text{diag}(\omega_1, \ldots, \omega_N), \qquad \text{where} \qquad \omega_j := \frac{\mu^2}{d_1^2} \csc^2\left(\frac{2\theta}{N}\right) \sin^2\left(\frac{(j-1)}{N}\pi\right) h_j, \quad j = 1, \ldots, N. \tag{F.10}$$

Here h_j, for $j = 1, \ldots, N$, are the diagonal entries of $\mathcal{H}$ that can be identified from (F.6).

Upon substituting (F.9) and $\mathcal{D}_g^{-1} = Q_g \mathcal{K}_g^{-1} Q_g^T$ into (F.7), and recalling (4.28), we obtain that the matrix eigenvalue problem for the small eigenvalues reduces to

$$\lambda \boldsymbol{c} \sim -\epsilon^3 \beta_0 \mathcal{M} \boldsymbol{c}, \qquad \text{where} \quad \mathcal{M} = Q_g\left(a\mathcal{K}_g^{-1} + bI - \frac{2v_{\max 0}^2 \zeta_0}{a_g}\Sigma\mathcal{K}_g^{-1}\right)Q_g^T. \tag{F.11}$$

This key result shows that $\mathcal{M}$ is diagonalizable by the eigenspace Q_g of the Green's dipole matrix. In (F.11),

$$a := \frac{2\bar{\chi}}{3}v_{\max 0}^3\left(\frac{\mu\theta}{d_1}\right), \qquad b := \frac{s_0\bar{u}\mu}{\epsilon d_1} = \frac{2\bar{\chi}}{3}v_{\max 0}^3\left(\frac{a_g\bar{u}\mu}{d_1}\right), \tag{F.12}$$

where we have used the result $s_0 \sim 2\bar{\chi}a_g v_{\max 0}^3\epsilon/3$ from (2.30) to simplify b.

Finally, by introducing $\tilde{\boldsymbol{c}} = Q_g^T \boldsymbol{c}$ in (F.11), we readily obtain from (F.12) that the small eigenvalues are given explicitly as in (4.33) of Proposition 4.3. The constants ω_j, as given in (4.34), are obtained from (F.10) by using the diagonal entries of $\mathcal{H}$ that can be identified from (F.6) and (F.2).

G   Bifurcation Point for the Emergence of Asymmetric Steady-States

In this appendix we verify that the simultaneous zero-eigenvalue crossing threshold for the small eigenvalues, as given in (4.40), coincides with the bifurcation point at which asymmetric steady-state solution branches bifurcate from the symmetric steady-state branches constructed in §2.

To do so, we proceed in a similar way as in [54] by constructing a steady-state solution of (1.2) on a canonical domain $|x| \leq \ell$, with $u_x = v_x = 0$ at $x = \pm\ell$ and with a spike centered at $x = 0$. On this domain, the leading-order outer solution $u_{o\ell}(x)$ satisfies (see (2.22))

$$\mathcal{L}_{0\ell}u_{o\ell} := \frac{d_1}{\mu}u_{o\ell xx} + \bar{u}u_{o\ell} = \frac{2\bar{\chi}\epsilon}{3}v_{\max \ell}^3 \delta(x), \quad |x| \leq \ell; \qquad u_{o\ell x}(\pm\ell) = 0, \tag{G.1}$$

where, in analogy with (2.33), $v_{\max \ell}$ satisfies the dominant balance

$$\frac{1}{2}v_{\max \ell}^2 \sim \frac{s_\ell}{\bar{\chi}}e^{\bar{\chi}v_{\max \ell}}, \qquad \text{with} \quad s_\ell = u_{o\ell}(0). \tag{G.2}$$

To solve (G.1) we let $G_\ell(x)$ be the Green's function satisfying $\mathcal{L}_{0\ell}G_\ell = \delta(x)$, with $G_{\ell x}(\pm\ell) = 0$. For $\theta \neq m\pi/\ell$ with $m = 1, 2, \ldots$, where $\theta = \sqrt{\mu\bar{u}/d_1}$, we obtain that

$$u_{o\ell}(x) = \frac{2\bar{\chi}}{3}\epsilon v_{\max\ell}^3 \, G_\ell(x), \qquad \text{where} \quad G_\ell(x) = \frac{\mu \cos\left[\theta(\ell - |x|)\right]}{2\theta d_1 \sin(\theta\ell)}. \tag{G.3}$$

By evaluating (G.3) at $x = 0$ we can calculate s_ℓ, which is needed in (G.2) for determining $v_{\max\ell}$. In this way, we obtain after some algebra that at $x = \ell$

$$u_{o\ell}(\ell) = c\mathcal{B}(\ell), \qquad \text{where} \quad \mathcal{B}(\ell) := \frac{v_{\max\ell}^3}{\sin(\theta\ell)}, \quad c := \frac{\epsilon\bar{\chi}}{3\bar{u}}\sqrt{\frac{\mu\bar{u}}{d_1}}. \tag{G.4a}$$

Here $v_{\max\ell}$ as a function of ℓ satisfies the nonlinear algebraic equation

$$v_{\max\ell}e^{\bar{\chi}v_{\max\ell}}\cot(\theta\ell) = \bar{\chi}/(2c). \tag{G.4b}$$

As similar to the analysis in [54] for the GM model, the construction of asymmetric steady-state patterns for (1.2) relies on determining ℓ_1 and ℓ_2 for which $\mathcal{B}(\ell_1) = \mathcal{B}(\ell_2)$. As a result, we have $u_{o\ell}(\ell_1) = u_{o\ell}(\ell_2)$, which allows for the construction of a C^1 global solution on $|x| \leq 1$ with M_1 and M_2 small and large spikes, respectively, when the length constraint $\ell_1 M_1 + \ell_2 M_2 = 1$ is satisfied (cf. [54]).

The bifurcation point along the steady-state symmetric branch where such asymmetric equilibria emerge is determined by setting $\mathcal{B}'(\ell) = 0$ with $\ell = 1/N$. From (G.4a) and the logarithmic derivative of (G.4b) we get

$$\mathcal{B}'(\ell) = \frac{v_{\max\ell}^2}{\sin(\theta\ell)}\left[3v'_{\max\ell} - \theta v_{\max\ell}\cot(\theta\ell)\right], \qquad v'_{\max\ell}\left(1 + \frac{1}{\bar{\chi}v_{\max\ell}}\right) = \frac{\theta}{\bar{\chi}\sin(\theta\ell)\cos(\theta\ell)}. \tag{G.5}$$

Upon combining these two equations we conclude that

$$\mathcal{B}'(\ell) = \frac{\theta\, v_{\max\ell}^3}{\sin^2(\theta\ell)\cos(\theta\ell)}\left[\frac{3}{1 + \bar{\chi}v_{\max\ell}} - \cos^2(\theta\ell)\right]. \tag{G.6}$$

By setting $\mathcal{B}'(\ell) = 0$ with $\ell = 1/N$, and using the double-angle formula for $\cos^2(\theta\ell)$, we readily obtain that the threshold value of θ is

$$\cos\left(\frac{2\theta}{N}\right) = \frac{1 - a_1}{1 + a_1}, \qquad \text{where} \quad a_1 = \frac{1}{3}(\bar{\chi}v_{\max} - 2). \tag{G.7}$$

This threshold agrees precisely with the zero-eigenvalue crossing result (4.40) for the small eigenvalues.

H   Computation of β_0 and β_j

In this appendix, we show how to obtain the estimate (5.26) for β_j, where β_j was defined in (5.17) of §5. For simplicity, in the analysis below we will drop the subscript j in V_{0j}, $v_{\max j}$, C_j, s_j, and $v_{\max j}$.

We begin by recalling from (2.3) that the leading order steady state v-equation for the spike profile is

$$V_0'' - V_0 + Ce^{\bar{\chi}V_0} = 0, \qquad -\infty < y < +\infty; \qquad V_0(0) = v_{\max}, \quad V_0(\infty) = s, \tag{H.1}$$

where $v_{\max}^2 = 2Ce^{\bar{\chi}v_{\max}} - 2s + s^2$ and $C = se^{-\bar{\chi}s}$.

From the results in Proposition 2.1 for the sub-inner region, we conclude that there exists a positive constant $y_0 = O(1/v_{\max}) \ll 1$ such that

$$V_0 \sim v_{\max} + \frac{1}{\bar{\chi}}\log\left[\text{sech}^2\left(\frac{v_{\max}\bar{\chi}y}{2}\right)\right], \quad 0 < y < y_0; \qquad U_0 \sim \frac{\bar{\chi}}{2}v_{\max}^2\text{sech}^2\left(\frac{v_{\max}\bar{\chi}y}{2}\right), \quad 0 < y < y_0.$$

49

The decay behavior of U_0 and V_0 is obtained by noting that $V_0'' - V_0 + \bar{\chi}sV_0 \approx 0$ for $y > y_0$. Since $s \ll 1$, this yields $V_0'' - V_0 \approx 0$. With this observation, and by enforcing continuity across $y = y_0$, we estimate

$$V_0 \sim \begin{cases} v_{\max} + \frac{1}{\bar{\chi}}\log\left[\operatorname{sech}^2\left(\frac{v_{\max}\bar{\chi}y}{2}\right)\right], & y < y_0, \\ v_{\max}e^{-(y-y_0)} + \frac{1}{\bar{\chi}}\log\left[\operatorname{sech}^2\left(\frac{v_{\max}\bar{\chi}y_0}{2}\right)\right], & y > y_0, \end{cases} , \qquad V_0' \sim \begin{cases} -v_{\max}\tanh(\frac{v_{\max}\bar{\chi}y}{2}), & y < y_0, \\ -v_{\max}e^{-(y-y_0)}, & y > y_0. \end{cases} \qquad \text{(H.2)}$$

Moreover, since $U_0 = Ce^{\bar{\chi}V_0}$, we obtain in a similar way that

$$U_0 \sim \begin{cases} \frac{\bar{\chi}}{2}v_{\max}^2\operatorname{sech}^2\left(\frac{v_{\max}\bar{\chi}y}{2}\right), & y < y_0, \\ Ce^{\bar{\chi}v_{\max}e^{-(y-y_0)}}\left(\operatorname{sech}^2\left(\frac{v_{\max}\bar{\chi}y_0}{2}\right)\right), & y > y_0. \end{cases} \qquad \text{(H.3)}$$

By using (H.3) we calculate that

$$\int_0^y \frac{1}{U_0}\,d\xi \sim \begin{cases} \frac{2}{\bar{\chi}v_{\max}^2}\left(\frac{y}{2} + \frac{\sinh(v_{\max}\bar{\chi}y)}{2\bar{\chi}v_{\max}}\right), & y < y_0, \\ \frac{2}{\bar{\chi}v_{\max}^2}\left(\frac{y_0}{2} + \frac{\sinh(v_{\max}\bar{\chi}y_0)}{2\bar{\chi}v_{\max}}\right) + \frac{1}{s}(y - y_0), & y > y_0. \end{cases}$$

Then, upon multiplying by U_0, we obtain

$$U_0\int_0^y \frac{1}{U_0}\,d\xi \sim \begin{cases} \frac{y}{2}\operatorname{sech}^2(\frac{v_{\max}\bar{\chi}y}{2}) + \frac{1}{2v_{\max}\bar{\chi}}\tanh(\frac{v_{\max}\bar{\chi}y}{2})\operatorname{sech}(\frac{v_{\max}\bar{\chi}y}{2}), & y < y_0, \\ (y - y_0) + \frac{2C}{\bar{\chi}v_{\max}^2}e^{\bar{\chi}v_{\max}e^{-(y-y_0)}}\operatorname{sech}^2\left(\frac{v_{\max}\bar{\chi}y_0}{2}\right)\left(\frac{y_0}{2} + \frac{\sinh(v_{\max}\bar{\chi}y_0)}{2\bar{\chi}v_{\max}}\right), & y > y_0. \end{cases} \qquad \text{(H.4)}$$

By multiplying (H.4) with V_0' from (H.2) and integrating, we observe that the dominant contribution to the integrand arises from multiplying the $y - y_0$ term in (H.4) with the $-v_{\max}e^{-(y-y_0)}$ term in (H.2). In this way,

$$\int_0^\infty U_0 V_0'\left(\int_0^y \frac{1}{U_0}\,d\xi\right)dy \sim -v_{\max}\int_{y_0}^{+\infty} e^{-(y-y_0)}(y - y_0)\,dy \sim -v_{\max}.$$

In a similar way, we estimate that $\int_0^{+\infty}\left(V_0'\right)^2 dy \sim v_{\max}^2\int_{y_0}^{+\infty} e^{-2(y-y_0)}\,dy \sim v_{\max}^2/2$. We conclude from (5.17) that $\beta_j \sim 2/v_{\max}$, as was claimed in (5.26).

Next, we recall from (4.28) in our analysis of the small eigenvalues that $\beta_0 = -\int_0^\infty yV_0'\,dy / \int_0^\infty \left(V_0'\right)^2 dy$. By using (H.4) and (H.2), we can readily verify that

$$\int_0^\infty yV_0'\,dy \sim \int_0^\infty U_0 V_0'\left(\int_0^y \frac{1}{U_0}\,d\xi\right)dy,$$

which establishes that $\beta_j \sim \beta_0$ when evaluated at the steady-state solution.

I   The Equivalence Between Some Matrices

In this appendix, we show the relationship between the matrices

$$\nabla\mathcal{G} := (\partial_{x_j}G(x_j^0; x_k^0))_{N\times N}, \qquad (\nabla\mathcal{G})^T := (\partial_{x_k}G(x_j^0; x_k^0))_{N\times N}, \qquad \nabla^2\mathcal{G} := (\partial_{x_j}\partial_{x_k}G(x_j^0; x_k^0))_{N\times N}, \qquad \text{(I.1)}$$

used in the linearization of the DAE system and the matrices $\mathcal{P}$, $\mathcal{P}_g$, and $\mathcal{G}_g$, as defined in (4.27), (4.24), and (4.27), respectively, that were used in §4 in our analysis of the small eigenvalues. Recall that the diagonal entries in the matrices in (I.1) were defined in (5.27) in terms of the regular part R of the Green's function (see (5.20)).

We first show that $\nabla G = \mathcal{P}$. To establish this, we use the decomposition (5.20) to obtain

$$G_x(x; x_k) = \begin{cases} \frac{\mu}{2d_1} + R_x(x; x_k), & x > x_k, \\ -\frac{\mu}{2d_1} + R_x(x; x_k), & x < x_k. \end{cases} \tag{I.2}$$

As such, we identify that the average across the kth spike is simply $\langle G_x \rangle_k = \left(G_x(x_k^+; x_k) + G_x(x_k^-; x_k) \right)/2 = R_x(x_k; x_k)$. By comparing (I.1) and (4.27), and recalling (5.27) for $j = k$, we conclude that $\nabla G = \mathcal{P}$.

Next, we show that $(\nabla \mathcal{G})^T = -\mathcal{P}_g$. We first differentiate the BVP (2.24) for $G(x; x_k)$ with respect to x_k to get

$$\frac{d_1}{\mu} \left(\partial_{x_k} G(x; x_k) \right)_{xx} + \bar{u} \left(\partial_{x_k} G(x; x_k) \right) = -\delta'(x - x_k); \qquad \partial_x \left(\partial_{x_k} G(x; x_k) \right)|_{x=\pm 1} = 0.$$

By comparing this result with the BVP (4.22) satisfied by the dipole Green's function, we conclude that

$$\partial_{x_k} G(x; x_k) = -g(x; x_k), \qquad -1 < x < 1, \tag{I.3}$$

so that for $j \neq k$ we have $\partial_{x_k} G(x_j; x_k) = -g(x_j; x_k)$. It follows that the off-diagonal entries in $(\nabla \mathcal{G})^T$ and $\mathcal{P}_g$ are identical. For the diagonal entries, where $j = k$, we use (I.3) and the decomposition (5.20) to obtain

$$g(x; x_k) = \begin{cases} \partial_{x_k} \left(\frac{\mu}{d_1}(x - x_k) + R(x; x_k) \right) = -\frac{\mu}{d_1} - \partial_{x_k} R(x; x_k), & x > x_k, \\ \partial_{x_k} \left(-\frac{\mu}{d_1}(x - x_k) + R(x; x_k) \right) = \frac{\mu}{d_1} - \partial_{x_k} R(x; x_k), & x < x_k, \end{cases} \tag{I.4}$$

Upon defining $\langle g \rangle_k = \frac{1}{2} \left(g(x_k^+; x_k) + g(x_k^-; x_k) \right)$, we conclude from (I.4) and the reciprocity $R(x; y) = R(y; x)$ of the Green's function that $\langle g \rangle_k = -\partial_{x_k} R(x; x_k)|_{x=x_k} = -\partial_{x_k} R(x_k; x)|_{x=x_k}$. This implies that the diagonal entries of $\mathcal{P}_g$ in (4.24) are the same as those of $(\nabla \mathcal{G})^T$ in (I.1). It follows that $(\nabla \mathcal{G})^T = \mathcal{P}^T = -\mathcal{P}_g$. We remark that the relation $\mathcal{P}^T = -\mathcal{P}_g$ was also derived using an alternative approach in (E.7) at the end of Appendix E.

Our next identity is to establish that $\nabla^2 \mathcal{G} = -\mathcal{G}_g$. The equivalence between the off-diagonal entries in these matrices, where $j \neq k$, is established by setting $x = x_j$ in (I.3) and differentiating in x_j to obtain

$$\partial_{x_j} \left[\partial_{x_k} G(x_j; x_k) \right] = -\partial_{x_j} g(x_j; x_k) = -\partial_x g(x; x_k)|_{x=x_j}.$$

Next, we differentiate (I.4) with respect to x and upon evaluating at $x = x_k$, we compare the resulting expression with (5.27) to obtain that

$$g_x(x : x_k)|_{x=x_k} = -\frac{\partial}{\partial x}|_{x=x_k} \frac{\partial}{\partial y}|_{y=x_k} R(x, y) = -\partial_{x_k}^2 G(x_j; x_k), \qquad j = k.$$

We conclude that the diagonal entries in $\nabla^2 \mathcal{G}$ and $-\mathcal{G}_g$ are also identical. It follows that $\nabla^2 \mathcal{G} = -\mathcal{G}_g$.

Finally, we calculate $R_{xx}(x; x_j)|_{x=x_j}$ as needed in (5.41). By using the decomposition (5.20) we write (I.2) as

$$G_x(x; x_j) = -\frac{\mu}{2d_1} + \frac{\mu}{d_1} H(x - x_j) + R_x(x; x_j),$$

where $H(z)$ is the Heavyside function. Therefore, $G_{xx}(x; x_j) = \frac{\mu}{d_1} \delta(x - x_j) + R_{xx}(x; x_j)$ on $|x| < 1$. Upon substituting this expression into the BVP (2.24) for G, we conclude that $R_{xx}(x; x_j) = \frac{\bar{u}\mu}{d_1} G(x; x_j)$, so that

$$R_{xx}(x_j; x_j) = \frac{\bar{u}\mu}{d_1} G(x_j; x_j). \tag{I.5}$$

51

References

[1] J. Adler. Chemotaxis in bacteria. *Ann. Rev. Biochem.*, 44(1):341–356, 1975.

[2] R. Bastiaansen, P. Carter, and A. Doelman. Stable planar vegetation stripe patterns on sloped terrain in dryland ecosystems. *Nonlineariy*, 32(8):2759–2814, 2019.

[3] N. Bellomo, A. Bellouquid, Y. Tao, and M. Winkler. Towards a mathematical theory of Keller-Segel models of pattern formation in biological tissues. *Math. Model. Meth. Appl. Sci.*, 25(9):1663–1763, 2015.

[4] V. Brinkmann, U. Reichard, C. Goosmann, B. Fauler, Y. Uhlemann, D. Weiss, Y. Weinrauch, and A. Zychlinsky. Neutrophil extracellular traps kill bacteria. *Science*, 303(5663):1532–1535, 2004.

[5] D. Brown and H. Berg. Temporal stimulation of chemotaxis in *escherichia coli*. *P. Natl. Acad. Sci.*, 71(4):1388–1392, 1974.

[6] W. Bühring. The behavior at unit argument of the hypergeometric function $_3F_2$. *SIAM J. Math. Anal.*, 18(5):1227–1234, 1987.

[7] J. Carrillo, J. Li, and Z-A. Wang. Boundary spike-layer solutions of the singular Keller–Segel system: existence and stability. *Proc. London Math. Soc.*, 122(1):42–68, 2021.

[8] W. Chen and M. Ward. The stability and dynamics of localized spot patterns in the two-dimensional Gray–Scott model. *SIAM J. Appl. Dyn. Syst.*, 10(2):582–666, 2011.

[9] X. Chen, J. Hao, X. Wang, Y. Wu, and Y. Zhang. Stability of spiky solution of Keller–Segel's minimal chemotaxis model. *J. Diff. Eq.*, 257(9):3102–3134, 2014.

[10] S. Childress and K. Percus. Nonlinear aspects of chemotaxis. *Math. Biosci.*, 56(3-4):217–237, 1981.

[11] M. del Pino and J. Wei. Collapsing steady states of the Keller–Segel system. *Nonlinearity*, 19(3):661, 2006.

[12] A. Doelman, T. Kaper, and K. Promislow. Nonlinear asymptotic stability of the semi-strong pulse dynamics in a regularized Gierer-Meinhardt model. *SIAM J. Math. Anal.*, 38(6):1760–1789, 2007.

[13] T. Engelmann. Über sauerstoffausscheidung von pflanzenzellen im mikrospektrum. *Pflüger, Arch.*, 27(1):485–489, 1882.

[14] FlexPDE. Solutions inc. *https://www.pdesolutions.com*, 2021.

[15] C. Gui and J. Wei. Multiple interior peak solutions for some singularly perturbed Neumann problems. *J. Diff. Eq.*, 158(1):1–27, 1999.

[16] M. Herrero and J. Velázquez. Chemotactic collapse for the Keller-Segel model. *J. Math. Biol.*, 35(2):177–194, 1996.

[17] T. Hillen and K. Painter. A user's guide to PDE models for chemotaxis. *J. Math. Biol.*, 58(1):183–217, 2009.

[18] T. Hillen and A. Potapov. The one-dimensional chemotaxis model: global existence and asymptotic profile. *Math. Methods Appl. Sci.*, 27(15):1783–1801, 2004.

[19] T. Hillen, J. Zielinski, and K. Painter. Merging-emerging systems can describe spatio-temporal patterning in a chemotaxis model. *Disc. Contin. Dyn. Syst. Ser. B*, 18(10):2513, 2013.

[20] D. Horstmann. The nonsymmetric case of the Keller-Segel model in chemotaxis: some recent results. *Nonl. Diff. Eq. Appl.*, 8(4):399–423, 2001.

[21] D. Horstmann. From 1970 until present: the Keller-Segel model in chemotaxis and its consequences I. *Jahresber Deutsch. Math.-Verein.*, 105:103–165, 2003.

[22] D. Horstmann. From 1970 until present: the Keller-Segel model in chemotaxis and its consequences II. *Jahresber Deutsch. Math.-Verein.*, 106:51–69, 2004.

[23] D. Iron and M. Ward. The dynamics of multi-spike solutions for the one-dimensional Gierer-Meinhardt model. *SIAM J. App. Math.*, 62(6):1924–1951, 2002.

[24] D. Iron, M. Ward, and J. Wei. The stability of spike solutions to the one-dimensional Gierer–Meinhardt model. *Physica D.*, 150(1-2):25–62, 2001.

[25] L. Jin, Q. Wang, and Z. Zhang. Pattern formation in Keller–Segel chemotaxis models with logistic growth. *Int. J. Bifur. Chaos*, 26(02):1650033, 2016.

[26] K. Kang, T. Kolokolnikov, and M. Ward. The stability and dynamics of a spike in the 1D Keller–Segel model. *IMA J. Appl. Math.*, 72(2):140–162, 2007.

[27] E. Keller and L. Segel. Initiation of slime mold aggregation viewed as an instability. *J. Theor. Biol.*, 26(3):399–415, 1970.

[28] E. Keller and L. Segel. Model for chemotaxis. *J. Theor. Biol.*, 30(2):225–234, 1971.

[29] T. Kolokolnikov, F. Paquin-Lefebvre, and M. J. Ward. Competition instabilities of spike patterns for the 1-d gierer-meinhardt and schnakenberg models are subcritical. *Nonlinearity*, 34(1):273–312, 2021.

[30] T. Kolokolnikov, W. Sun, M. J. Ward, and J. Wei. The stability of a stripe for the Gierer-Meinhardt model and the effect of saturation. *SIAM J. Appl. Dyn. Sys.*, 5(2):313–363, 2006.

[31] T. Kolokolnikov, J. Wei, and A. Alcolado. Basic mechanisms driving complex spike dynamics in a chemotaxis model with logistic growth. *SIAM J. Appl. Math.*, 74(5):1375–1396, 2014.

[32] T. Kolokolnikov, J. Wei, and M. Winter. Existence and stability analysis of spiky solutions for the Gierer–Meinhardt system with large reaction rates. *Physica D.*, 238(16):1695–1710, 2009.

[33] F. Kong, J. Wei, and L. Xu. The existence and stability of spikes in the one-dimensional Keller-Segel model with logistic growth. *preprint*, 2022.

[34] F. Kong, J. Wei, and L. Xu. Existence of multi-spikes in the Keller-Segel model with logistic growth. *preprint*, 2022.

[35] C-S. Lin, W-M. Ni, and I. Takagi. Large amplitude stationary solutions to a chemotaxis system. *J. Diff. Eq.*, 72(1):1–27, 1988.

[36] K. Lin and C. Mu. Convergence of global and bounded solutions of a two-species chemotaxis model with a logistic source. *Disc. Contin. Dyn. Syst. Ser. B*, 22(6):2233, 2017.

[37] T. Nagai. Blow-up of radially symmetric solutions to a chemotaxis system. *Adv. Math. Sci. Appl.*, 5:581–601, 1995.

[38] T. Nagai, T. Senba, and K. Yoshida. Application of the Trudinger-Moser inequality to a parabolic system of chemotaxis. *Funkc. Ekvacioj*, 40:411–433, 1997.

[39] V. Nanjundiah. Chemotaxis, signal relaying and aggregation morphology. *J. Theor. Biol.*, 42(1):63–105, 1973.

[40] W-M. Ni and I. Takagi. Locating the peaks of least-energy solutions to a semilinear Neumann problem. *Duke Math. J.*, 70(2):247–281, 1993.

[41] J. Oppenheim and D. Yang. Alarmins: chemotactic activators of immune responses. *Curr. Opin. Immunol.*, 17(4):359–365, 2005.

[42] K. Osaki and A. Yagi. Finite dimensional attractor for one-dimensional Keller-Segel equations. *Funkc. Ekvacioj*, 44(3):441–470, 2001.

[43] K. Painter. Mathematical models for chemotaxis and their applications in self-organization phenomena. *J. Theor. Bio.*, 481(21):162–182, 2019.

[44] K. Painter and T. Hillen. Spatio-temporal chaos in a chemotaxis model. *Physica D.*, 240(4-5):363–375, 2011.

[45] D. Rossi and A. Zlotnik. The biology of chemokines and their receptors. *Annu. Rev. Immunol.*, 18(1):217–242, 2000.

[46] T. Senba and T. Suzuki. Some structures of the solution set for a stationary system of chemotaxis. *Adv. Math. Sci. Appl.*, 10(1):191–224, 2000.

[47] L. Slater. *Generalized hypergeometric functions*. Cambridge university press, 1966.

[48] W. H. Tse and M. J. Ward. Hotspot formation and dynamics for a continuum model of urban crime. *Europ. J. Appl. Math.*, 27(3):583–624, 2016.

[49] A. Turing. The chemical basis of morphogenesis. *Philos. Trans. Royal Soc.*, 237(641):37–72, 1952.

[50] G. Wang and J. Wei. Steady state solutions of a reaction-diffusion system modeling chemotaxis. *Math. Nachr.*, 233(1):221–236, 2002.

[51] Q. Wang, J. Yan, and C. Gai. Qualitative analysis of stationary Keller–Segel chemotaxis models with logistic growth. *Z. Angew. Math. Phys.*, 67(3):1–25, 2016.

[52] X. Wang and Q. Xu. Spiky and transition layer steady states of chemotaxis systems via global bifurcation and Helly's compactness theorem. *J. Math. Biol.*, 66(6):1241–1266, 2013.

[53] M. J. Ward. Spots, traps, and patches: Asymptotic analysis of localized solutions to some linear and nonlinear diffusive processes. *Nonlinearity*, 31(8):R189 (53), 2018.

[54] M. J. Ward and J. Wei. Asymmetric spike patterns for the one-dimensional Gierer-Meinhardt model: Equilibria and stability. *Europ. J. Appl. Math.*, 13(3):283–320, 2002.

[55] M. J. Ward and J. Wei. Hopf bifurcation and oscillatory instabilities of spike solutions for the one-dimensional Gierer-Meinhardt model. *J. Nonl. Sci.*, 13(2):209–264, 2003.

[56] J. Wei. On single interior spike solutions of the Gierer–Meinhardt system: uniqueness and spectrum estimates. *Eur. J. Appl. Math.*, 10(4):353–378, 1999.

[57] J. Wei and M. Winter. Critical threshold and stability of cluster solutions for large reaction-diffusion systems in R^1. *SIAM J. Math. Anal.*, 33(5):1058–1089, 2002.

[58] J. Wei and M. Winter. Existence, classification and stability analysis of multiple-peaked solutions for the Gierer-Meinhardt system in R^1. *Methods Appl. Anal.*, 14(2):119–164, 2007.

[59] J. Wei and M. Winter. *Mathematical aspects of pattern formation in biological systems*, volume 189 of *Appl. Math. Sci.* Springer, London, 2014.

[60] M. Winkler. Chemotaxis with logistic source: very weak global solutions and their boundedness properties. *J. Math. Anal. Appl.*, 348(2):708–729, 2008.

[61] M. Winkler. Boundedness in the higher-dimensional parabolic-parabolic chemotaxis system with logistic source. *Comm. Part. Diff. Eq.*, 35(8):1516–1537, 2010.

[62] M. Winkler. Global asymptotic stability of constant equilibria in a fully parabolic chemotaxis system with strong logistic dampening. *J. Diff. Eq.*, 257(4):1056–1077, 2014.

[63] T. Xiang. How strong a logistic damping can prevent blow-up for the minimal Keller–Segel chemotaxis system? *J. Math. Anal. Appl.*, 459(2):1172–1200, 2018.

[64] T. Xiang. Sub-logistic source can prevent blow-up in the 2D minimal Keller-Segel chemotaxis system. *J.*

Math. Phys., 59(8):081502, 2018.